NASA CR-134745
ORNL-TM-4775

EVALUATION OF T-111 FORCED-CONVECTION LOOP TESTED WITH LITHIUM AT 1370°C

by

J. H. DeVan and E. L. Long, Jr.

OAK RIDGE NATIONAL LABORATORY

prepared for

NATIONAL AERONAUTICS AND SPACE ADMINISTRATION

NASA Lewis Research Center

Contract C-54-555-B

Robert L. Davies, Project Manager

OAK RIDGE NATIONAL LABORATORY
OPERATED BY UNION CARBIDE CORPORATION • FOR THE U.S. ATOMIC ENERGY COMMISSION

NASA CR-134745
ORNL-TM-4775

EVALUATION OF T-111 FORCED-CONVECTION LOOP TESTED WITH LITHIUM AT 1370°C

J. H. DeVan and E. L. Long, Jr.

Contract No. W-7405-eng-26

OAK RIDGE NATIONAL LABORATORY
operated by
Union Carbide Corporation
Nuclear Division
Post Office Box X
Oak Ridge, Tennessee 37830

for U.S. Energy Research and Development Administration

prepared for

NATIONAL AERONAUTICS AND SPACE ADMINISTRATION

CONTRACT C-54-555-B

APRIL 1975

NASA Lewis Research Center
Cleveland, Ohio
Robert L. Davies, Project Manager

1. Report No.	2. Government Accession No.	3. Recipient's Catalog No.
NASA CR-134745		

4. Title and Subtitle	5. Report Date
Evaluation of T-111 Forced-Convection Loop Tested with Lithium at 1370°C	April 1975
	6. Performing Organization Code
7. Author(s)	8. Performing Organization Report No.
J. H. DeVan and E. L. Long, Jr.	ORNL-TM-4775
	10. Work Unit No.
9. Performing Organization Name and Address Oak Ridge National Laboratory P.O. Box X Oak Ridge, TN 37830	11. Contract or Grant No. C-54-555-B
	13. Type of Report and Period Covered Contractor Report
12. Sponsoring Agency Name and Address National Aeronautics and Space Administration Washington, D.C. 20546	14. Sponsoring Agency Code

15. Supplementary Notes

Topical Report
Project Manager, R. L. Davies, Materials and Structures Division, NASA Lewis Research Center, Cleveland, Ohio

16. Abstract

A T-111 alloy (Ta—8% W—2% Hf) forced-convection loop containing molten lithium was operated 3000 hr at a maximum temperature of 1370°C. Flow velocities up to 6.3 m/sec were used. The results of this forced-convection loop are very similar to those observed in lower velocity thermal-convection loops of T-111 containing lithium.

Weight changes were determined at 93 positions around the loop. The maximum dissolution rate occurred at the maximum wall temperature of the loop and was less than 1.3 μm/year. Mass transfer of hafnium, nitrogen, and, to a lesser extent, carbon occurred from the hotter to cooler regions. Exposed surfaces in the highest temperature region were found to be depleted in hafnium to a depth of 60 μm with no detectable change in tungsten content.

There was some loss in room-temperature tensile strength for specimens exposed to lithium at 1370°C, attributable to depletion of hafnium and nitrogen and to attendant grain growth.

17. Key Words (Suggested by Author(s))	18. Distribution Statement
Lithium Corrosion Tantalum Alloys Liquid Metals Power Systems	Unclassified-Unlimited

19. Security Classif. (of this report)	20. Security Classif. (of this page)	21. No. of Pages	22. Price*
Unclassified	Unclassified	154	$ 7.60

* For sale by the National Technical Information Service, Springfield, Virginia 22151

CONTENTS

SUMMARY

This report describes the design, operation, and post-test evaluation of a tantalum alloy forced-convection loop, which circulated molten lithium. The loop operated for 3000 hr at a maximum temperature of 1370°C. The system piping was constructed of T-111 alloy (Ta—8% W—2% Hf) and was enclosed in an ultrahigh vacuum chamber to prevent oxidation at the operating temperature. Lithium was circulated at 509—575 kg/hr (141—160 g/sec) at flow velocities up to 6.3 m/sec. Tubular and sheet specimens of the T-111 alloy were contained within the loop to evaluate mass transfer behavior and changes in mechanical properties.

One test interruption occurred after 1735 hr, when a lithium leak developed in a vent line leading from the hot leg. The leak was associated with metallic contaminants, principally nickel, that apparently were present on the vent line before the test. The leak was successfully repaired, and the test run completed.

Weight changes were determined at 93 positions around the loop. The maximum dissolution rate occurred at the maximum wall temperature of the loop, and, in terms of uniform wall thinning, was less than 1.3 μm/year. Chemical analyses of loop sections and insert specimens showed mass transfer of hafnium, nitrogen, and, to a lesser extent, carbon from the hotter to cooler regions. Microprobe examination of T-111 from the highest temperature region indicated the exposed surface to be depleted of hafnium to a depth of 60 μm with no detectable change in tungsten content.

The room-temperature tensile strength of insert specimens exposed at 1205°C compared with that of control specimens vacuum-annealed at 1205°C. However, there was a loss in room-temperature tensile strength for specimens exposed at 1370°C compared with specimens vacuum-annealed at 1370°C. The loss is attributable to depletion of hafnium and nitrogen and to attendant grain growth.

Metallographic examination showed no microstructural changes in the inserts and loop tubing other than grain growth at exposure temperature above 1300°C.

The results of this forced-convection loop are very similar to those observed in lower velocity thermal-convection loops of T-111 containing lithium.

EVALUATION OF T-111 FORCED-CONVECTION LOOP TESTED WITH LITHIUM AT 1370°C

J. H. DeVan and E. L. Long, Jr.

INTRODUCTION

Nuclear reactors that are cooled by liquid lithium can be designed to operate at relatively high temperatures, since the boiling point of lithium is above 1300°C. Such reactors would be effective heat sources for Rankine-cycle or thermionic power conversion systems to generate electricity for space applications. The high operating temperatures not only imply high conversion efficiencies but also minimize the radiator area required to dissipate waste heat.

For several years we have studied the corrosion properties of liquid lithium pursuant to its use as a high-performance heat-transfer fluid in advanced energy systems. Early studies centered on niobium-base alloys as container materials; however, to meet demands for higher heat sink temperatures, interest shifted to tantalum alloys, which allowed higher operating temperatures. Our early corrosion studies with lithium were made in small closed loop systems[1,2] in which we imposed a temperature gradient to induce flow by natural convection. As an outgrowth of these studies, we constructed and operated an engineering-scale forced-circulation liquid lithium loop (FCLLL) fabricated from the tantalum-base alloy T-111 (Ta—8% W—2% Hf). This report describes the design and operating history of this T-111 loop and presents the results of a chemical and metallurgical examination of the loop following a 3000-hr test run. The construction and operation of the loop were conducted under the auspices of the Atomic Energy Commission. The metallurgical and chemical examinations of the loop were done under contract with National Aeronautics and Space Administration-Lewis Research Center.

DESIGN CONCEPT

This loop was constructed as a test bed for studying the corrosion properties of tantalum-base and, ultimately, tungsten-base alloys in liquid lithium under forced-convection conditions. We had originally planned to conduct three sequential test runs of 3000 hr each and to replace the heated sections of the loop between successive runs. However, the development program supporting the loop was terminated following the first test run.

---

[1]J. H. DeVan and C. E. Sessions, "Mass Transfer of Niobium-Base Alloys in Flowing Nonisothermal Lithium," *Nucl. Appl.* 3: 102—09 (1967).

[2]C. E. Sessions and J. H. DeVan, "Thermal Convection Loop Tests of Nb—1% Zr Alloy in Lithium at 1200 and 1300°C," *Nucl. Appl.* 9: 250—59 (1970).

The loop is shown schematically in Fig. 1. It was designed to provide lithium flow velocities up to 6.3 m/sec (21 fps), a maximum temperature capability of 1500°C (intended for the third test run), and a temperature difference not exceeding 200°C. The test parameters realized in the first run are summarized in Table 1. The lithium was heated by passing electrical current directly through one leg of the loop. Heat was rejected as radiant energy to a water-cooled bell-jar enclosure, which also protected the loop from external oxidation. The heater and radiator were connected through a concentric-tube heat exchanger (economizer), where heat was exchanged between counterflowing streams of lithium. The heater and economizer sections were positioned so that they could be conveniently cut away from the rest of the loop and required only two field welds to replace.

Every section of the main loop except the radiator contained corrosion coupons, which, at the end of a test run, could be weighed, metallurgically examined, and mechanically tested.

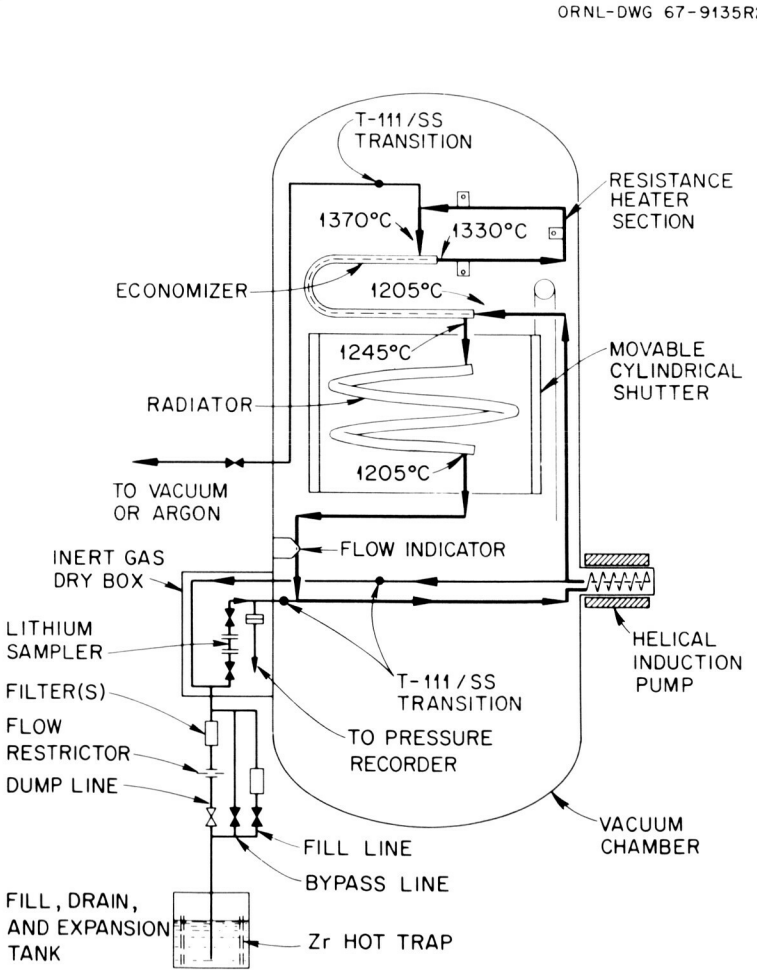

Fig. 1. Forced-Circulation Liquid Lithium Loop (FCLLL) Schematic.

Table 1. Engineering Design Information for Forced-Circulation Liquid Lithium Loop FCLLL-1

Table 1. Engineering Design Information for Forced-Circulation Liquid Lithium Loop FCLLL-1

General Information	
Material of construction	T-111 (Ta–8% W–2% Hf)
Heat-transfer fluid	Lithium
Flow rate	141–160 g/sec (≈5.8 gpm)
Maximum Reynolds number	99,000 at heater outlet
Total system pressure drop	283 kPa (41 psi)
Pressure drop in 9.40-mm-ID (0.370 in.) tubing	20 kPa/m (0.9 psi/ft)
Maximum temperature	1370°C
Minimum temperature	1200°C
Number of test specimens in loop	93
Resistance-Heated Section and Electrical Equipment	
Heated section length	2.4 m (8 ft) 13-mm-OD × 1.65-mm-wall tubing (1/2 × 0.065 in.)
Heat input for 43°C ΔT	26 kW (88,550 Btu/hr)
Current	2800 A
Electromotive force across heater	9.31 V
Transformer rating	60 kVA
Cross-section dimensions of copper bus bars	13 × 100 mm (1/2 × 4 in.)
Power loss in 4.6-m (15-ft) bus bar system	1.0 kW
Emissivity coating on bus bars	75–130 μm (3–5 mils) iron titanate
Maximum temperature of bus bars	425°C
Lithium velocity	5.58–6.32 m/sec (18.3–20.7 fps)
Economizer	
Heat transfer for 128°C ΔT	82 kW
Length of economizer	3.05 m (10 ft)
Outer-tube size	22 mm OD × 1.65 mm wall (7/8 × 0.065 in.)
Inner-tube size	13 mm OD × 1.65 mm wall (1/2 × 0.065 in.)
Lithium velocity in annulus	2.32–2.65 m/sec (7.6–8.7 fps)
Radiator	
Type of construction	0.71-m-diam (28 in.) coiled tube
Tubing size	6.7 m (22 ft) 25 mm OD × 1.65 mm wall (1 × 0.065 in.)
Surface area of coil	0.535 m^2 (5.76 ft^2)
Heat loss at design conditions	23.3 kW
Heat loss with reflective shields	20.6 kW
Heat loss with no shield	31.6 kW
Lithium velocity	0.88–1.01 m/sec (2.9–3.3 fps)
Reflective Shielding for Radiator	
Diameter of outer shell	0.86 m (34 in.)
Diameter of inner shell	0.48 m (19 in.)
Height of shield	0.66 m (26 in.)
Number of reflective layers on each shell	2
Maximum temperature of second layer	620°C
Method of operation	Cables and pulleys

A helical induction pump and magnetic flowmeter were located downstream from the radiator. Coupled to the same pump was a stainless steel bypass loop for sampling the lithium. A vent line was connected to the top of the loop, and an expansion tank was tied into the bottom of the loop ahead of the pump suction. The expansion tank doubled as the fill and drain tank and also as the site for final lithium purification. The drain tank, vent line, and lithium sampler were constructed of type 321 stainless steel and attached to T-111 lines at a distance of approximately 0.9 m (3 ft) from the main loop. The T-111 and type 321 stainless steel sections were joined through a transition joint composed of Nb—1% Zr on the end facing the T-111 alloy and type 316 stainless steel on the opposite end. The joint was a coextruded type made by Nuclear Metals, Inc. The Nb—1% Zr end of the transition joint was braze-welded to T-111 with Nb—1% Zr filler wire. During normal operation, the lithium in the stainless steel portions of the loop was static and below 400°C.

The T-111 piping was enclosed in an ultrahigh vacuum chamber to prevent oxidation at elevated temperatures. The vacuum pumps were of two types: continuous getter-ion with capacity of 2400 liters/sec and continuous titanium sublimation with capacity of about 250 liters/sec.

Within the bell-jar enclosure but distinct from the loop were two furnace assemblies containing control specimens exposed to the same external environment and temperature as the hottest and coldest sections of the loop but without the presence of lithium.

DESCRIPTION OF LOOP

Materials

Tha main loop was made from three sizes of T-111 tubing having a constant wall thickness of 1.65 mm (0.065 in.) and outside diameters of 13, 22, and 25 mm (0.5, 0.875, and 1.0 in.). Table 2 lists the tubing compositions and that of T-111 sheet used for specimens and specimen holders. Bar stock shown in Table 2 was used to make reducers for joining different tubing sizes and to make the electromagnetic flowmeter. All materials were furnished in the solution-annealed, fully recrystallized condition.

Resistance-Heated Section

Approximately 30 kW of electrical energy was transferred to the lithium as heat in the loop section shown in Fig. 2. The 13-mm-diam (1/2-in.) tubing composing this section was intercepted by three tantalum lugs, and parallel ac voltages were impressed from outboard lugs to the central lug to achieve ohmic heating. The lug geometry was selected on the basis of heat transfer studies to minimize heat conduction to current-carrying copper bus bars bolted to the lugs. The lugs and the copper

Table 2. Composition of T-111 Used in FCLLL-1

Heat	Form	Dimension (mm)		Analyst	Content,[a] wt %		Content, ppm					
					W	Hf	C	O	N	H	Zr	Nb
8171	Tubing	13	OD	Vendor	7.55	2.18	<10	39	23	3	b	b
				ORNL	8.0	2.0	40	40	8	<1	900	100
8227	Tubing	13	OD	Vendor	7.44	2.30	<10	42	18	1	b	b
				ORNL	7.9	2.1	70	27	4	<1	900	200
8227	Tubing	22	OD	Vendor	7.44	2.30	<10	31	20	4	b	b
				ORNL	7.9	2.0	40	35	12	<1	900	200
8171	Tubing	25	OD	Vendor	7.55	2.18	40	45	21	3	b	b
				ORNL	7.2	2.0	40	26	8	<1	900	100
	Sheet	0.76		Vendor	8.5	2.0	75	80	20	1.4	<200	<2000
				ORNL	8.2	1.9	60	150	19	<1	700	1000
	Bar	25	diam	Vendor	8.5	2.0	<20	90	17	3.2	<200	<2000
				ORNL	8.4	2.1	30	90	14	<1	1000	1000

[a] Balance tantalum.

[b] Not reported.

Photo 75827

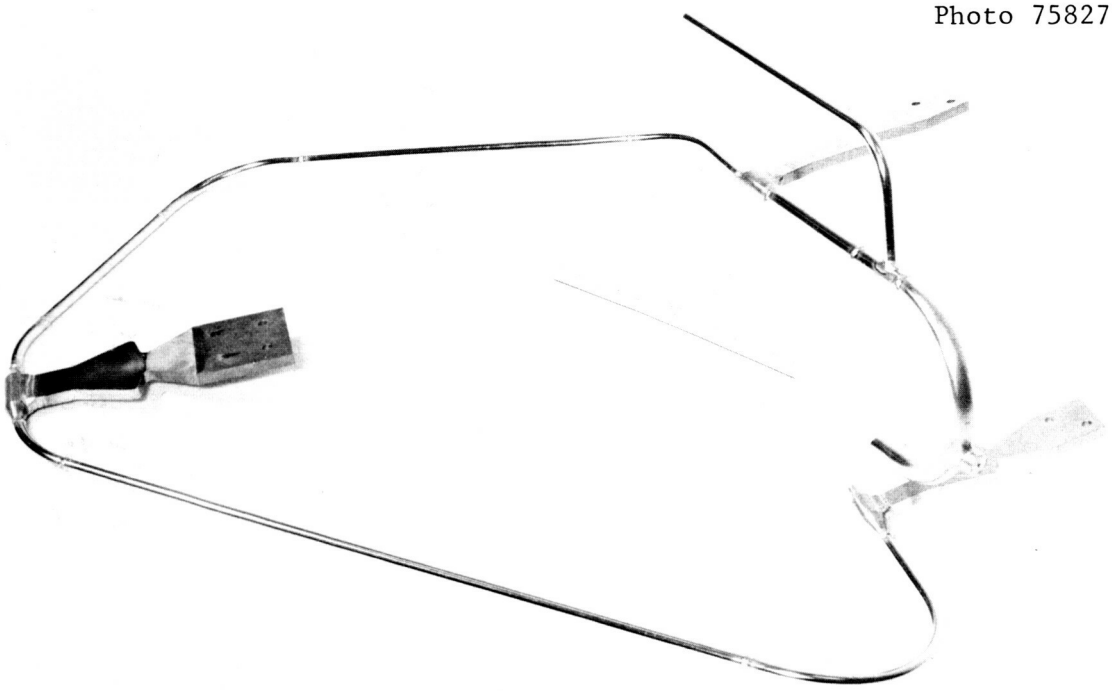

Fig. 2. Resistance-Heated Section with Bus Bar Attachment Lugs (Before Titanate Coating). Scale is 305 mm.

bus bars were plasma sprayed with iron titanate, a high-emissivity coating, to help cool these components.

The outlet of the heater section connected through a reducer to a 22-mm-diam (7/8-in.) U-bend, which matched the outer diameter of the economizer section. A 25-mm-diam (1-in.) right cylinder with a small centrally drilled cavity was welded onto the U-bend, as shown in Fig. 2, to provide a blackbody for optical pyrometer sighting.

The T-111 resistivity-heated sections were thermally insulated by several concentric layers of 50-μm-thick (0.002-in.) tantalum foil. A herringbone pattern embossed on the foil provided constant spacing between the layers.

Economizer Section

Lithium leaving the heater section entered the annulus of the concentric-tube heat economizer pictured in Fig. 3. A colder counter-current lithium stream from the radiator flowed through the inner tube of the economizer, and approximately 80 kW of thermal energy exchanged between the respective streams. The inner and outer economizer tubes were 13 and 22 mm (1/2 and 7/8 in.) in diameter, respectively, and the velocity of lithium in the inner tube was approximately twice that in the annulus. The outside surface of the economizer was thermally insulated in the same manner as the resistively heated section.

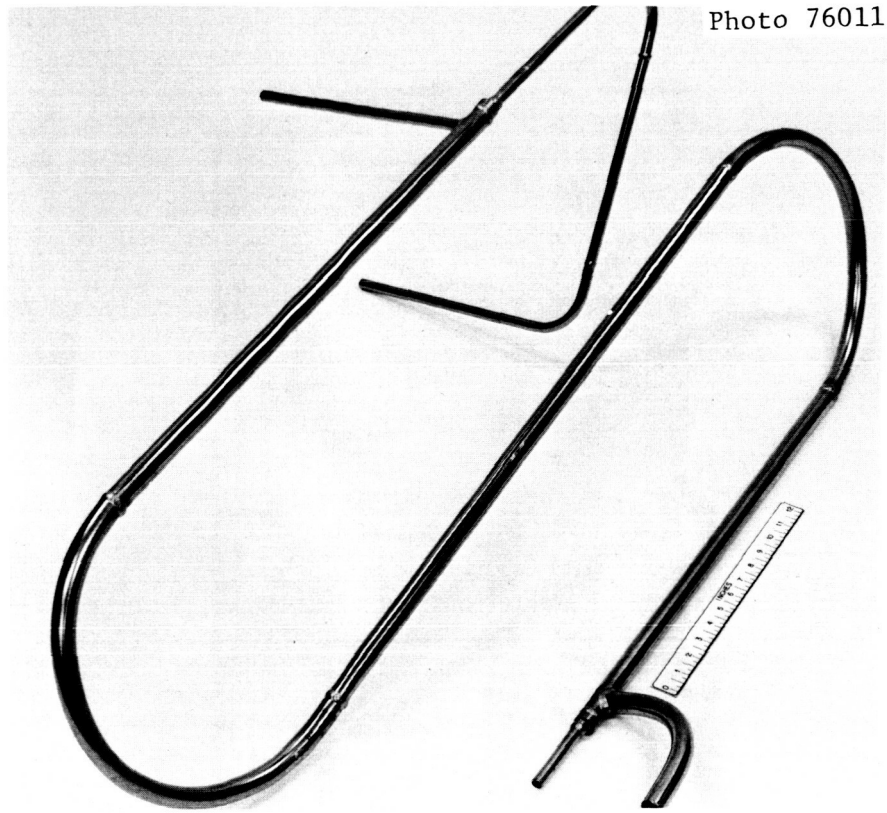

Fig. 3. Economizer Section of FCLLL, which Connected Electrically Heated Section (Fig. 2) with Radiator (Fig. 4). Scale is 305 mm.

Radiator Section

A vertical length of 13-mm (1/2-in.) tubing connected the economizer annulus to a coiled length of 25-mm-diam (1-in.) tubing located below. This coiled section was not thermally insulated and radiated thermal energy to the vacuum bell jar that housed the loop. The amount of heat radiated was controlled by a movable shutter (shown in Fig. 4), which was located concentrically between the radiator and the bell jar. The shutter was raised and lowered by a stainless steel cable, which was strung over alumina pulleys and connected to a magnetically driven winch. The alumina pulleys were mounted on stainless steel shafts with Stellite 12 hard-facings and were lubricated with niobium diselenide.

Electromagnetic Pump

The helical induction pump used in this experiment was designed by General Electric Company for the CANEL facility of Pratt and Whitney Aircraft Corporation. The helical pump duct was redesigned by ORNL for service at 1370°C and 85 psig (0.59 MPa gage) using T-111 alloy. The pump cell, fabricated by ORNL, is shown in Fig. 5. A cross-sectional view of the complete pump is shown in Fig. 6.

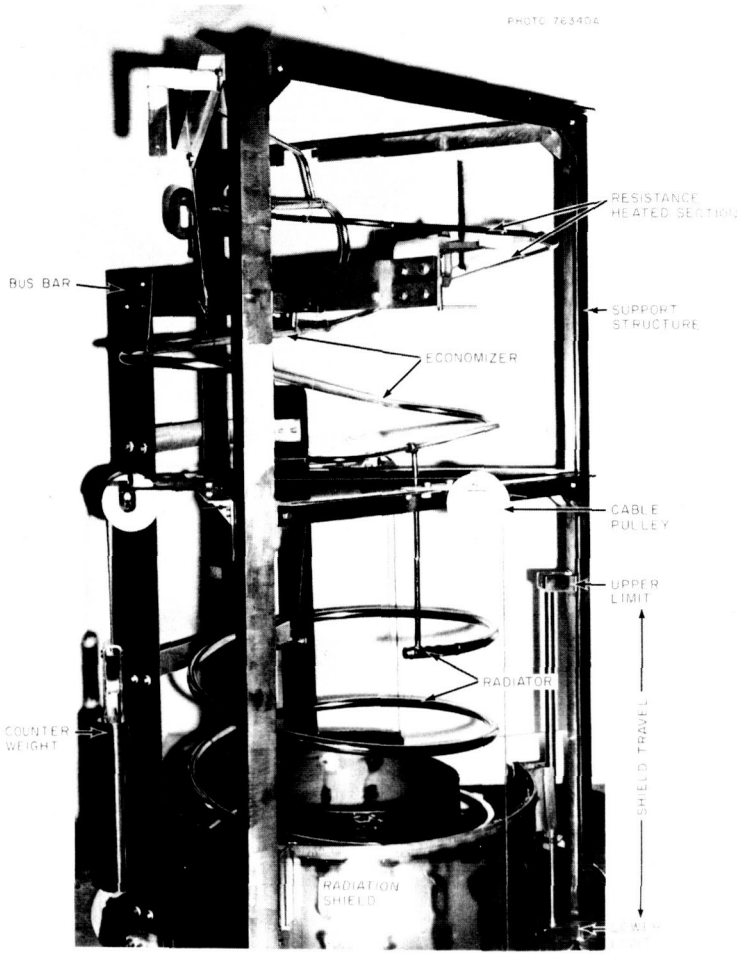

Fig. 4. As-Assembled View of FCLLL Showing Placement of Radiator and Radiation Shield.

The performance characteristics of the T-111 pump were evaluated in a stainless steel test facility using potassium at temperatures up to 800°C. This pump test and its results are described elsewhere.[3] The test data developed in potassium confirmed that the pump could accommodate the 160 g/sec (≈6 gal/min) and 283-kPa (41-psi) pressure drop flow requirements of the lithium loop.

---

[3]H. C. Young and D. L. Clark, *Hydraulic Performance and Cavitation Characteristics of an Electromagnetic Helical Induction Pump Operating with Potassium and Prediction of Performance with Lithium at 2200°F*, ORNL-TM-2995 (November 1970).

Photo 76154

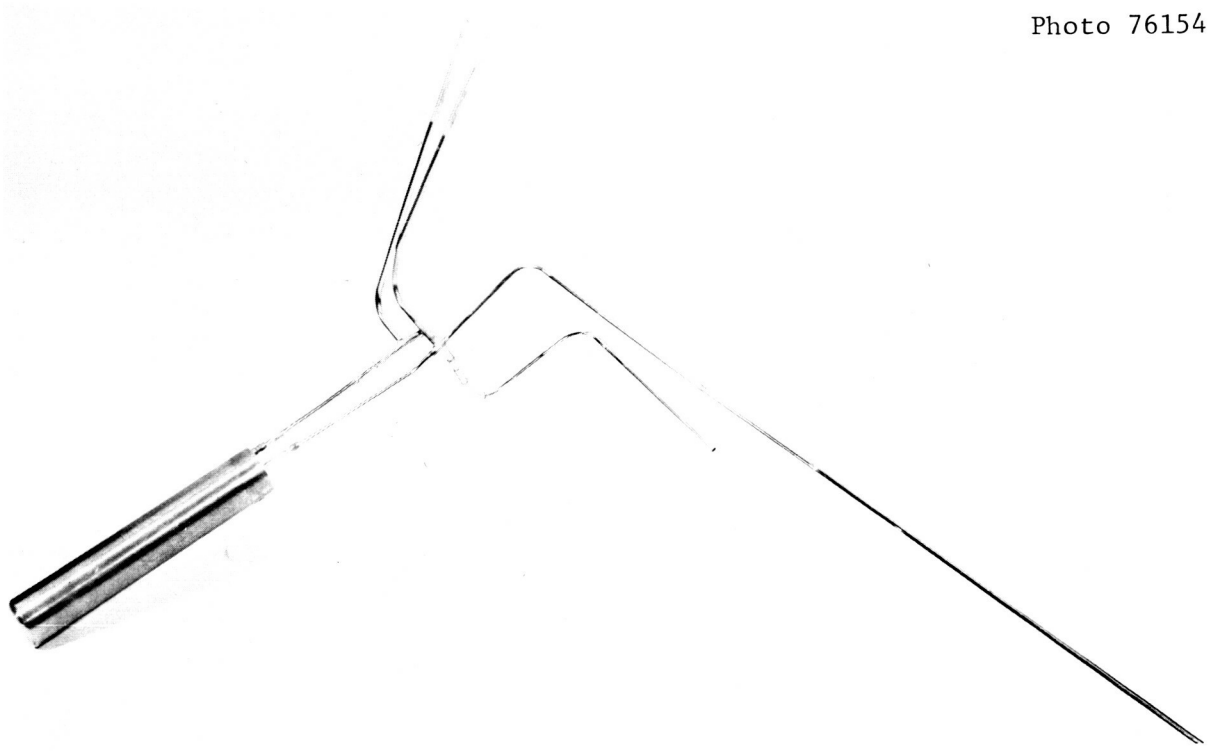

Fig. 5. T-111 Pump Cell with Primary Loop Attachment Lines (Downward Facing) and By-Pass Sampling Load Lines (Upward Facing). Pump cell (extreme left) is approximately 460 mm long by 90 mm diam (18 by 3 1/2 in.).

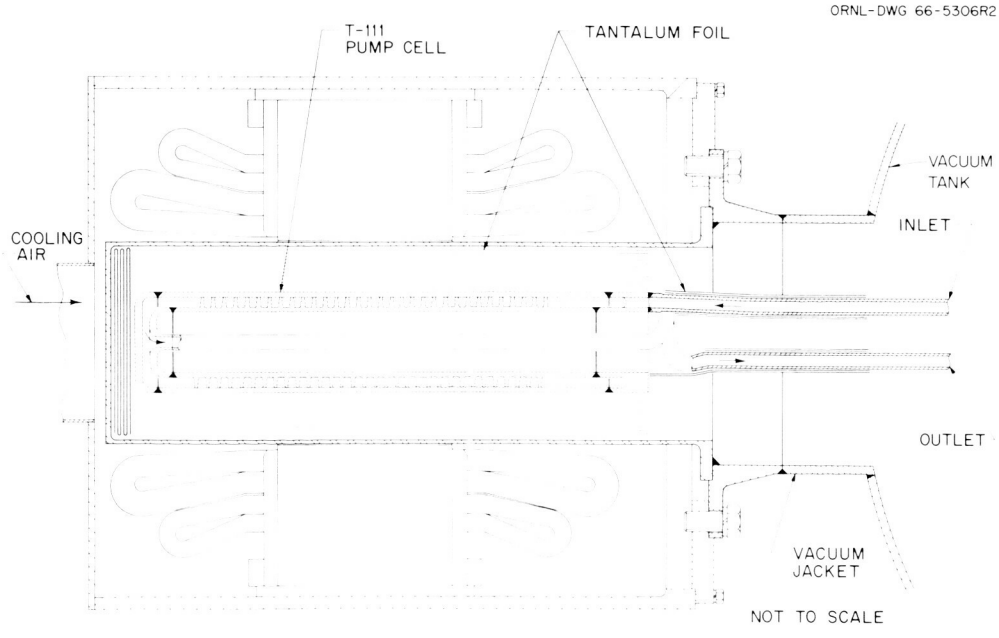

Fig. 6. Schematic of Helical Induction Pump with T-111 Pump Cell.

DESCRIPTION OF TEST SPECIMENS

Two types of removable specimens were incorporated in the loop to record weight changes at various loop positions. The first type was in the form of a flat tab, 70 by 3.2 by 0.76 mm (2 3/4 by 1/4 by 0.03 in.), whose longest axis coincided with the longitudinal axis of the loop piping. From three to ten of the tabs were mounted end-to-end on stringers, as shown in Fig. 7. Each stringer was then tack-welded into an equivalent length of tubing, which was butt-welded into the loop. In addition to the tab specimens, the loop also contained three annular (tubular) specimens, 18.8 mm OD by 0.48 mm wall by 19.2 mm long (0.742 by 0.019 by 0.75 in.) and six annular specimens 10.4 mm OD by 0.48 mm wall by 19.2 mm long (0.408 by 0.019 by 0.75 in.). These annular specimens were placed in groups of three against recessed tubing sections and were located around stringers containing tab specimens.

Photo 2978-74

Fig. 7. Three Flat Specimens Showing Assembly into the Holder. Also shown is the tube into which the assembled specimens were placed and fastened by tack-welding each end of the holder.

Within the same vacuum chamber that housed the loop were two tungsten-mesh furnaces containing control specimens of T-111. These furnaces were operated for 1735 hr at the highest and lowest loop temperatures. The T-111 specimens in these furnaces were in the form of sheet, 35 by 54 by 0.76 mm (1 3/8 by 2 1/8 by 0.03 in.), and were assembled in holders shown in Fig. 8.

Photo 75889

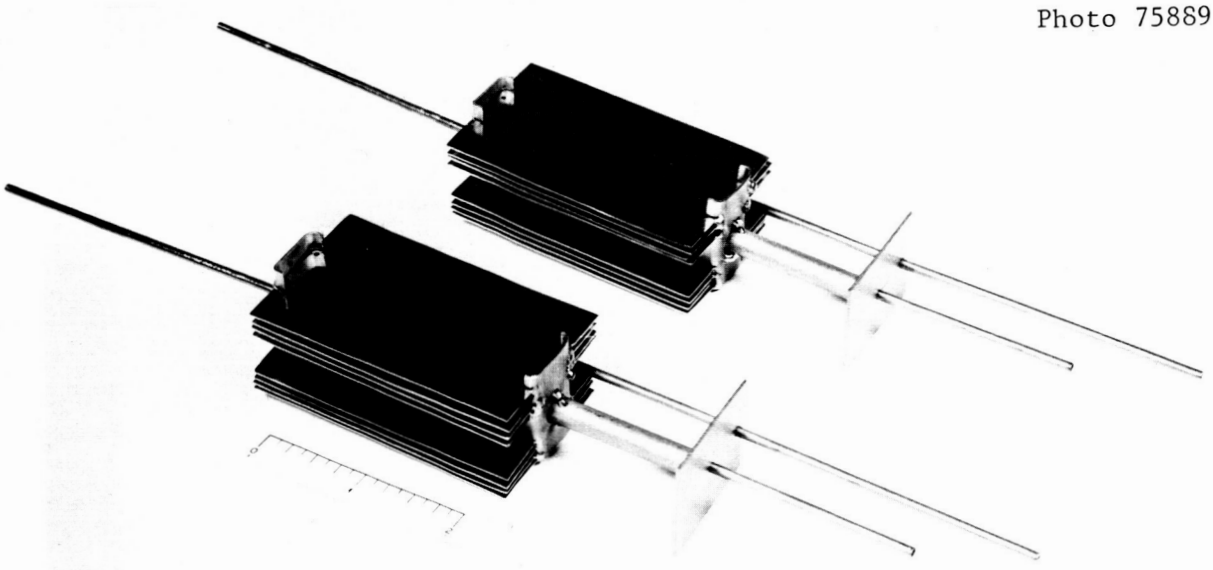

Fig. 8. Control Specimens of T-111 Alloy for FCLLL. Scale is 51 mm.

FABRICATION AND HEAT TREATMENT

Piping subassemblies were welded in inert-gas glove boxes by the gas tungsten-arc process with T-111 filler metal. Welding procedures are discussed elsewhere.[4] Before final assembly in the vacuum chamber, loop subassemblies consisting of the resistance heater, economizer, radiator, and helical induction pump were vacuum annealed for 2 hr at 1325°C. Appendix A describes the annealing conditions and the results of chemical analyses of control specimens carried through the annealing cycle. After annealing, the T-111 pump cell with attached tubing (Fig. 5) was installed in the vacuum vessel. Type 321 stainless steel tubing was then attached to the transition joints, and trace heaters were mounted on stainless steel sections between the transition joints and the vacuum vessel penetrations. The T-111 radiator section and the economizer and heater sections were next assembled on the test stand frame along with the copper bus bars. One field weld between the radiator and economizer and another between the heater and economizer

[4]E. A. Franco-Ferreira and G. M. Slaughter, "The Welding of Refractory-Metal Components for Liquid Metal Service," *Weld. J. (N.Y.)* 45: 835–42 (1966).

completed the assembly. The field welds were made with a remotely controlled welding head mounted in a glass tee envelope "inerted" with high-purity helium.[4] Figure 9 shows the assembly for the final field weld with the automatic welder in place.

Following loop assembly a crack was detected near a tack weld that anchored a specimen holder to the loop wall (Fig. 7). Without removing the loop from the test stand, we were able to repair the crack by brazing an overlay with Nb—1% Zr filler metal. The filler metal was deposited over the cracked region in six passes.

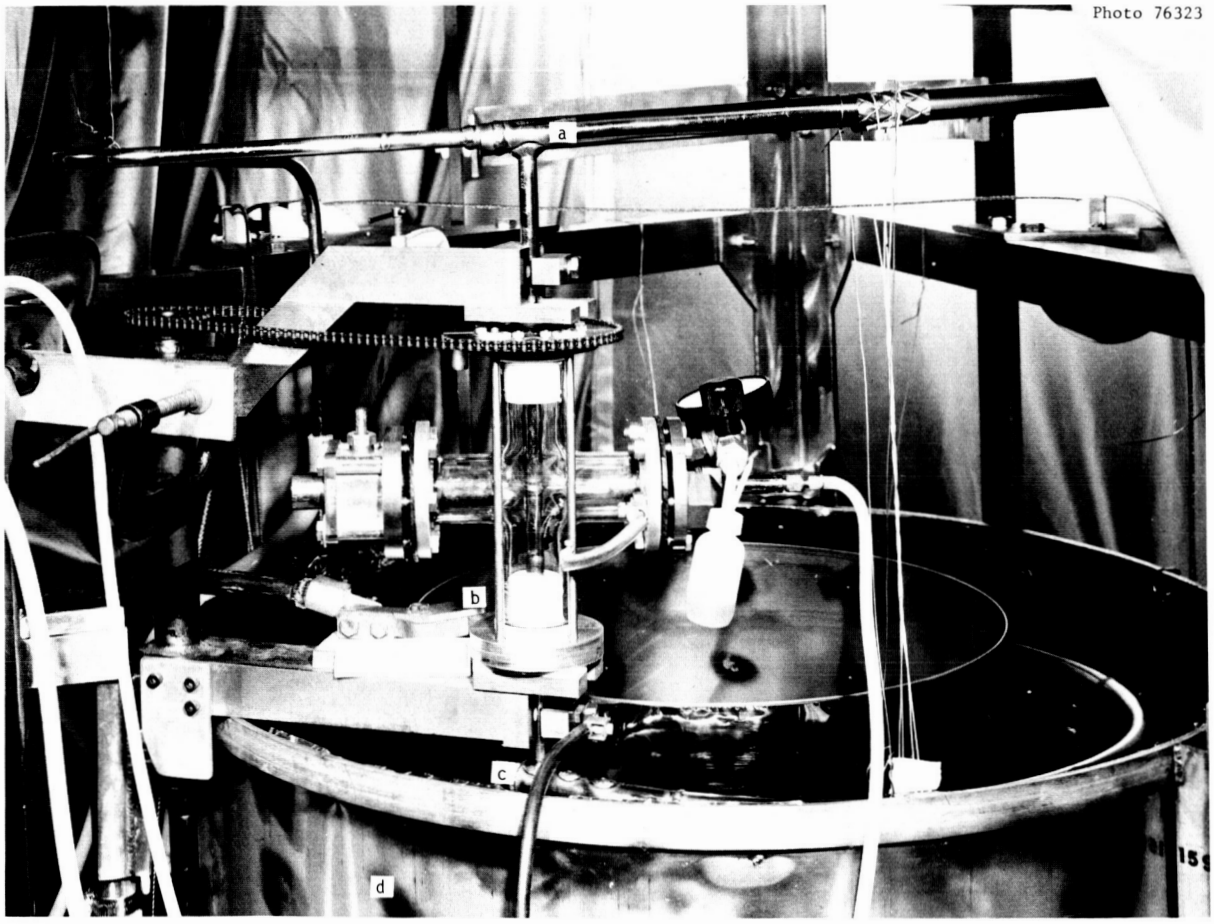

Fig. 9. Field Welding Assembly Used to Join Radiator and Economizer Sections After Installation of These Sections in the Vacuum Vessel. (a) Economizer, (b) pyrex cross for welding, (c) radiator, (d) shutter assembly, and (e) rotation drive unit.

To achieve a protective atmosphere during the repair, we fabricated a square glove box from plexiglass and mounted it on the portion of the pipe to be repaired. One side of the box was closed with a large plastic bag that served as a bladder for displacement of gas from the inside of the box. The bag could be pushed into the box to displace about 90% of the volume and could then be inflated with inert gas to at least twice the volume of the glove box. A heavier plastic bag protected the bladder bag during expansion. The glove box was purged and backfilled five times before welding, and during welding the gas flow on the welding torch served as an additional purge. Welding periods were limited to about 10 sec to minimize outgassing of the materials composing the containment vessel. To assure cleaniness, we made a practice pass on a sample of T-111 tube before each pass on the part to be repaired. There was no hardening of the Nb—1% Zr weld metal or adjacent surfaces as determined by light abrasion with a file. Neither dye penetrant inspection nor helium leak checking showed any indication of cracks in the repaired area. The practice weld was exposed to lithium at 816°C in a stainless steel capsule for 100 hr to verify that adequate cleanliness had been achieved.

This same basic braze welding procedure using a temporary glove box also enabled us to repair a vent line leak that developed later in loop operation.

TEMPERATURE MEASUREMENT

Temperatures at the external surface of the T-111 loop piping were recorded by means of thermocouples, a two-color optical pyrometer, and a brightness pyrometer. Three configurations of W—25% Re vs W—3% Re thermocouples were used: (1) 0.13-mm-diam (0.005-in.) bare wires individually spot welded to the piping, (2) bare wires with a mechanical junction that was held against the pipe by a tantalum foil cover, and (3) wires sheathed with 1.6-mm-OD (1/16-in.) tantalum, insulated with BeO, and held in place with a foil cover.

The integral or spot-welded thermocouples were joined to the loop wall by three spot welds about 1.6 mm (1/16 in.) apart on each wire, as shown in Fig. 10. The welds were made at three different power settings starting with 7 W-sec nearest the ceramic insulator and increasing to 9 and 11 W-sec for consecutive welds. An expansion loop, also shown in Fig. 10, was incorporated between the ceramic insulator and the first weld.

Because of the inherent brittleness of the spot-welded thermocouples, additional thermocouple wires were mechanically attached to the loop wall by inserting the 0.13-mm-diam wires into a 0.51-mm-diam (0.020-in.) cylinder of 0.13-mm-thick tantalum shim stock and flattening the cylinder onto the wires. The flattened cylinder was then folded back upon itself at the midpoint and flattened again to produce a junction about 0.53 mm thick by 6 mm wide by 3.2 mm long (0.21 by 1/16 by 1/8 in.). The assembly steps are illustrated in Fig. 11. The junction was then fastened to the pipe wall by a 51-mm-thick (0.002-in.) tantalum strap

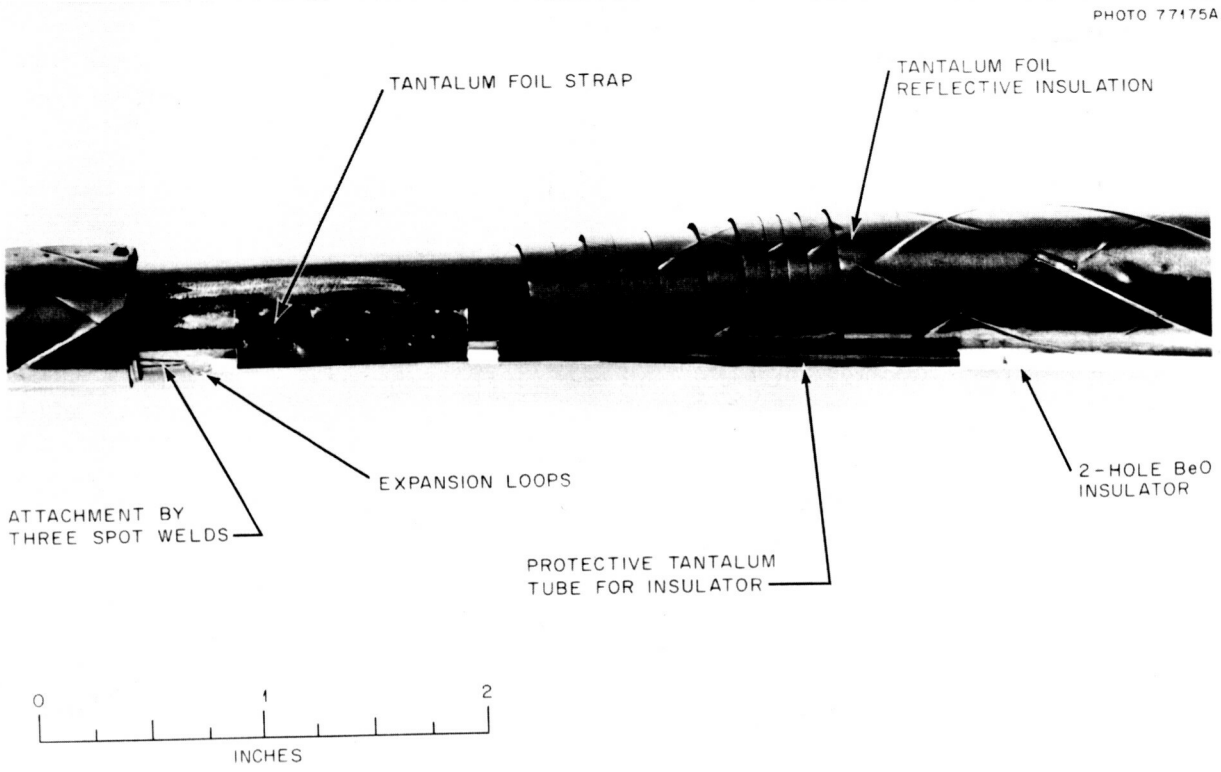

Fig. 10. Method of Attaching Bare-Wire Thermocouples to Insulated Piping of FCLLL. Scale is 51 mm.

that was spot welded to the pipe as shown in Fig. 11. To avoid any possibility of embtittlement, we made no spot welds on the junction itself. Sheathed thermocouples were attached to the loop wall similarly to the nonwelded bare-wire thermocouples.

The bare-wire thermocouples entered the vacuum system through ceramic feedthroughs that contained a bundle of eight electrically isolated 23-mm-OD by 18-mm-ID (0.090-by 0.070-in.) stainless steel tubes. Each thermocouple wire was centered in the tube with alumina sleeves, leaving a recess about 3 mm (1/8 in.) into the tube, and the recess was filled with RTSN solder (60% Ag—30% Cu—10% Sn).

Optical pyrometer sightings were made at a point near the heater outlet (maximum loop temperature) using the previously described black-body sighting cavity. A prism and shutter arrangement was used to avoid deposits collecting on the sight port installed on the vacuum chamber.

The maximum loop temperature was controlled within ±5°C measured by emf readings from spot-welded thermocouples. Temperatures recorded by the optical pyrometer were in close agreement with the control temperature. However, the mechanically joined bare-wire thermocouples read approximately 20°C lower, while sheathed thermocouples read approximately 30° lower. The differences in temperature readings among the various thermocouples decreased with decreasing temperature level.

Y-96727

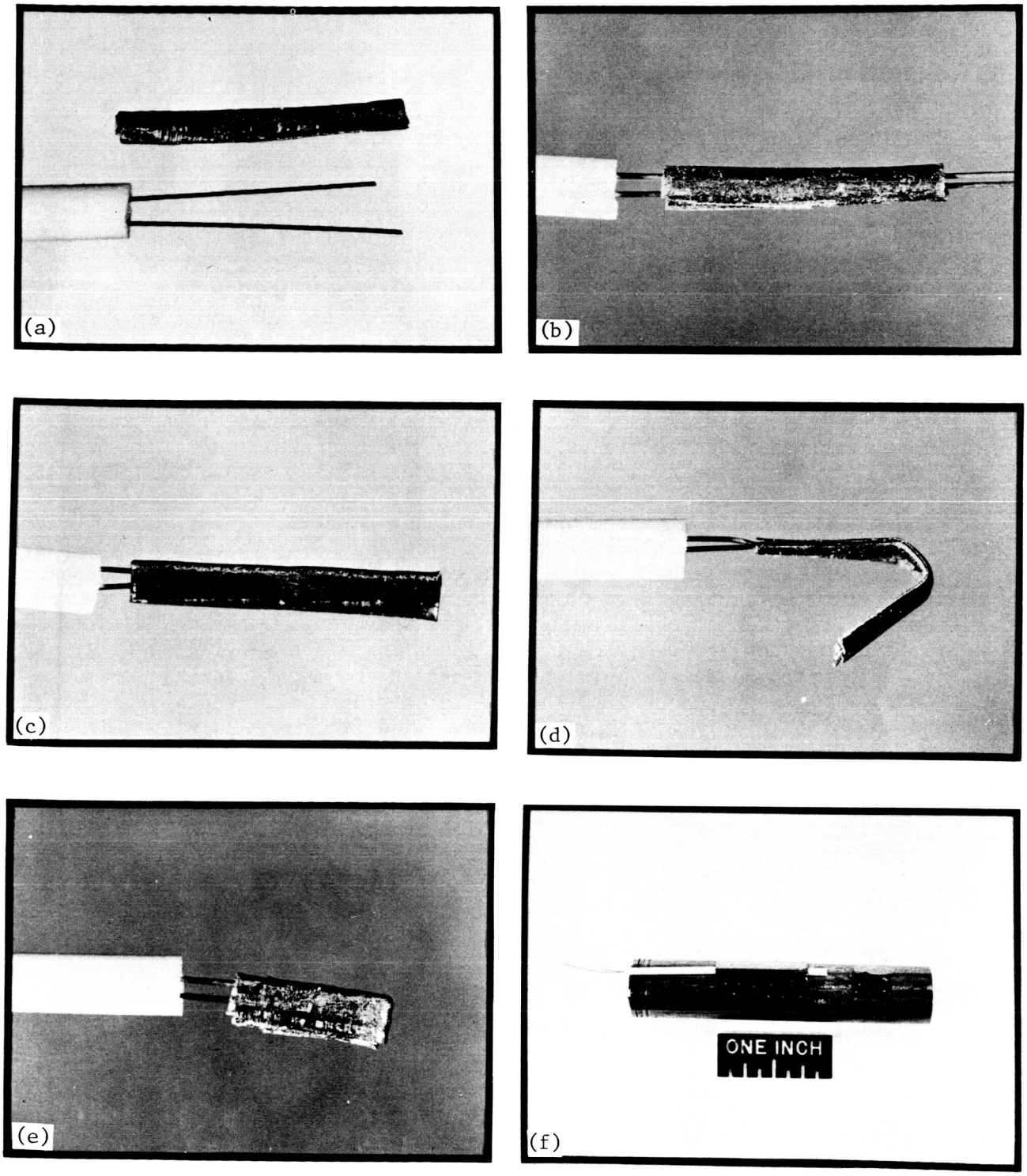

Fig. 11. Sequence for Assembly of Mechanical Joint for Bare-Wire Thermocouples.

LITHIUM PURIFICATION AND SAMPLING

Approximately 11 kg (25 lb) of commercially pure lithium was transferred into the fill-and-drain tank for purification before filling the loop. Lithium was at 200°C during the transfer and passed through a 10-μm filter in the transfer line. The fill-and-drain tank, which contained approximately 6.5 m^2 (10,000 $in.^2$) of zirconium foil, was heated for 40 hr at 815°C to reduce the nitrogen and oxygen concentrations of the lithium. The foil, which was 0.25 mm (0.010 in.) thick, had been specially fabricated from zone-refined crystal bar stock and before lithium exposure contained less than 50 ppm O and N each. The analyses of the lithium before and after zirconium gettering are compared in Table 3 and show that the zirconium significantly reduced both the oxygen and nitrogen concentrations.

The initial loop fill was intended to flush any impurities out of the loop, and, depending on the impurity increases in the flush charge, we had the option of returning it to the fill-and-drain tank for repurification or using it as the operating charge. As shown in Table 3, the impurity increases were inconsequential, and the flush charge was used as the operating charge without further purification.

Samples of lithium were withdrawn from the loop by means of a bypass circuit connected in parallel with the electromagnetic pump. The bypass loop, constructed of 9.5-mm-OD (3/8-in.) type 321 stainless steel tubing, passed through an argon-filled glove box, where a flow-through sampling section could be removed. Figure 12 shows the glove box including 9.5-mm valves on either end of the sampling section and metal-gasketed Marmon "Conoseal" flanges connecting the sampler to the loop. The bypass loop was opened only during lithium sampling. The flow rates during sampling were 76 ml/sec (1.2 gpm) in the primary circuit and 32 ml/sec (0.5 gpm) in the bypass, the temperature was held at 300 to 350°C (570–660°F) in both circuits. After at least 150 volume changes in the bypass circuit, this circuit was valved off, the lithium frozen in place, and a sample removed.

OPERATING HISTORY

Loop start-up involved the following sequence of operations:

1. The vacuum chamber containing the loop was evacuated with an auxiliary roughing system consisting of an oil diffusion pump with a liquid-nitrogen-cooled optically baffled trap. The chamber was heated to 315°C and, within 24 hr, the pressure fell to 1.1 mPa (8×10^{-6} torr). The chamber pressure was held below 7 mPa (5×10^{-5} torr) during subsequent heating of the loop to design conditions.

2. Lithium was pushed from the dump tank, circulated, and sampled. Once the oxygen and nitrogen concentrations in the lithium were found to be within predetermined limits (≤50 ppm each) the loop was heated to design temperature. When the loop reached design conditions, the auxiliary pump was valved off, and the ion pumps and sublimation pump were started.

Table 3. Chemical Analysis of Lithium Used in Forced-Circulation Liquid Lithium Loop (FCLLL-1)

Element	Concentration, ppm		
	As Received	After Hot Trapping[a]	After Loop Flush[b]
O	48	12,23[c]	9,11,16[d]
N	201,224[c]	<5[c]	<5[c]
Ag	<1	<1	<1
Al	<10	<10	<10
B	<1	<1	<1
Ba	<5	<5	<5
Be	<1	<1	<1
Bi	<2	<2	<2
Ca	<100	<100	<100
Co	<5	<5	<5
Cr	5	5	5
Cu	10	10	10
Fe	50	50	20
Hf	<20	<20	<20
K	30	30	30
Mg	≤1	≤1	≤1
Mn	3	7	2
Mo	≤1	<1	<1
Na	50	70	30
Nb	<20	<20	<20
Ni	20	10	10
Pb	<3	<3	<3
Sb	<5	<5	<5
Si	≤5	≤5	≤5
Sn	<3	<3	<3
Ta	<20	<20	<20
V	<3	<3	<3
W	<20	<20	<20
Zr	<20	<20	<20

[a]After hot trapping 40 hr at 815°C.

[b]Flushing consisted of more than 100 volume changes at 300°C in both the primary and bypass circuit over a period of 2 hr.

[c]Duplicate samples.

[d]Triplicate samples.

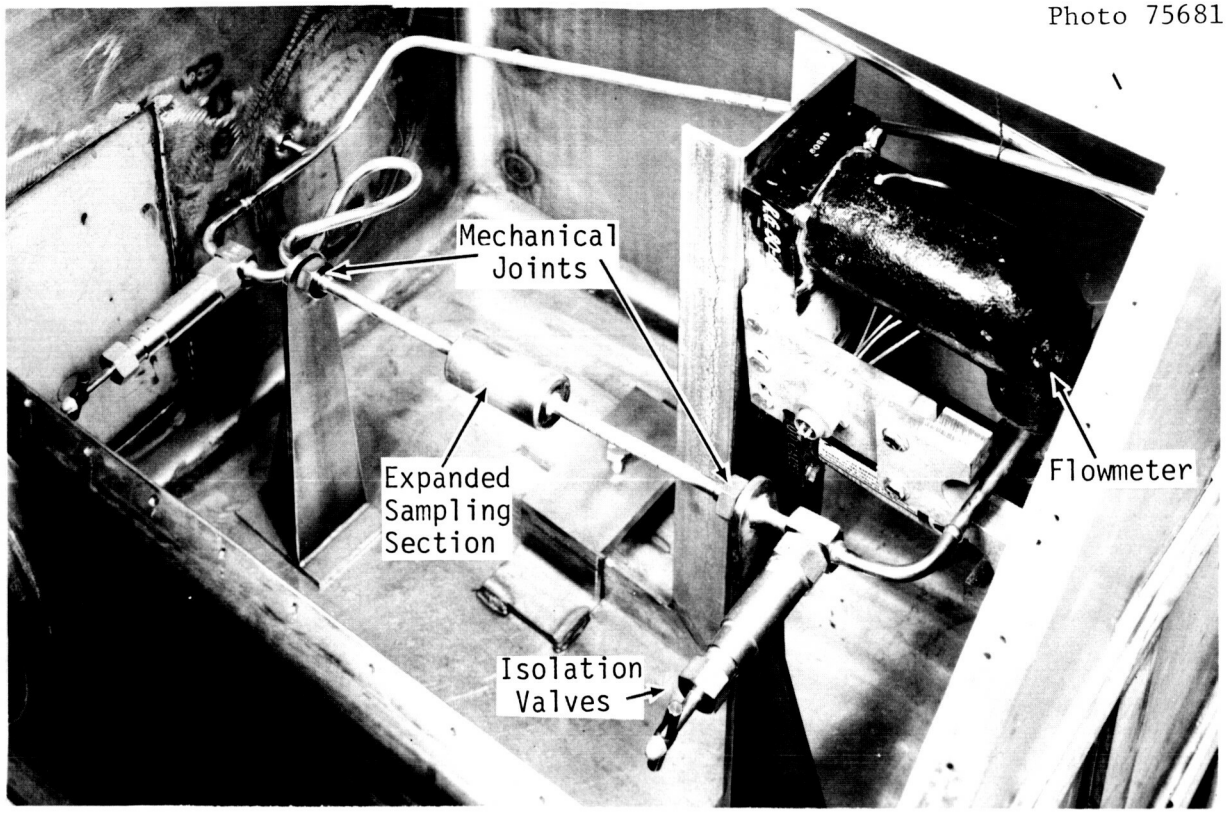

Fig. 12. Internal View of FCLLL-1 Glove Box for Lithium Sampling.

Hydrogen constituted the principal gas impurity within the vacuum chamber during the period when the chamber walls were water cooled and the loop was being heated to design conditions. Water vapor and organic materials were detected after the chamber bakeout period, but these disappeared with time. Typical gas analyses are given in Table 4. After 1517 hr of operation at design conditions, a lithium leak was detected by the residual gas analyzer. A routine scan of the peak currents for residual gas in the vacuum chamber at 1517 hr showed peaks at the mass-to-charge ratios of 6 and 7. These peaks were absent in a scan made 22 hr earlier. We decided to continue operating the loop until the relative size of the leak could be assessed and until we could assure that the leak could be located. Continued monitoring with the residual gas analyzer showed that the leak was increasing with time. Finally, the appearance of lithium deposits on colder surfaces inside the vacuum chamber indicated that the leak was of a size to preclude further operation. Accordingly, the loop was shut down with the lithium *in situ* after 1735 hr (218 hr after the leak was detected).

Readings of partial pressures before and during the leak are shown in Table 4. In addition to lithium, the analyzer detected potassium and sodium as well as the residual gases normally expected. The source for the potassium and sodium is believed to have been impurities in the lithium.

Table 4. Concentrations of Residual Gases in Vacuum Chamber Containing Liquid-Lithium-Loop Test (FCLLL-1)

Gas Species	Pressure, torr[a] for various times from start-up in hr					
	141	580	1495	1517[b]	1686	1734[c]
	$\times 10^{-8}$	$\times 10^{-8}$	$\times 10^{-8}$	$\times 10^{-8}$	$\times 10^{-8}$	$\times 10^{-8}$
H_2	16.5	4.10	2.13	6.18	2.79	7.53
N_2-CO	6.6	0.82	0.26	0.38	0.29	0.55
Ar	3.1	0.46	0.15	0.31	0.31	0.52
CH_4	1.0	0.18	0.06	0.21	0.12	0.32
CO_2	0.6	0.11	0.01	0.003	0.002	0.003
H_2O	0.6	0.07	0.01	0.005	0.007	0.003
^{7}Li	0.00	0.00	0.000	0.0035	0.039	0.89
^{6}Li	0.00	0.00	0.000	0.0003	0.003	0.08
^{39}K	0.08	0.01	0.001	0.0076	0.017	0.38
^{23}Na	0.00	0.00	0.000	0.0019	0.015	0.24
TOTAL[d]	28.5	5.75	2.60	7.10	3.60	10.5

[a]Based on total pressure and ratio of peak current to sum of peak currents. Ionization probability relative to N_2-CO was taken as 2 for H_2 and 1 for other components. To convert to pascals, multiply by 133.3.

[b]Lithium leak first detected.

[c]Last scan before shutdown.

[d]Based on hot-filament ionization gage.

Figure 13 shows the leak site, which was in a 13-mm-OD (1/2-in.) vent line leading from the resistance-heated section of the primary loop. The leak was approximately 25-mm (1 in.) away from where the vent line tied into the loop. The vent line had been valved off after the loop was filled, and, assuming the lithium in the line was stagnant, the temperature at the leak site would have been about 1125°C.

To repair the loop, we severed the vent line below the leak site and then capped off the remaining tube stub, as shown schematically in Fig. 14. Although this precluded our venting the loop during filling and draining, we encountered no subsequent problems with either operation. Lithium was left solidified in the loop during the repair operation, and we mechanically removed the lithium from within the tube stub. A T-111 plug was first welded into the tube stub, and this cap was braze-welded with Nb—1% Zr to the original T-111 weld that had joined the vent line to the primary loop. The welding procedure was the same as that used to effect an earlier repair and discussed in a preceding section.

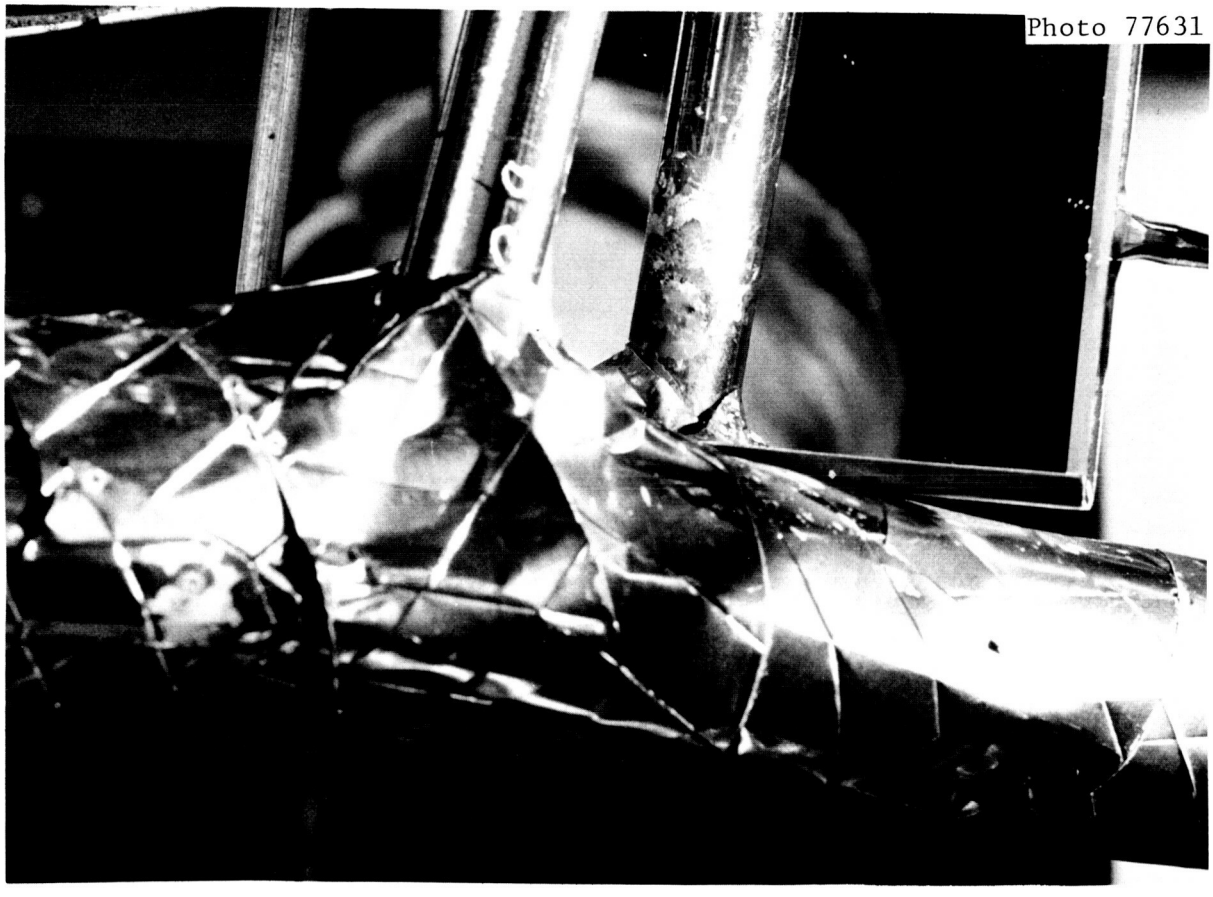

Fig. 13. Site of Lithium Leak in 13-mm-OD (1/2-in.) Vent Line as Viewed with a Mirror. The leaking line is shown at top center emerging from the foil-wrapped primary loop. The leak is seen on the back side of the tube in the bottom center of the mirror.

ORNL-DWG 70-7774

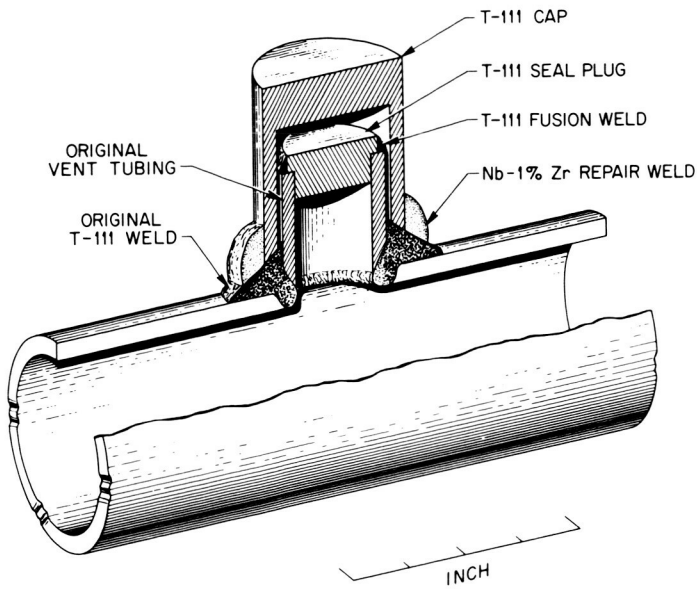

Fig. 14. Vent Line Closure Weld. Scale is 25 mm.

After the repair, the loop was brought to design conditions by the same general procedures discussed above in the initial start-up. However, on reaching 315°C the loop was drained and refilled three times in succession, and on the fourth drain the lithium was hot trapped in the dump tank 24 hr at 815°C. The loop was refilled and a lithium sample taken. As a result of the analysis of this sample, the loop was dumped, and the lithium was hot trapped another 7.5 hr at 815°C. The loop was again filled with lithium and another sample taken, which showed less than 20 ppm O and less than 5 ppm N. Loop operation resumed at this point and continued for an additional 1265 hr to complete the 3000-hr test period. The furnaces containing T-111 control specimens were not restarted after the initial 1735-hr operating period.

The chamber pressure peaked at 13 mPa (1×10^{-4} torr) when the loop reached design conditions after the repair. This pressure decayed to 0.13 mPa (1×10^{-6} torr) within 24 hr, to 13 μPa (1×10^{-7} torr) within 48 hr, and to 1.3 μPa (1×10^{-8} torr) at the end of the test. The relative proportions of residual gases at the end of the test period were estimated to be 72% H_2, 15% Ar, 10% N_2+CO, and 3% methane.

The rate of heat transfer from the radiator to the vacuum bell jar was lower after the repair than before. A similar effect was seen during the leak and was apparently caused by the deposition of lithium on the chamber walls. Although we cleaned the inner surface of the bell jar with alcohol before the repair, it is likely that sufficient lithium reaction products remained to decrease the emissivity. The lower rate of heat removal necessitated a lower heat input and a lower lithium flow rate to maintain the desired minimum loop operating temperature. Figure 15

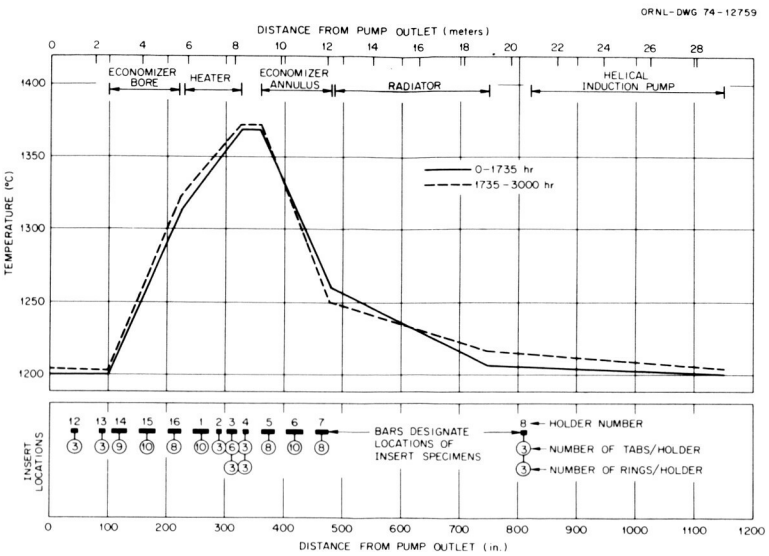

Fig. 15. Variation of Temperature with Distance from Pump Outlet, Showing the Position of Test Specimens.

compares the loop temperature profiles before and after the leak. The flow rate before the repair was 160 g/sec (6.1 gal/min) and after the repair was 141 g/sec (5.4 gal/min).

The heat-transfer performance of the tube-and-shell lithium economizer was within 5% of the performance predicted with the standard calculations for heat transfer in liquid metal. Heat balances across the resistance-heated section indicated flow rates in close agreement with those measured by the electromagnetic flowmeter.

Near the end of the 3000-hr test run, we performed a series of cavitation tests on the electromagnetic helical induction pump. Nine cavitation tests were made with the loop at design conditions, and the temperature profile in the circulating portions of the loop was not disturbed. However, the onset of cavitation was noted by pressure fluctuations and by temperature changes in the static drain line as lithium was expelled from the loop.

On shutdown, a final lithium sample was taken and the lithium was drained into the dump tank. The oxygen impurity concentrations throughout the test program were as follows:

Sampling Time	Concentration, ppm
Start of test	12
1735 hr	
Before repair	58
After repair	20
3000 hr	50

The nitrogen concentration remained below 5 ppm.

When the loop was removed from the vacuum chamber, a collection of lithium droplets was noted on the exterior surface of the drain line at a point 115 mm (4 1/2 in.) from the tee on the 1200°C pump discharge line. The droplets were located on opposite sides of the pipe on the neutral axis of a bend in the 13-mm (1/2-in.) line. We subsequently dye-checked this region and found tiny cracks running perpendicular to the tubing axis. The point of failure was estimated to have been at approximately 1200°C during normal loop operation, although the dump line was subjected to substantial thermal cycling during the pump cavitation tests (see Appendix B). Since the leak was not in evidence during operation, its occurrence appears to coincide with the pump test.

FAILURE ANALYSIS

The T-111 vent line, which developed a lithium leak and was removed after 1735 hr, was metallurgically examined to determine the cause of failure. The outer surface of the failed area, pictured in Fig. 16, was generally eroded to a depth of about 0.8 mm (1/32 in.) over an area about 9.5 mm (3/8 in.) in diameter. The inner surface, pictured in Fig. 17, contained several mounds as well as crater-like spots. A crack through one of these spots appeared to be linked to the external eroded area. There were additional smaller cracks that did not penetrate to the outside surface, suggesting that the crack that caused the failure had emanated from the inside surface.

Bulk chemical analysis of the wall of the tubing adjacent to the failure showed no significant changes in the quantities of C, O, and N present from that present in the material before the test. Analysis of the inside surface by the electron beam microprobe showed that the mounds were enriched in hafnium compared with the base metal. A metallic film was deposited uniformly around the inner surface of the tube about 25 mm (1 in.) from the failure; this film also was quite rich in hafnium. We next examined a metallographic section through the failure site and through one of the mounds. The section through the failure site revealed a wide intergranular crack, with smaller separations of grain boundaries connecting to this crack near the outside surface of the tubing. As shown in Fig. 18, several light and dark phases were noted in the grain bundaries near the crack. Electron microprobe analysis showed that hafnium was depleted from these grain-boundary areas and also from the corroded area near the outer surface. A slight trace of nickel was found in several small locations in the corroded materials at the outer surface. No other foreign elements were detected. Further details on the electron microprobe examination of this sample are presented in Appendix C.

A cross section through one of the mounds revealed two phases, one of which (the more predominant) was rich in hafnium and the other depleted in it. (See Appendix C.) The surface under the mound showed no depletion of hafnium. No foreign elements were found except for zirconium, which occurs naturally in hafnium. Further visual examination of the tubing surface adjacant to the failed section about 50 mm (2 in.) from the failure site showed some slight traces of what appeared to be foreign metallic-like material smeared on the inner surface.

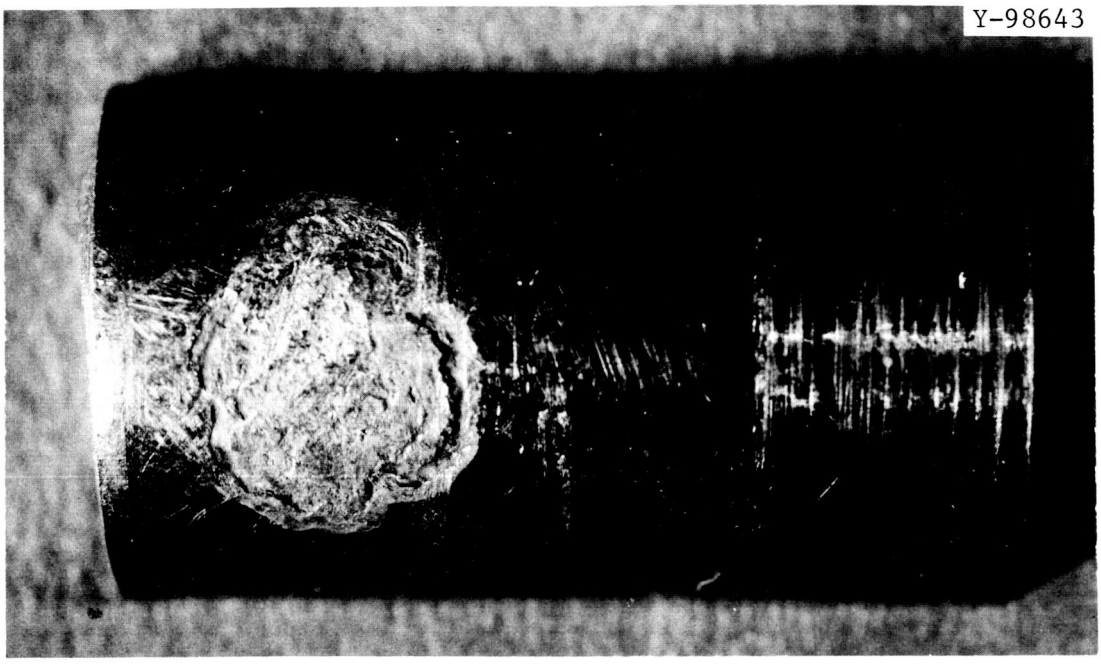

Fig. 16. Outer Surface of Failed Vent Line Showing the Corroded Area Surrounding the Failure Site. About 5×.

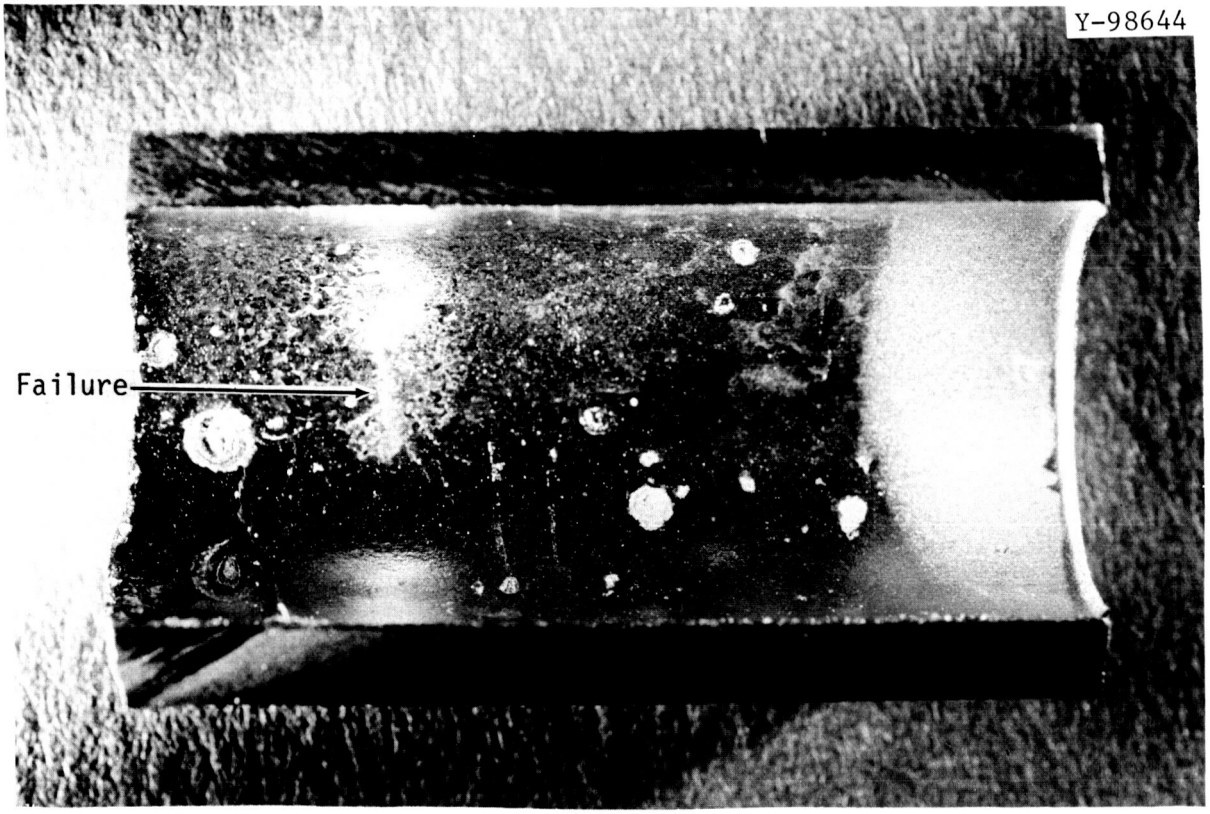

Fig. 17. Inside Surface of Failed Vent Line at the Failure Site. About 5×.

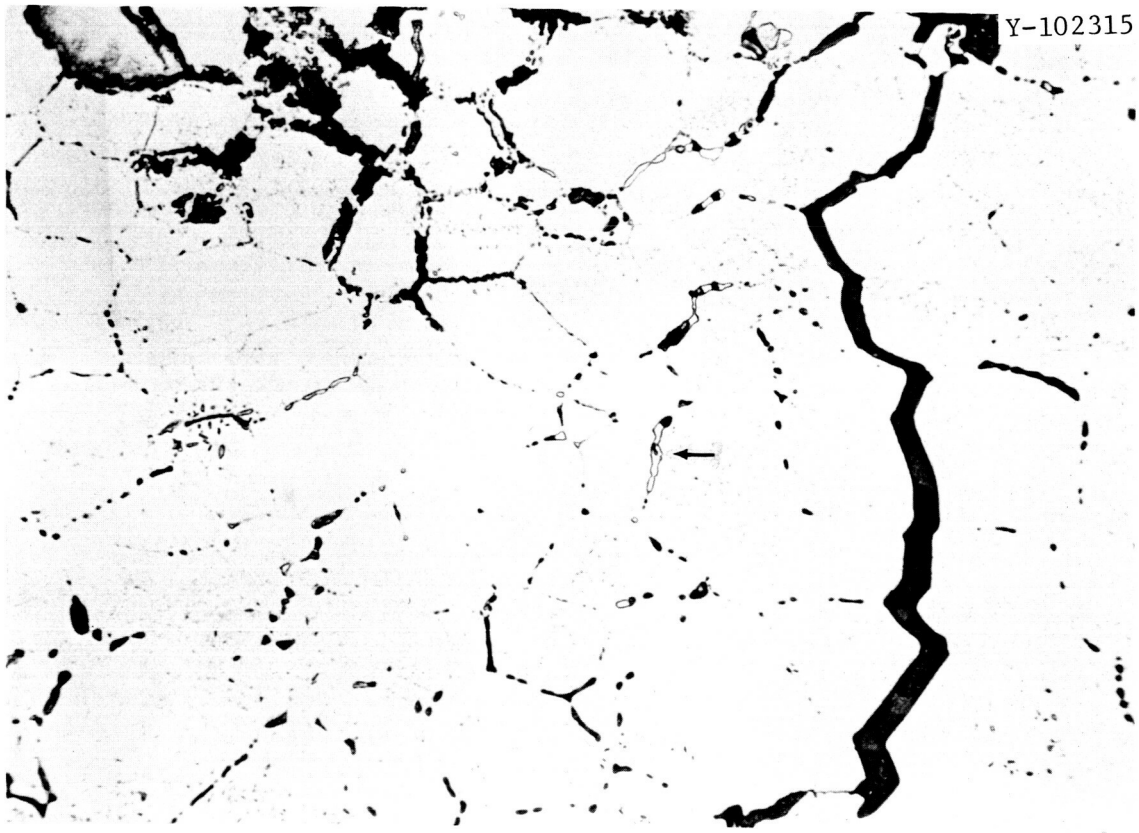

Fig. 18. Appearance of Grain Boundaries Near Failure of T-111 Vent Line. Note the light phase indicated ay arrow. 500×.

The above findings and the general asymmetrical arrangement and appearance of the internal spots and mounds near the weld and failure site lead us to believe that a foreign material was spattered over the inner and possibly the outer surface during welding. The existence of trace quantities of nickel suggests that a nickel-hafnium eutectic was present at some stage during welding; however, we believe that most of the nickel originally present was subsequently leached out by lithium during operation. This could account for the hafnium-rich mounds deposited on the surface of the tubing. The hafnium-rich film observed about 25 mm (1 in.) from the failure site appears to be the result of conventional solution mass transfer, as discussed in the next section, and not to be related to the failure.

A second lithium leak was discovered when the loop was being removed from the vacuum chamber after completing the 3000-hr test run. Like the first leak, it occurred in a 13-mm-OD (1/2-in.) T-111 tube that tied into the main loop and contained static lithium during normal operation. The latter tube was part of the drain line that attached to the pump discharge line at the bottom of the loop and was normally exposed to colder lithium than was the vent line. The leak was manifested by small droplets of lithium on the exterior surface of the tube at a point 115 mm (4 1/2 in.) from the point of attachment to the discharge line. Removing lithium

from the outside surface revealed no visible damage, and there were no mounds or craters on the interior of the tube, such as were visible with the earlier failure. We sectioned a 38-mm (1 1/2-in.) length that contained the leak zone and found three intergranular cracks that originated at the inside surface and two that traversed the 1.65-mm (0.065-in.) wall. The outside surface also exhibited a number of superficial grain boundary grooves or fissures, and the inside surface was covered by a discontinuous deposit.

A typical intergranular crack in the leak area is pictured in Fig. 19. Comparison with Fig. 18 shows that the cracking in the drain line was less extensive than in the vent line. Also the cracking in the drain line appears to have been associated with a light-etching grain boundary film (Fig. 19). The surface deposit and the grain boundary film were analyzed by the electron microprobe, and the results are given in Table 5. Additional electron-microprobe results are presented in Appendix D.

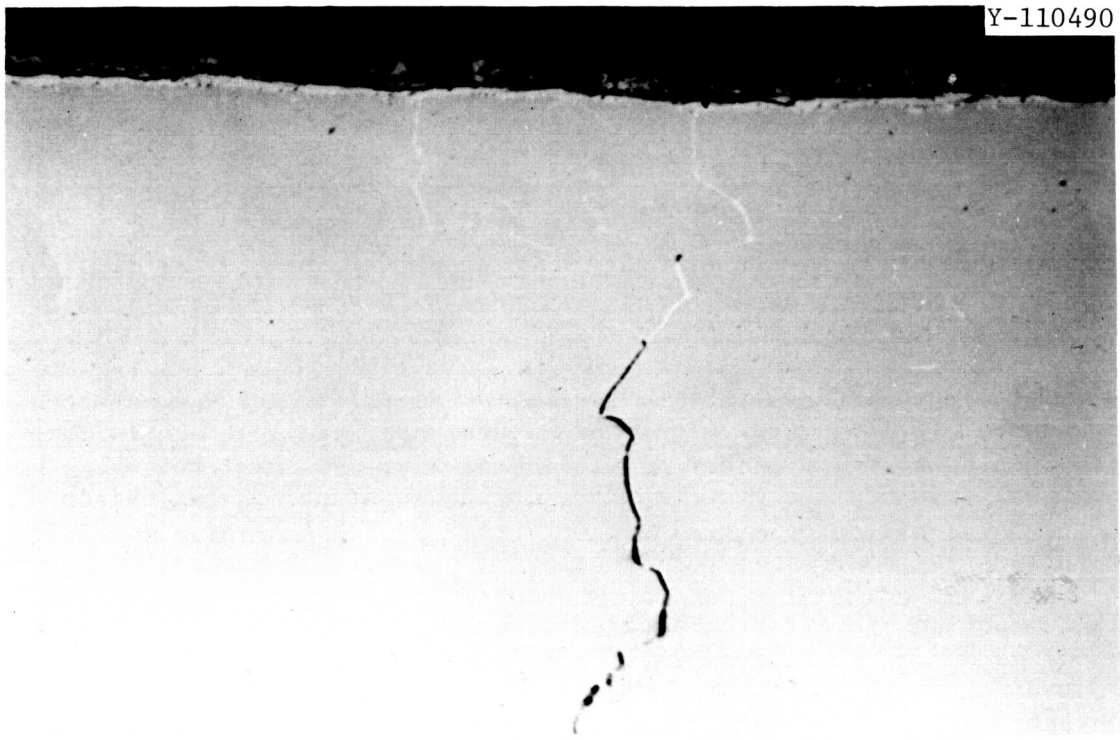

Fig. 19. Intergranular Crack in Drain Line Near Lithium Leak. 500×.

The relatively high concentrations of nickel and hafnium in the grain boundary film are indicative of a nickel-hafnium eutectic. The failure in the vent line showed a similar association with this eutectic, but the source of the nickel in that case appeared to have been different (i.e., it was associated with isolated mounds and craters).

Table 5. Electron-Microprobe Analysis of Deposits Associated with Drain Line Leak

Area Examined	Concentrations, wt %				
	Fe	Ni	Ta	W	Hf
Tube Matrix	<0.5	<0.5	92.0	10.5	2.8
Inner Surface Deposit	1.9	7.5	11.4	1.0	49.5
Grain Boundary Film	1.7	23.2			41.2

In the case of the drain line, we can identify three possible nickel sources: (1) a conventional alloy residue picked up in the tubing manufacturing process, (2) the type 321 stainless steel tubing that led to the dump tank and attached directly to the drain line, and (3) trace quantities of nickel picked up by the electromagnetic pump during a prior performance test with potassium in a stainless steel circuit. It is not possible to assess the probability of the first source, although we did not see evidence of nickel in any other T-111 loop components built from the same tubing. As will be shown in the next section, there were no indications of measurable lithium attack of any of the stainless steel sections used in the loop. However, as discussed in Appendix B, the drain line did experience temperature transients during pump cavitataion tests near the end of the test run. Although the maximum temperatures during these transients were sufficiently high to account for nickel transport via the lithium, the transient periods were quite short. Relative to the third source, it is conceivable that any trace quantities of nickel present on the pump surfaces could have been rapidly dissolved by the lithium and re-deposited over a relatively narrow temperature range down the stagnant drain leg. However, we elected not to destructively examine the electromagnetic pump (due to its potential usefulness), so there is no way to assess this later source.

POST-TEST EXAMINATION

Loop Dissection

The loop was removed from the vacuum chamber in three sections; (1) heater and economizer, (2) pump cell and associated inlet and outlet lines, and (3) radiator. To prepare for further sectioning and specimen removal, each section was flushed with anhydrous ammonia to remove residual lithium. Insert specimens were removed in reverse order of loop fabrication: specimen-containing sections were cut adjacent to the butt welds joining them into the loop. These cut sections were flushed again with anhydrous ammonia, and the tack welds holding the

specimen stringers were severed to free the specimens. After verification that all residual lithium had been removed, the specimens were rinsed in ethyl alcohol before weighing.

In subsequent analyses of the loop specimens, we attempted to discern between temperature effects and corrosion effects by referring to control specimens that had been thermally aged for 1735 hr in the loop vacuum chamber at the highest and lowest loop operating temperatures. Additional comparisons were made with as-received tubing and insert specimens (i.e., archive material).

The tab specimens are identified by a two-part number, the first part referring to the specimen holder and the second part designating the sequential position of the tab in a downstream direction from the pump outlet. Annular specimens carry the same number as the position number of insert tab they surrounded. Tubing specimens from the loop are referred to by the number of the specimen holder that they contained.

Weight Changes

The mass of constituents transferred into and out of the lithium was determined by weighing the 93 insert specimens, which were spaced at intervals around the loop. The position of each insert specimen in relationship to temperature and distance from the pump outlet is shown in Fig. 15. The weights before and after test are tabulated in Appendix E. The weight changes are plotted as a function of loop position in Fig. 20 and as a function of temperature in Fig. 21.

The maximum dissolution rate occurred at the maximum wall temperature of the loop and, in terms of uniform wall thinning, represents a surface loss of less than 1.27 μm/year (0.05 mil/year). The specimens in the 1200°C pump inlet and outlet lines showed essentially constant weight gains of 0.6 to 0.7 mg/cm^2. The only other specimens to show weight gains were those just inside the economizer, where the weight gains decreased from about 0.7 mg/cm^2 at 1200°C to essentially zero at 1225°C (Fig. 21).

The weight changes of three groups of annular test specimens, which were set into the loop wall, are noted in Table 6. Because the specimens fit tightly against the loop wall, the corrosion effects on these specimens should have been confined to the inner surface. When computed on this basis, the weight changes per unit area of annular specimens from isothermal sections of the loop were in good agreement with corresponding tab specimens. However, on the same basis, the annular specimens from the heater section showed a measurably greater weight loss than corresponding tab specimens. Although part of this difference may reflect a wrong surface area assumption, the annular specimen in the heater would be expected to show a somewhat higher weight loss, since heat transfer calculations predict a 3 to 5°C film temperature drop between the inside wall and bulk lithium in this region.

An effect of flow velocity on weight change is evident in Fig. 21. When compared at an equivalent temperature, specimens from the economizer section of the loop show a consistently smaller weight loss than specimens from the heater section. This difference is observed immediately

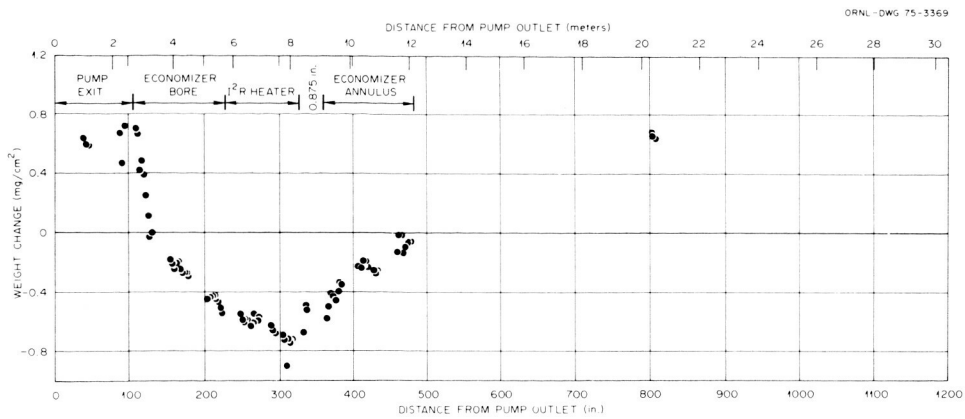

Fig. 20. Weight Change Profile for Insert Specimens Around FCLLL-1.

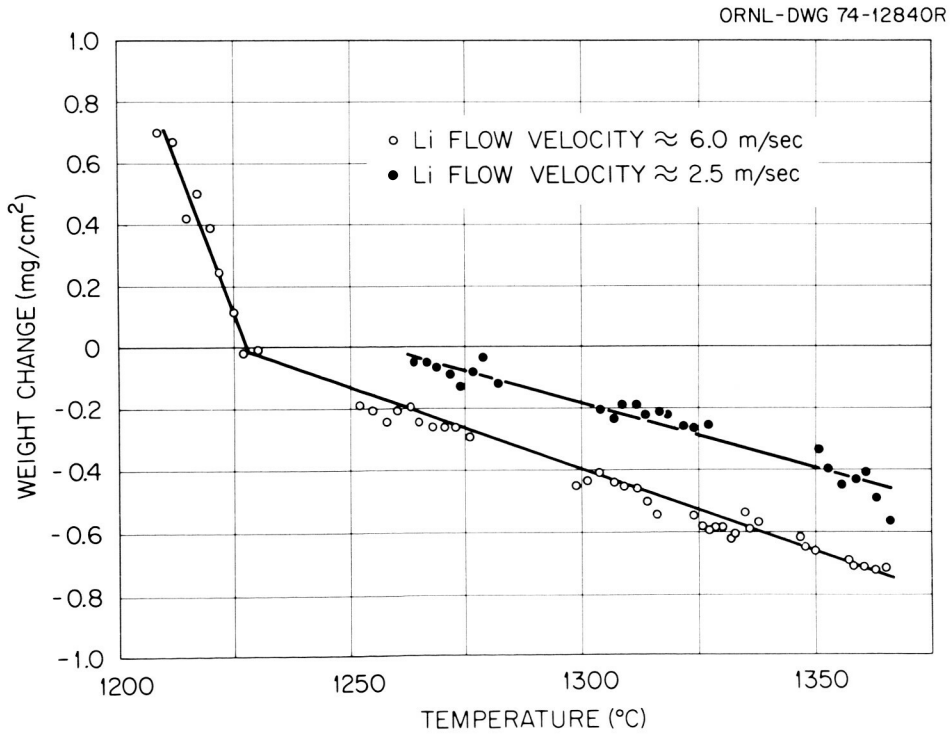

Fig. 21. Weight Change as a Function of Temperature for Insert Specimens in Heater-Economizer Section of FCLLL-1.

Table 6. Comparative Weight Changes of Annular (Ring) Specimen and Flat Tab Specimens

Location	Specimen	Geometry	Wetted Surface Area[a] (cm^2)	Weight Change (mg/cm^2)
Heater Exit	3-52	Tab	9.03	−0.72
	52A	Ring	5.63	−1.43
	52C	Ring	5.64	−1.14
Economizer Entrance (Isothermal)	4-55	Tab	9.03	−0.52
	55A	Ring	11.32	−0.52
	55C	Ring	11.34	−0.56
Pump Exit (Isothermal)	8-87	Tab	9.03	+0.65
	87C	Ring	5.64	+0.45

[a]Wetted surface of ring geometry = π(inside diam) × length.

upon leaving the heater and entering the economizer, and does not increase as a function of wetted area down the economizer. Therefore the difference reflects the tubing size and velocity change between the heater and economizer sections and does not seem to be a function of the downstream distance *per se*.

The surfaces of the specimens that gained weight were covered with a gold-colored crystalline deposit, and specimens that lost weight exhibited superficial grain-boundary grooving. These contrasting surface features, as revealed by scanning electron microscopy, are shown in Fig. 22.

Metallographic Examination of T-111 Inserts and Piping Specimens

We metallographically examined transverse sections of at least one insert tab specimen from each specimen holder and one annular specimen from each of three specimen groups (Fig. 15). In addition, we examined five T-111 tubing samples from positions opposite five tab specimens.

The positions of the various insert samples and tubing specimens are given in Table 7. Figure 23 compares the microstructure of the as-received (before-test) insert tabs with control specimens thermally aged at 1204 and 1370°C. Figures 24 through 31 are illustrative of the microstructures of the after-test tab specimens.[5] Note the relatively large grain size and absence of second phase precipitates in specimens 1-36,

[5]The etching process used to delineate the grain structure of the specimens sometimes caused the specimens to pit. The pitting observed in the microstructures is in all cases an etching artifact and was not observed in as-polished microstructures.

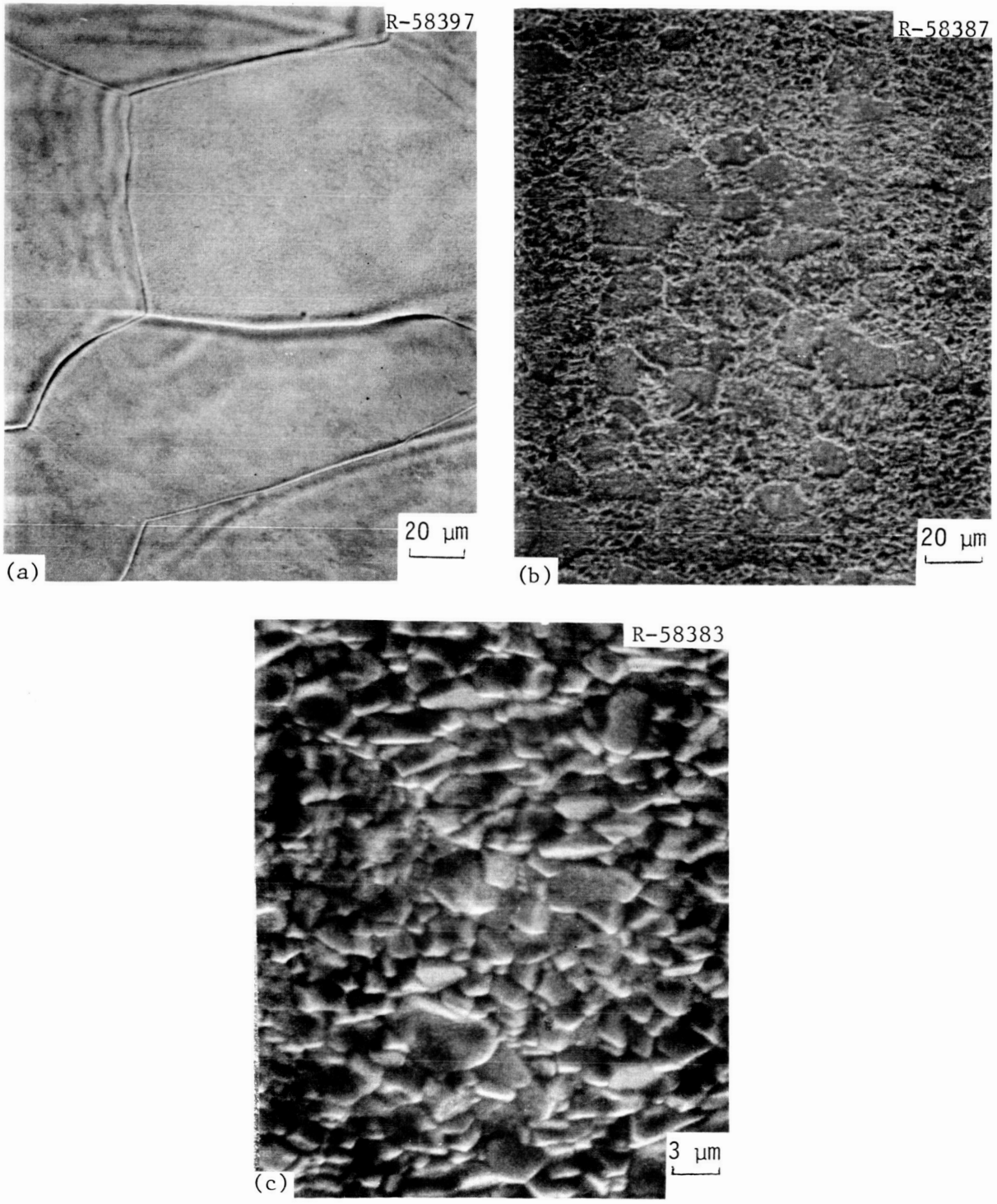

Fig. 22. Surfaces of T-111 Sheet Specimens from the Forced-Circulation Lithium Loop. (a) Maximum weight loss location; (b) maximum weight gain location; (c) higher magnification of (b).

Table 7. Locations of T-111 Specimens Examined Metallographically

Insert Tab Specimen	T-111 Tubing Sample	Annular Specimen	Position in Loop[a] (m)	Position in Loop[a] (in.)	Approximate Temperature (°C)
13-6	13		2.35	92 1/2	1200
15-18	15		4.05	159 1/2	1258
15-22			4.33	170 1/2	1268
16-26	16		5.17	203 3/4	1299
1-36			6.42	252 3/4	1327
3-52	3	52B	8.08	318 1/4	1365
4-55		55B	8.51	335	1369
5-64			9.72	382 3/4	1348
6-71	6		10.74	423	1312
7-77			11.72	461 1/2	1277
8-87	8	87B	20.39	802 3/4	1204

[a]From pump outlet to midlength of insert tab specimen.

3-52, 4-55, and 5-64. At higher magnification the surfaces of specimens 13-6 and 8-87 revealed the presence of a thin, tightly adherent film about 1 μm thick, which corresponds to the gold-colored surface film seen visually. The nature of this film is discussed in the sections covering scanning electron microscopy and electron microprobe analysis.

The microstructures of annular insert specimens are shown in Fig. 32, and they essentially match those of the insert tab specimens that they surrounded. Specimens 52-B and 55-B from the maximum temperature region of the loop showed considerable grain coarsening, while annular specimen 87-B from the cooler region of the loop was unchanged from the as-received condition.

The microstructural details near the inner and outer surfaces of the loop tubing samples are shown in Figs. 33 through 37. The appearance of these samples again is similar to that of the specimens that they surrounded.

The mean grain diameters of the tab, annular, and tubing specimens can be compared for various loop positions in Table 8. The onset of grain growth in the tab specimens becomes apparent about 5 m (200 in.) downstream from the pump outlet. A slight increase in grain size of the loop tubing was measured about 4.3 m (170 in.) from the pump outlet.

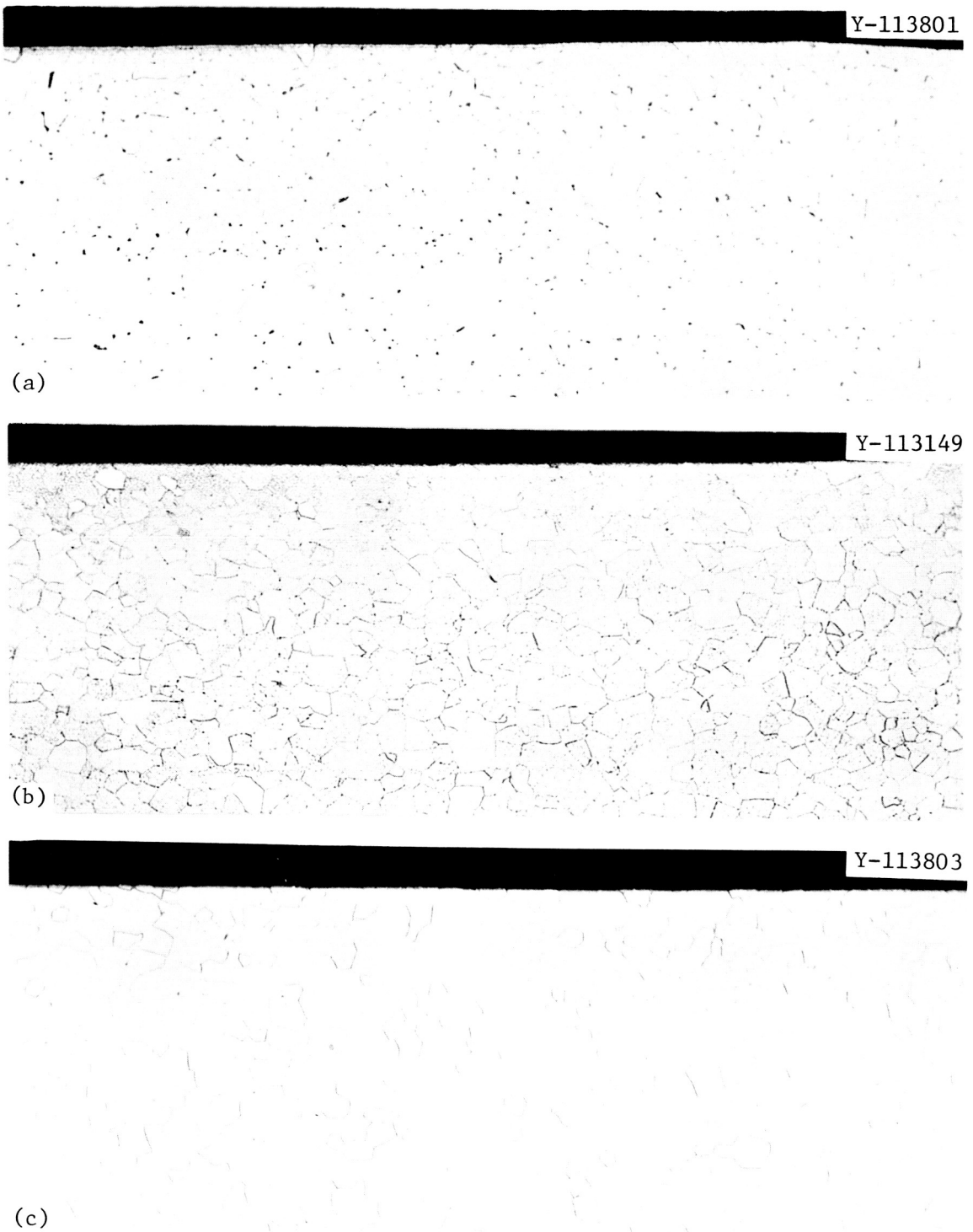

Fig. 23. Microstructures of Tab Insert Specimens, Etched, 200×. (a) As received. (b) 1204°C control. (c) 1370°C control.

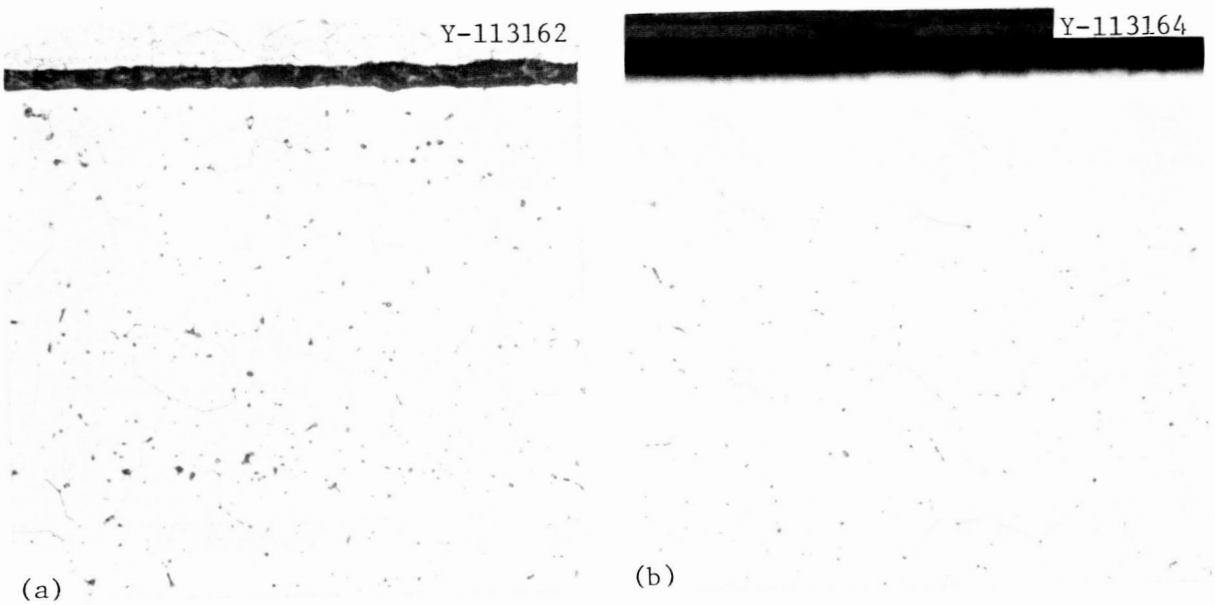

Fig. 24. Typical Microstructures of Insert Tab Specimens, Etched, 500×. (a) 13-6 and (b) 15-18.

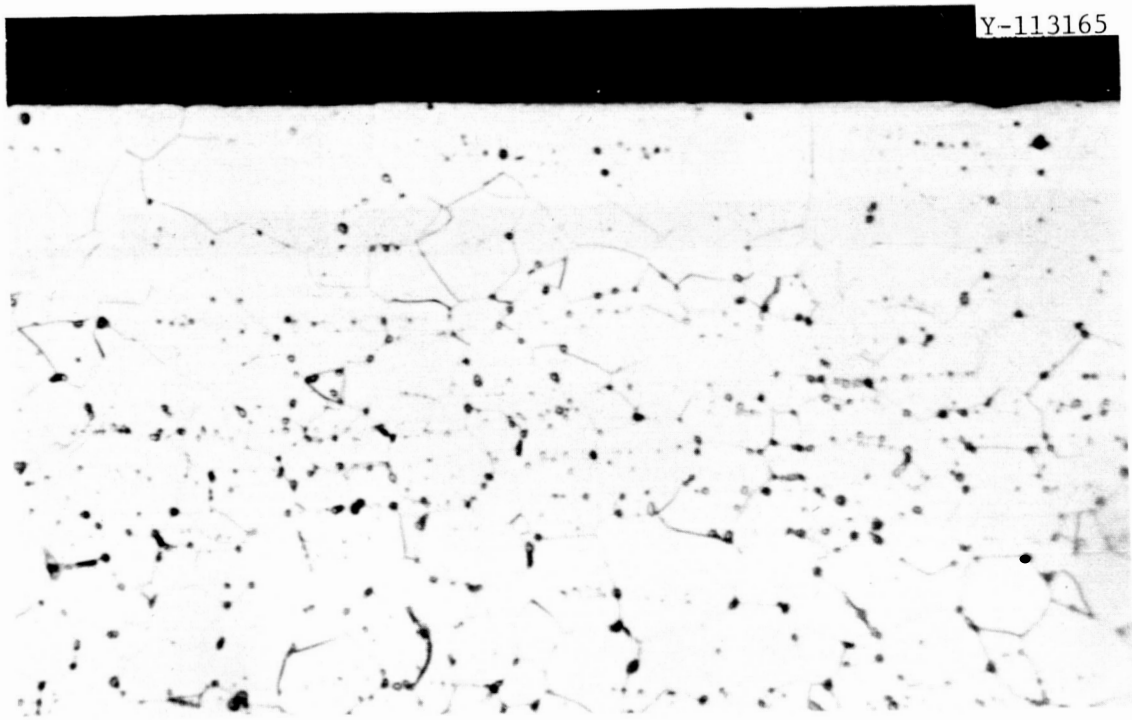

Fig. 25. Microstructure of Insert Tab Specimen 15-22. Grain boundary precipitate particles were exaggerated by etchant in order to reveal grain boundaries. Etched, 500×.

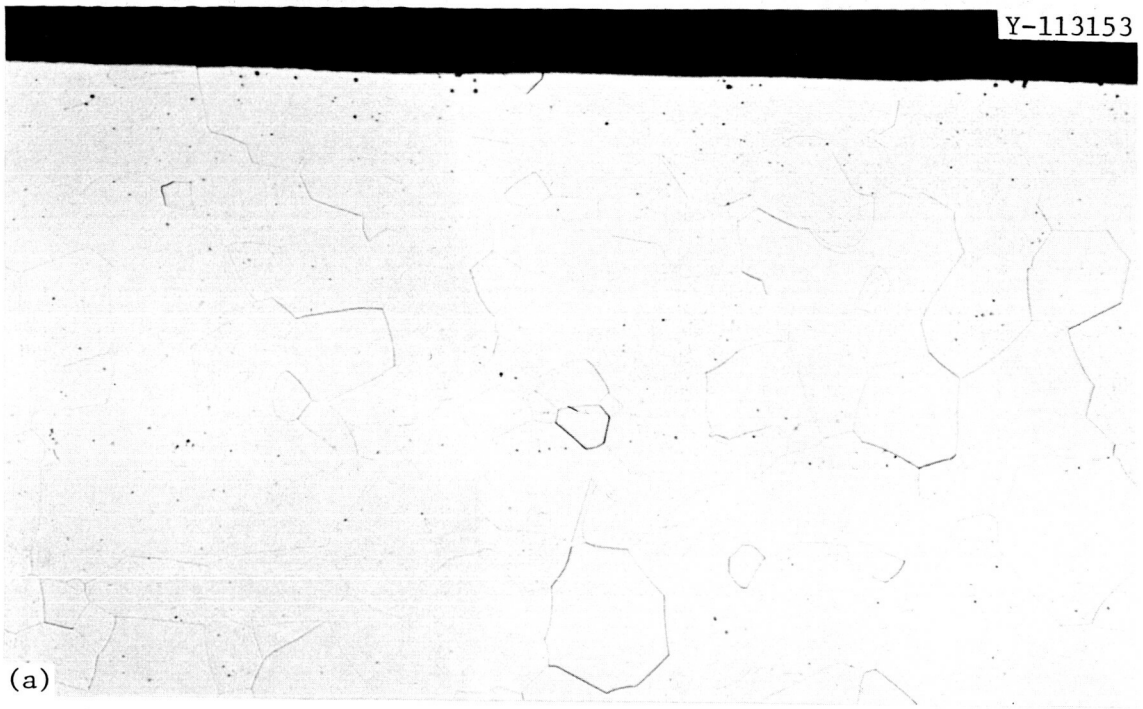

(a)

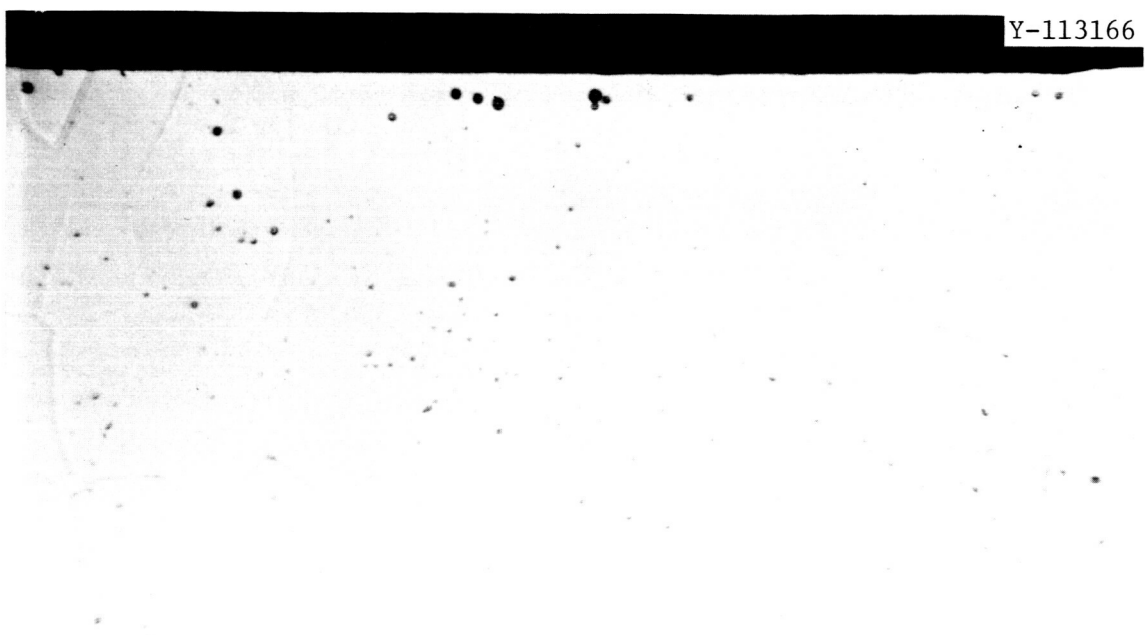

(b)

Fig. 26. Microstructure of Insert Tab Specimen 16-26, Etched. (a) 200×. (b) 500×.

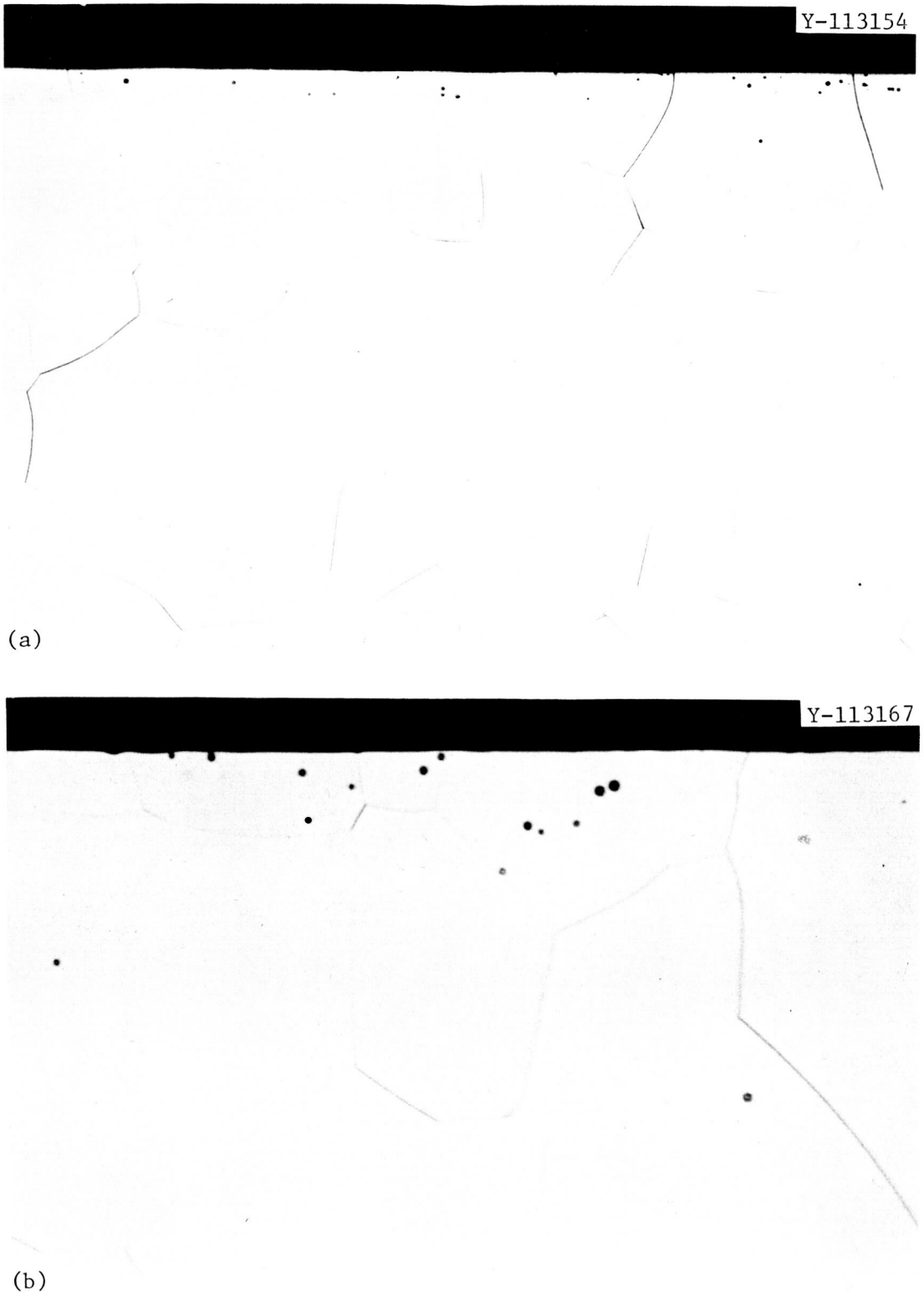

Fig. 27. Microstructure of Insert Tab Specimen 1-36, Etched. (a) 200×. (b) 500×.

(a)

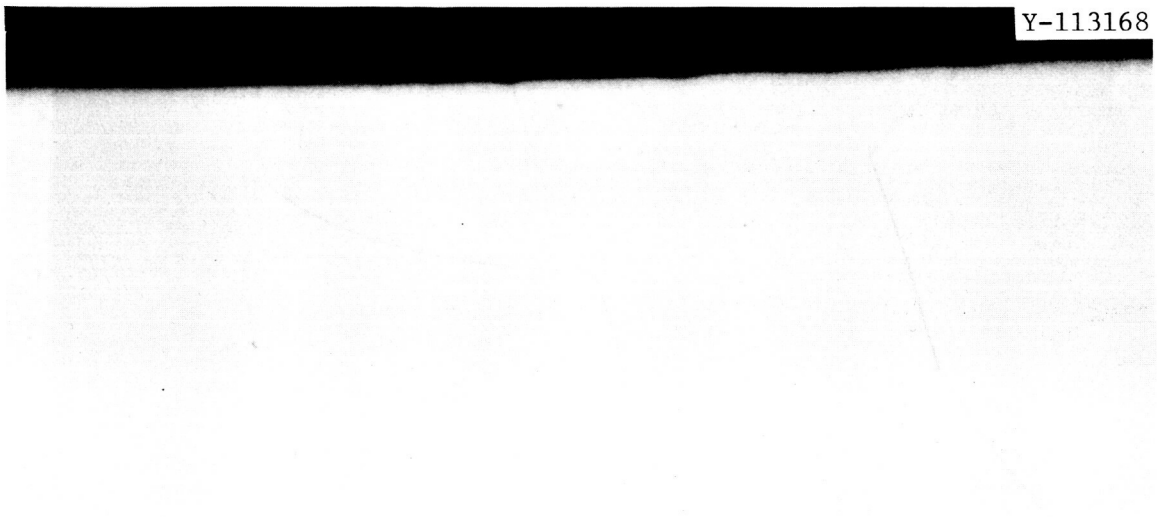

(b)

Fig. 28. Microstructure of Insert Tab Specimen 3-52, Etched. (a) 200×. (b) 500×.

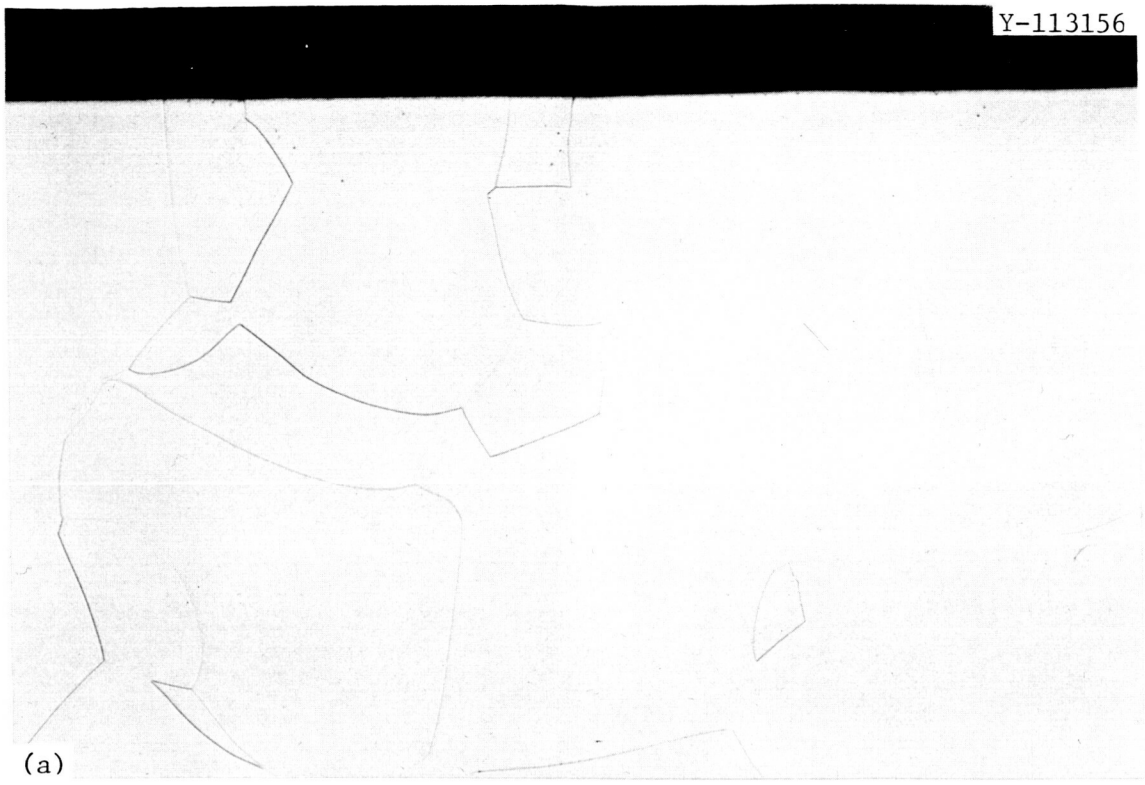

(a)

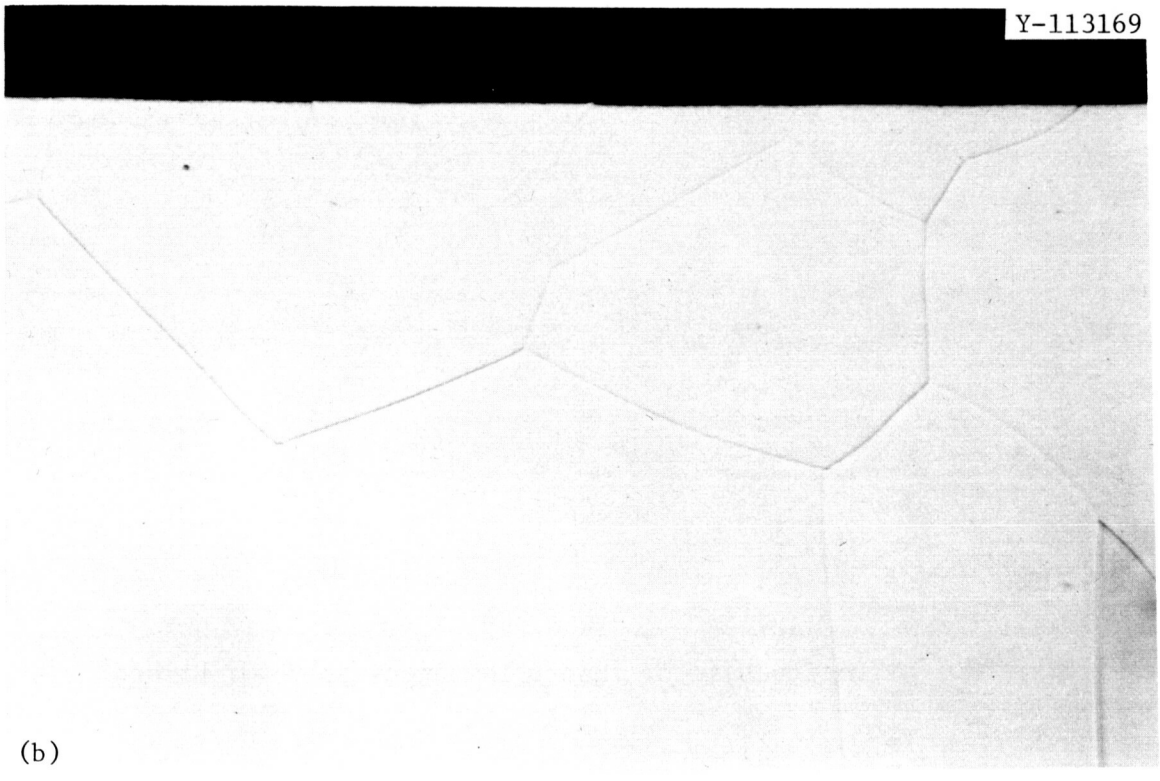

(b)

Fig. 29. Microstructure of Tab Insert Specimen 4-55, Etched. (a) 200×. (b) 500×.

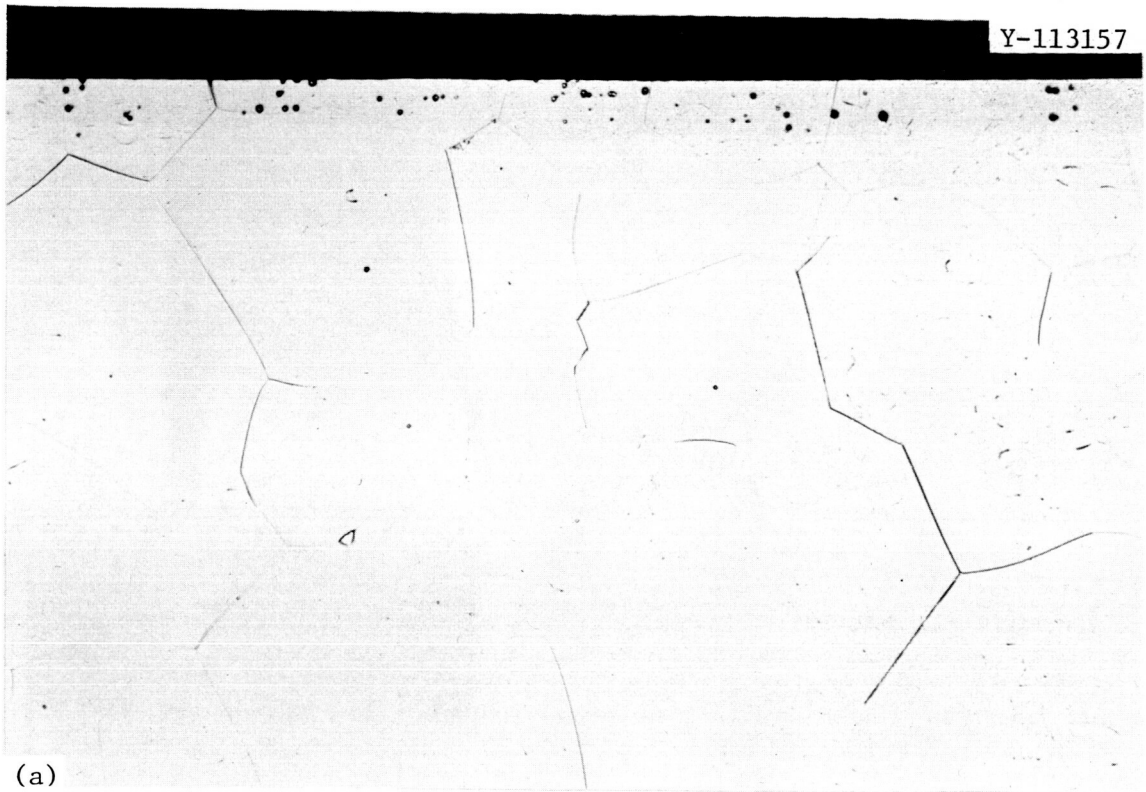

(a)

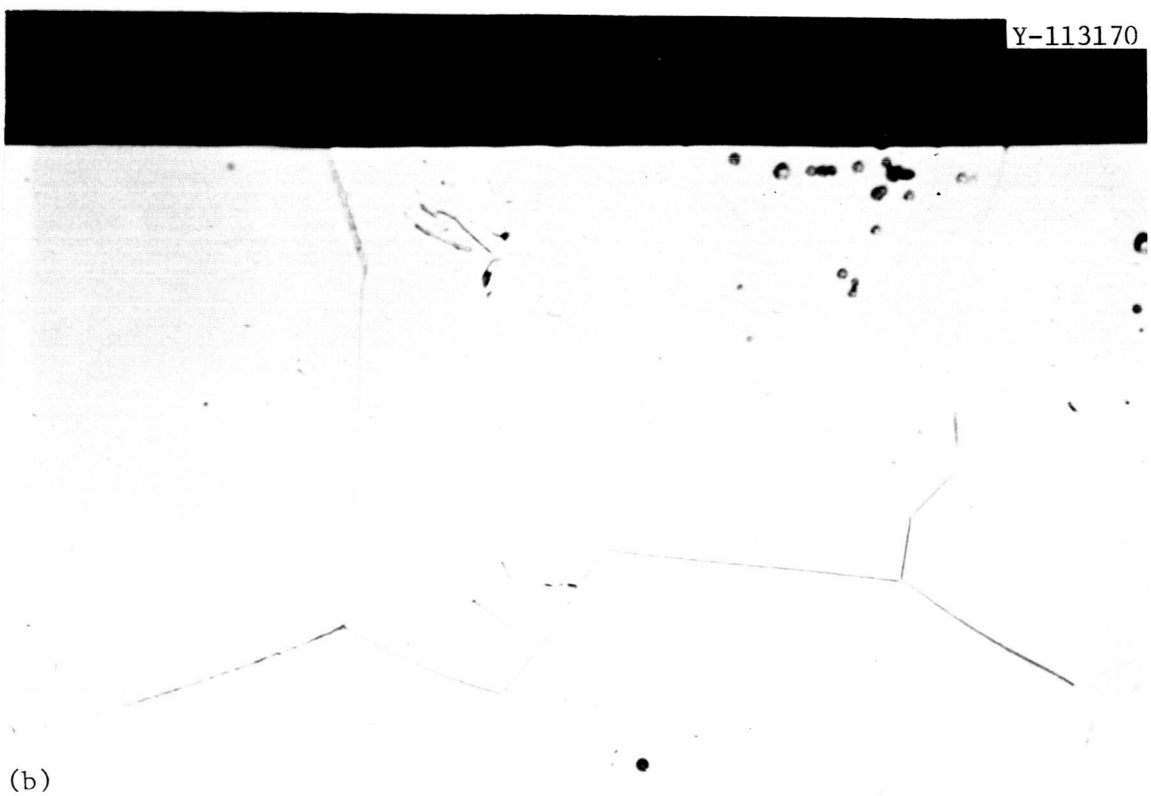

(b)

Fig. 30. Microstructure of Tab Insert Specimen 5-64, Etched. (a) 200×. (b) 500×.

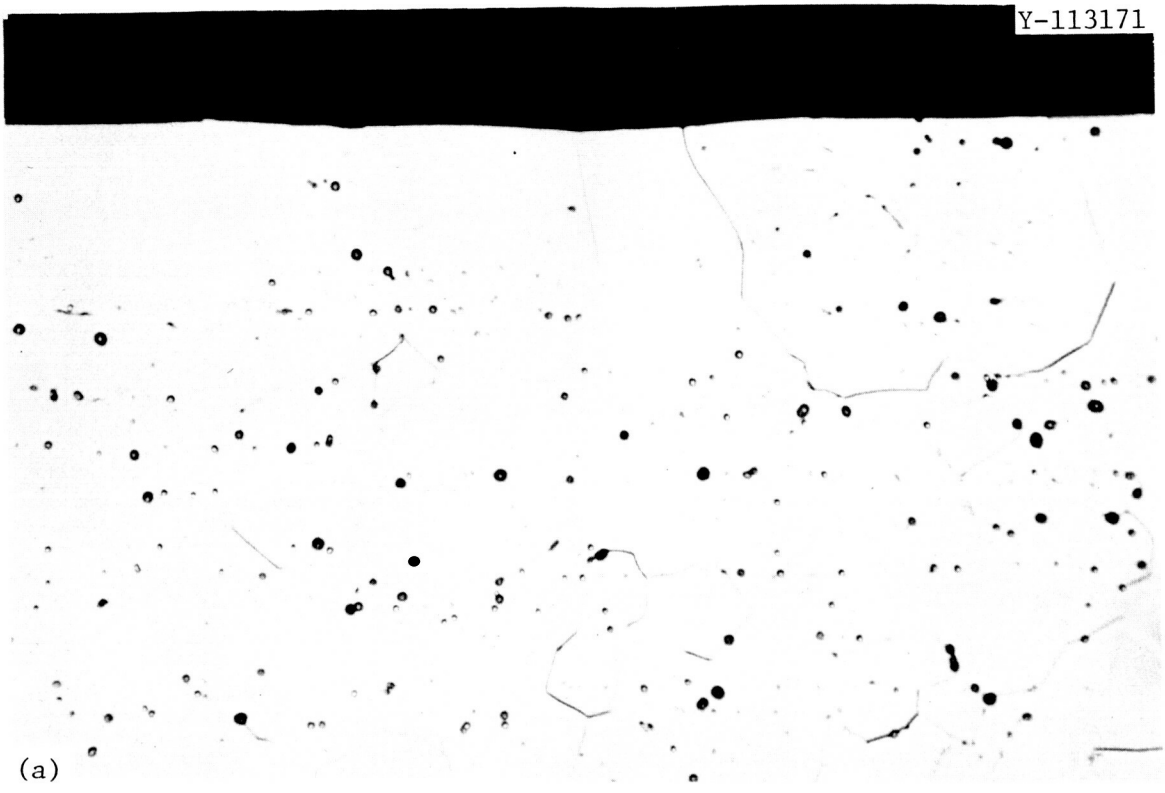

(a)

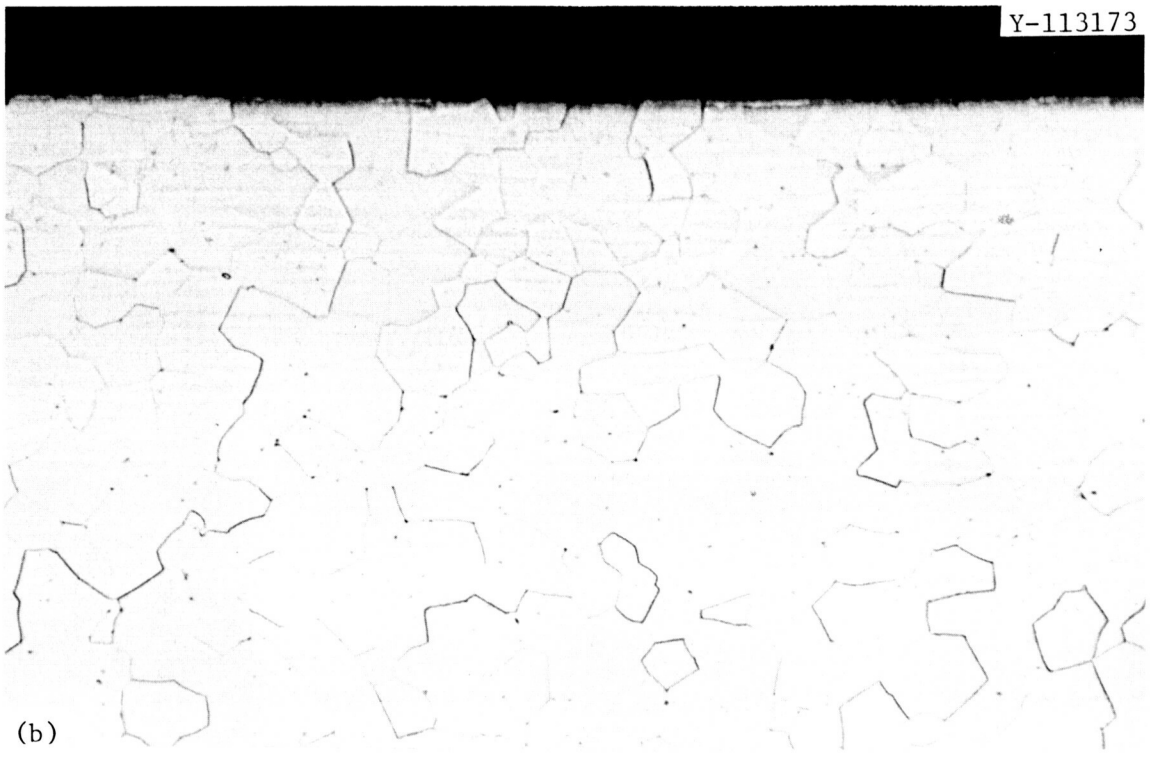

(b)

Fig. 31. Microstructure of Tab Insert Specimens, Etched, 500×. (a) 6-71 and (b) 8-87.

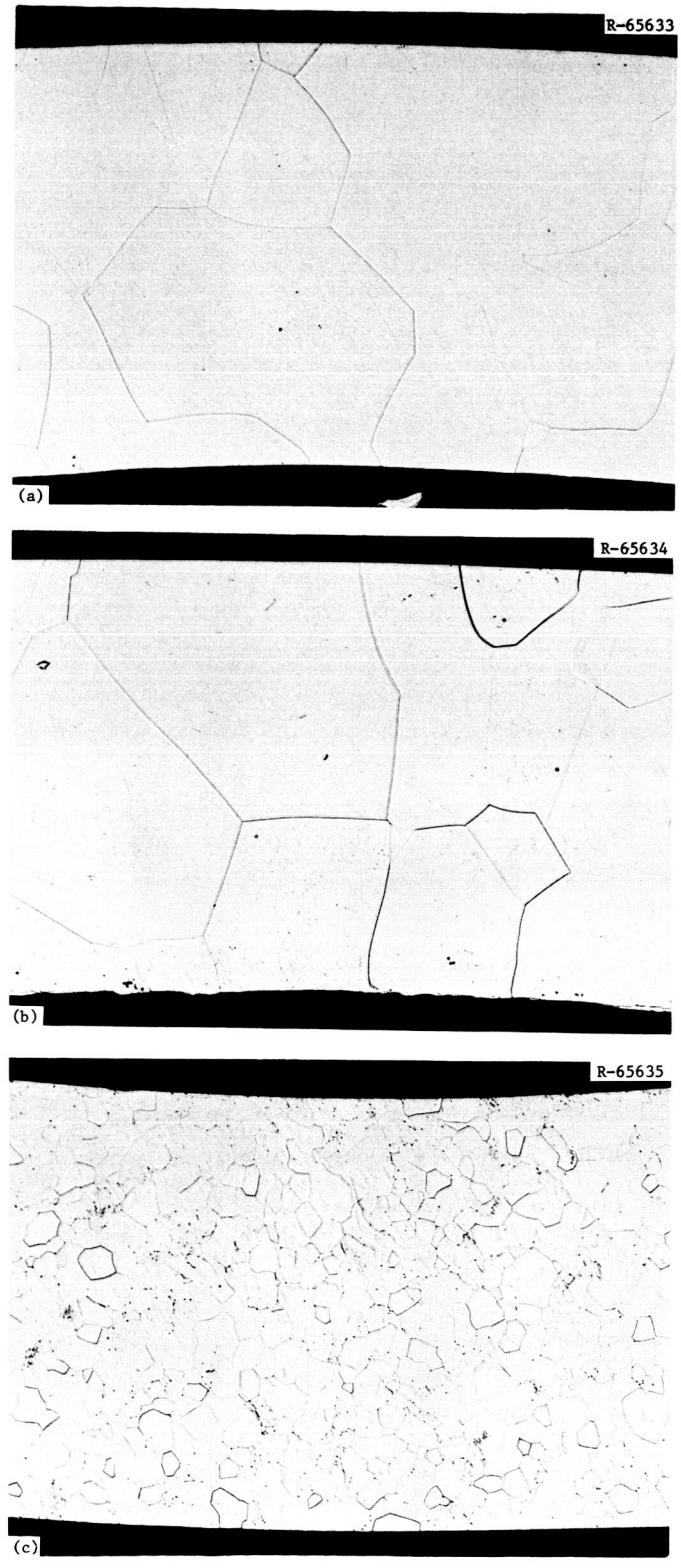

Fig. 32. Transverse Sections Through T-111 Annular Specimens, Etched, 200×. Reduced 40%. (a) 52-B. (b) 55-B. (c) 87-B.

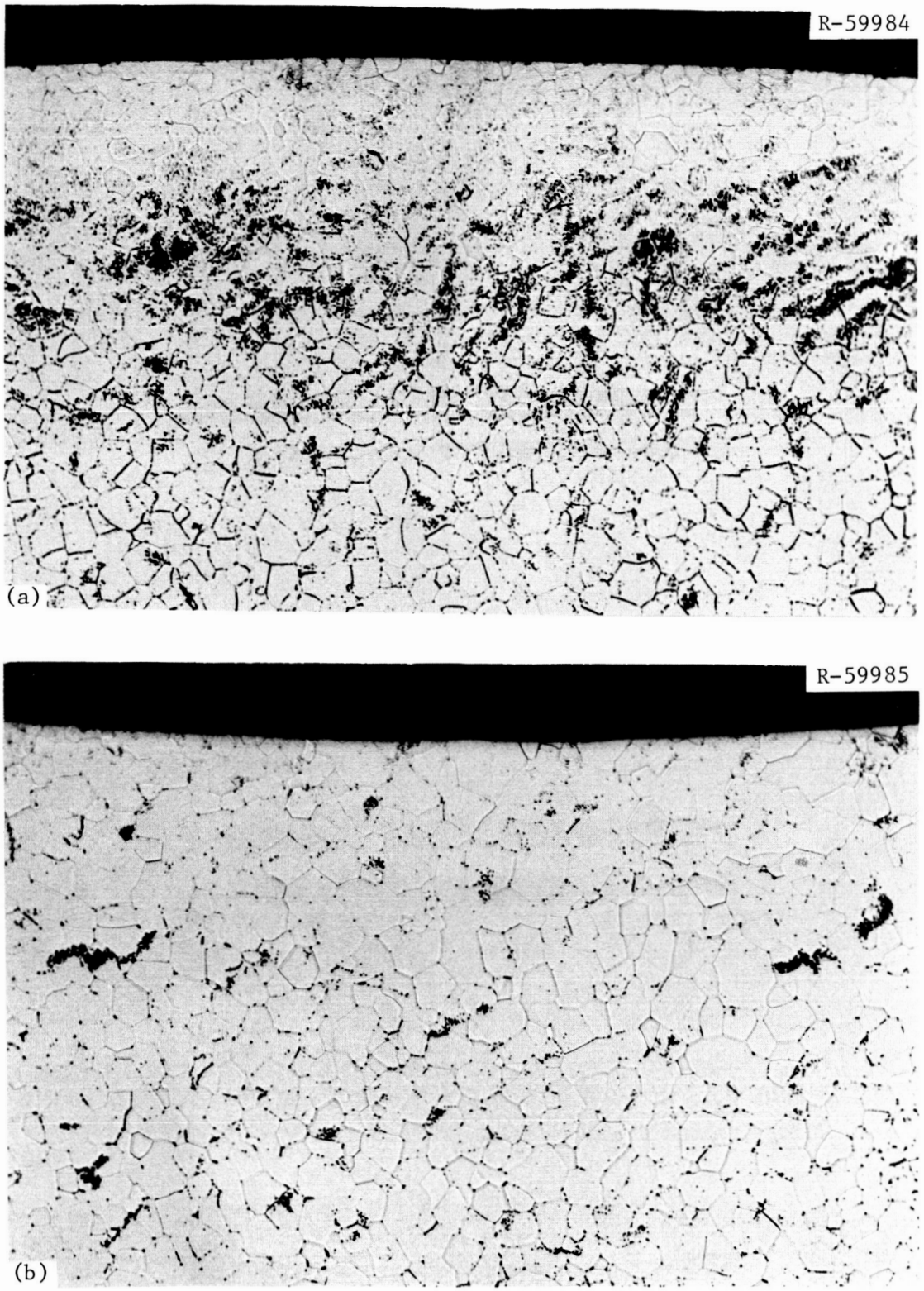

Fig. 33. Microstructure of (a) Outer and (b) Inner Surface Regions of T-111 Tubing Sample 13. The apparent "precipitates" are actually etch pits that developed during attempts to reveal grain boundaries. Etched, 200×.

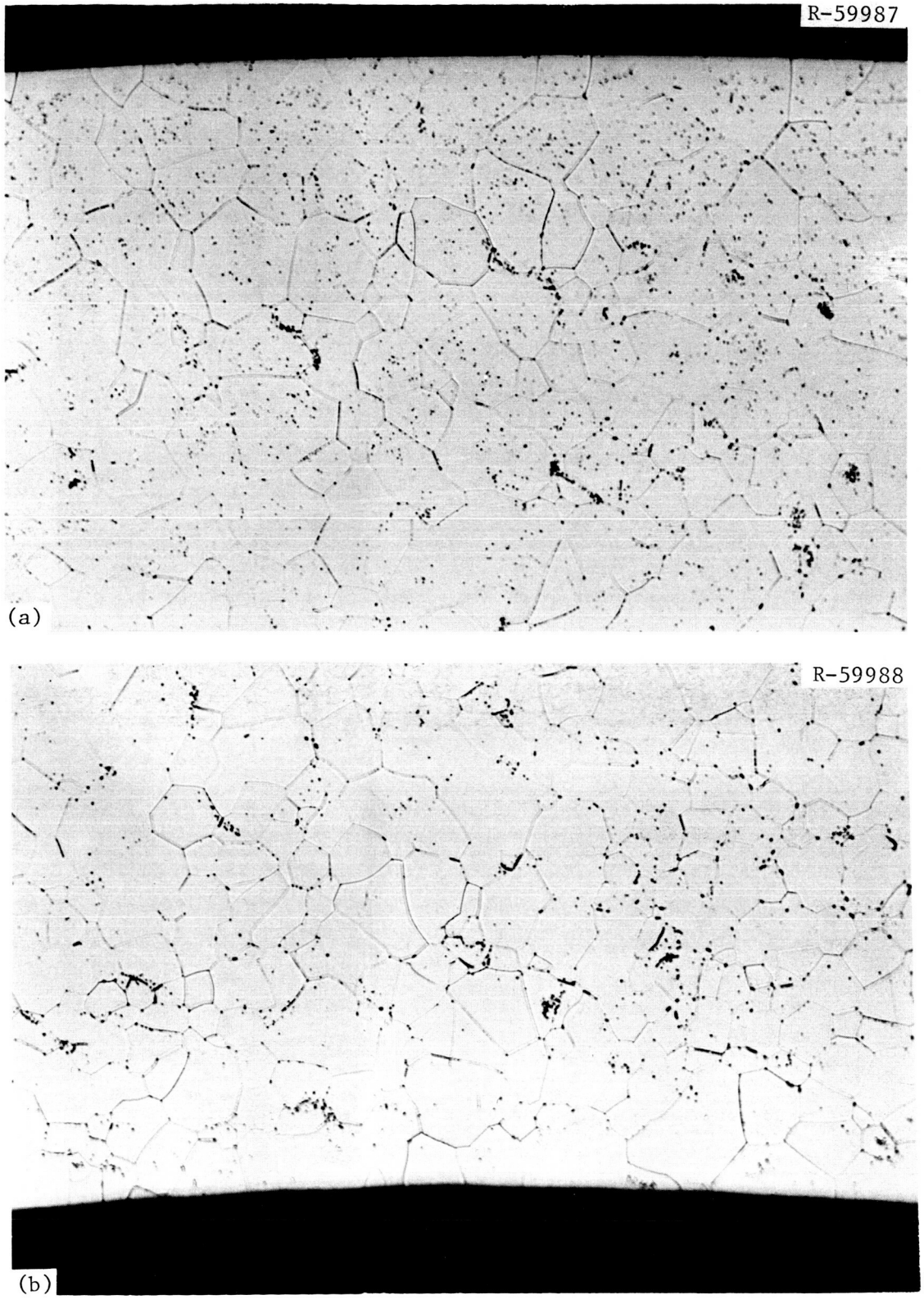

Fig. 34. Microstructure of (a) Outer and (b) Inner Surface Regions of T-111 Tubing Sample 15. Etched, 200×.

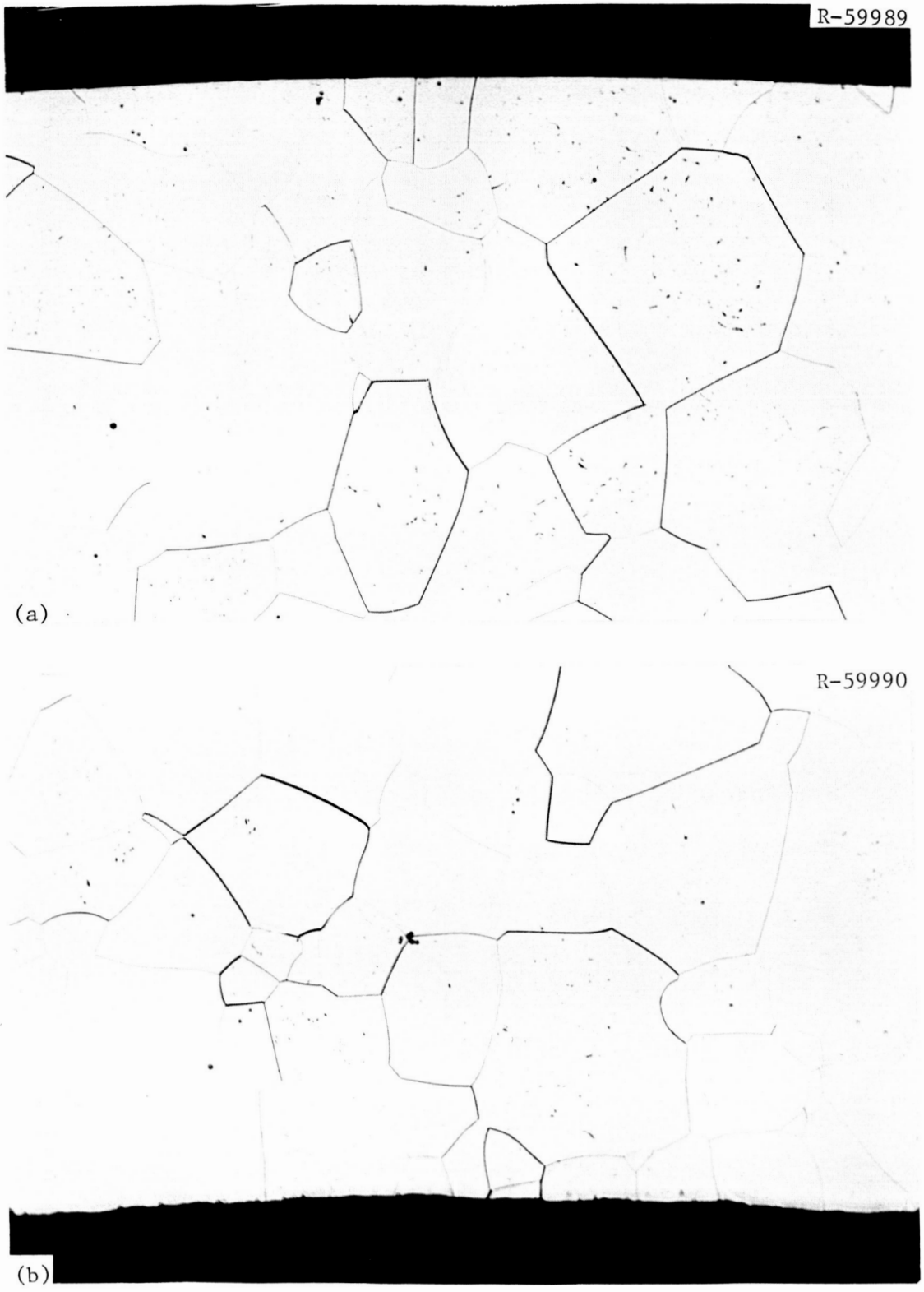

Fig. 35. Microstructure of (a) Inner and (b) Outer Surface Regions of T-111 Tubing Sample 16. Etched, 200×.

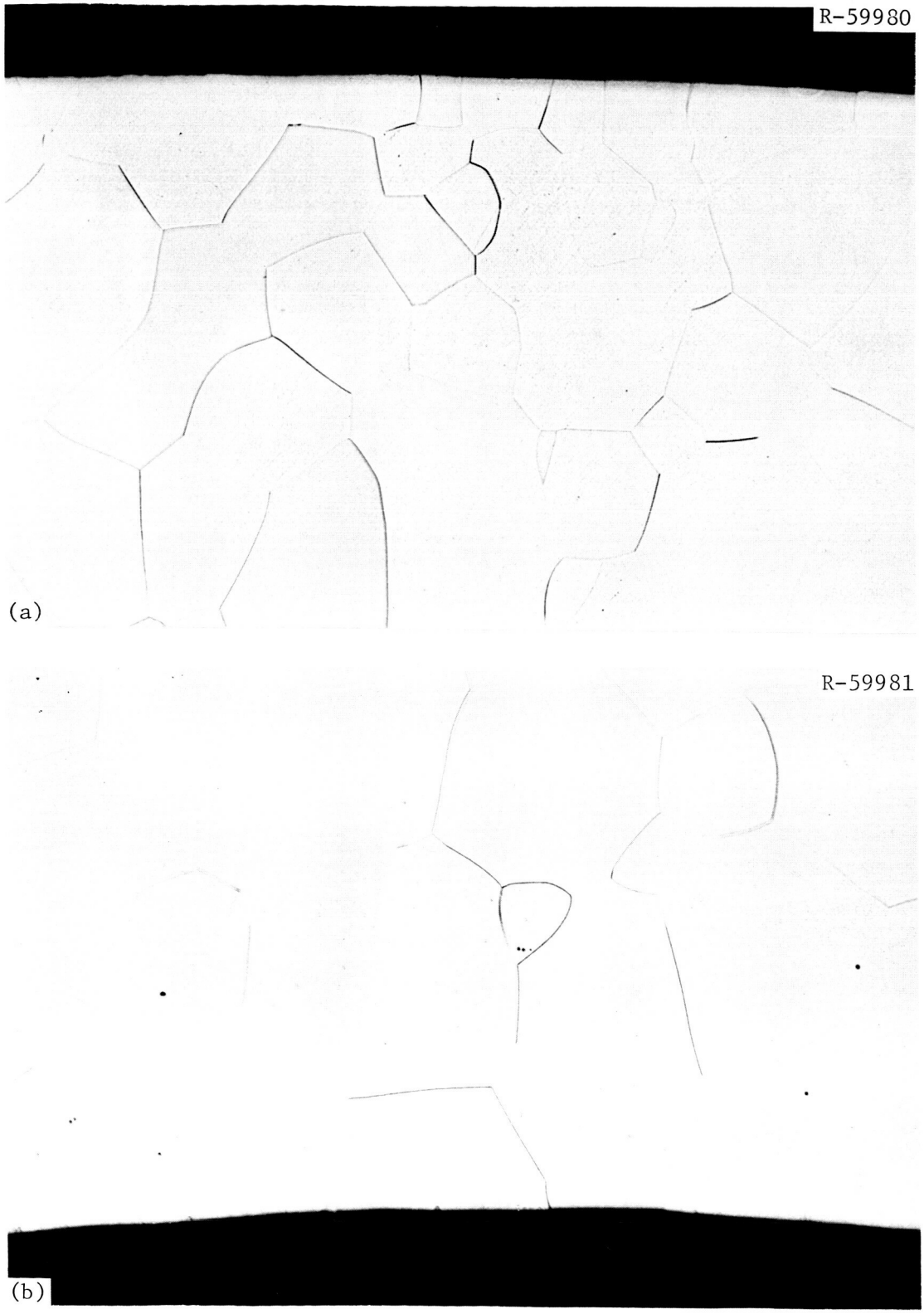

Fig. 36. Microstructure of (a) Inner and (b) Outer Surface Regions of T-111 Tubing Sample 3. Etched, 200×.

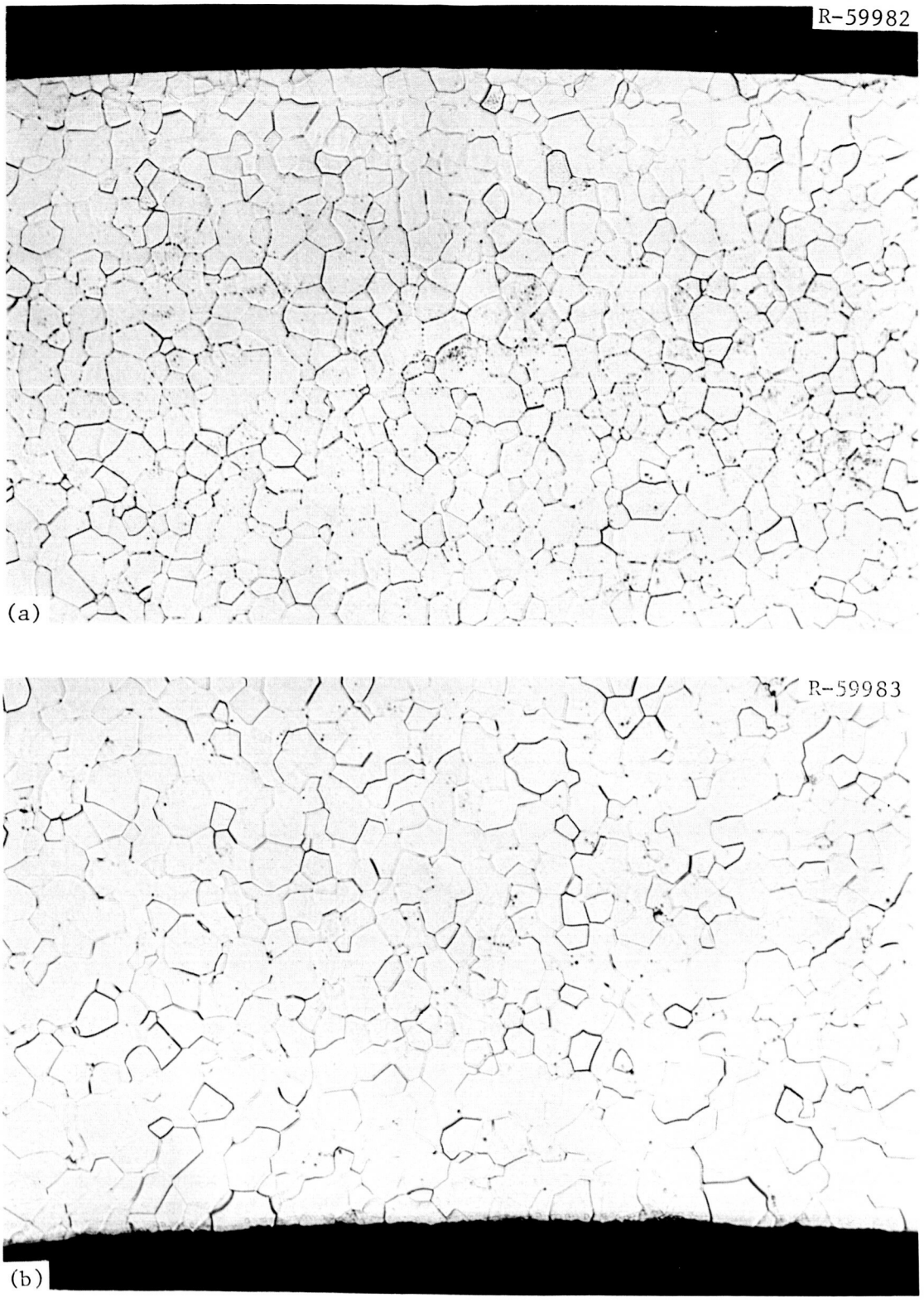

Fig. 37. Microstructure of (a) Inner and (b) Outer Surface Regions of T-111 Tubing Sample 8. Etched, 200×.

Table 8. Correlation of the Grain Size of the T-111 Tab Insert, Annular Insert, and Tubing Specimens with Loop Position and Temperature

Distance from Pump Outlet		Approximate Temperature (°C)	Mean Grain Diameter, mm			
			Insert Specimens	Annular Specimens	Loop Tubing Specimens	
(m)	(in.)				Inside	Outside
As received			0.018			
Control		1204	0.016			
Control		1370	0.016			
2.35	92 1/2	1200	0.019		0.023	0.021
4.05	159 1/2	1258	0.020			
4.33	170 1/2	1268	0.019		0.033	0.038
5.17	203 3/4	1299	0.057		0.077	0.086
6.42	252 3/4	1327	0.084			
8.08	318 1/4	1365	0.087	0.138	0.118	0.085
8.51	355	1369	0.130	0.138		
9.72	382 3/4	1348	0.119			
10.74	423	1312	0.023			
11.72	461 1/2	1277	0.019			
20.39	802 3/4	1204	0.019	0.022	0.020	0.024

All three types of specimens showed a 5-to-7-fold increase in grain size in a region of the loop located from about 8.1 to 9.1 m (320—360 in.) from the pump outlet.

The control specimen thermally aged at 1370°C (Fig. 23) showed little if any grain growth (Table 8), in contract to the tubing and insert specimens exposed to lithium at this temperature. Thus the grain growth of the latter specimens was obviously promoted by lithium-produced changes in interstitial impurities, which are described later in this report.

Except for the changes in grain size, the microstructures of T-111 tubing and insert samples from this loop showed no other manifestations of lithium attack.

Metallographic Examination of Loop Welds

The locations of welds selected for metallographic examination are shown in Fig. 38. The welds that had been made before loop assembly and had received a solution heat treatment (Appendix A) are designated as "fabrication welds." The two welds made during final loop assembly, which received no postweld heat treatment are designed as "field welds." Finally we examined the vent line repair weld and two transition joints between Nb—1% Zr and type 316 stainless steel from the drain line and lithium sampler.

Fabrication Welds

Fabrication welds 7, 9, and 10 (Fig. 38) were sectioned longitudinally to include base metal as well as weldment. Weld 7 was a T-joint that had been made at the junction of the downstream side of the resistance heater section and the economizer. This weld is shown at two magnifications in Fig. 39. There were no incipient defects.

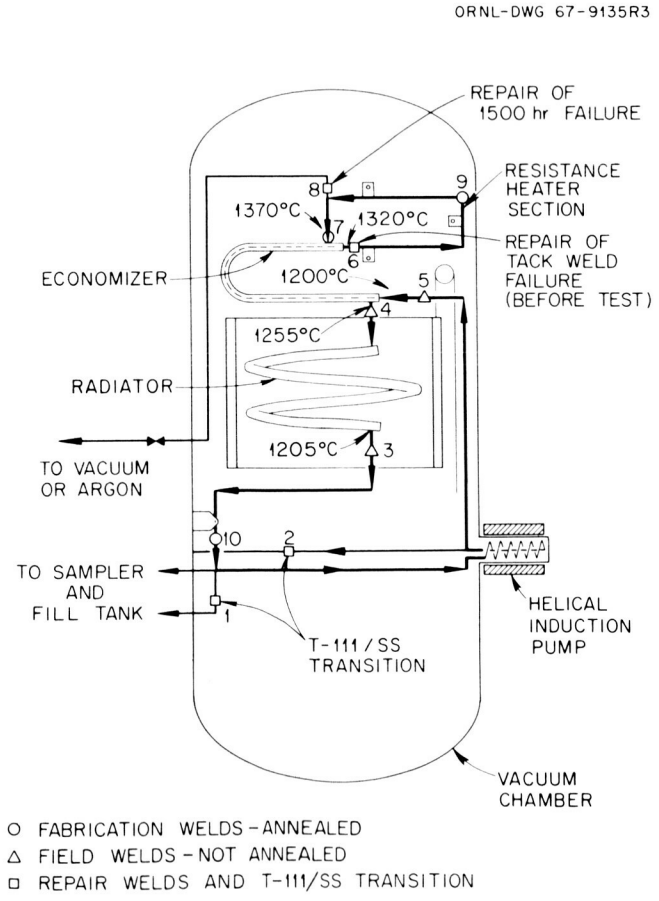

Fig. 38. Location of Various Types of Welds and Identification of Welds Selected for Metallographic Examination. Welds examined metallographically were: fabrication welds 7, 9, and 10; field welds 4 and 5; T-111-to-stainless-steel transition weld 1; and repair welds 6 and 8.

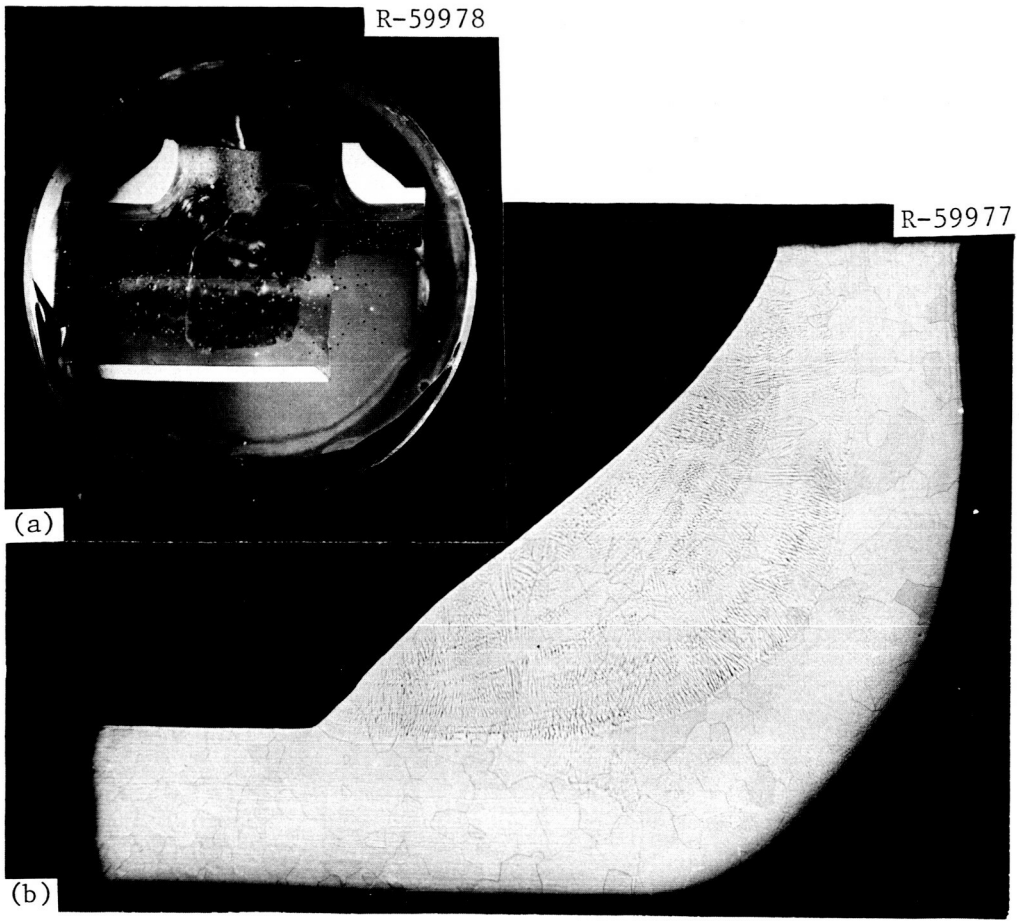

Fig. 39. Metallographic Section Through Fabrication Weld 7. (a) 1.8×. (b) 20×.

One of the longitudinal sections of welds 9 and 10 was examined metallographically and the other half was partially flattened in a vise at room temperature. The latter samples were also chemically analyzed for interstitial content. The samples after flattening are shown in Fig. 40. Note that weld 10 from the lower temperature region of the loop cracked in the fusion zone, while weld 9 from a higher temperature region did not. The chemical analyses of the two welds can be compared in Table 9; both show only minor amounts of interstitials, although weld 10 contains the greater concentration. The metallographic appearance of welds 9 and 10 is shown in Fig. 41. Full penetration was achieved during welding, and there were no obvious weld defects.

Field Welds

Field welds 4 and 5 were sectioned longitudinally; one half of each weld was examined metallographically and the other half was flattened in a vise and chemically analyzed. The appearance of the flattened specimens is shown in Fig. 42. The results of the crush test and the

R-59478

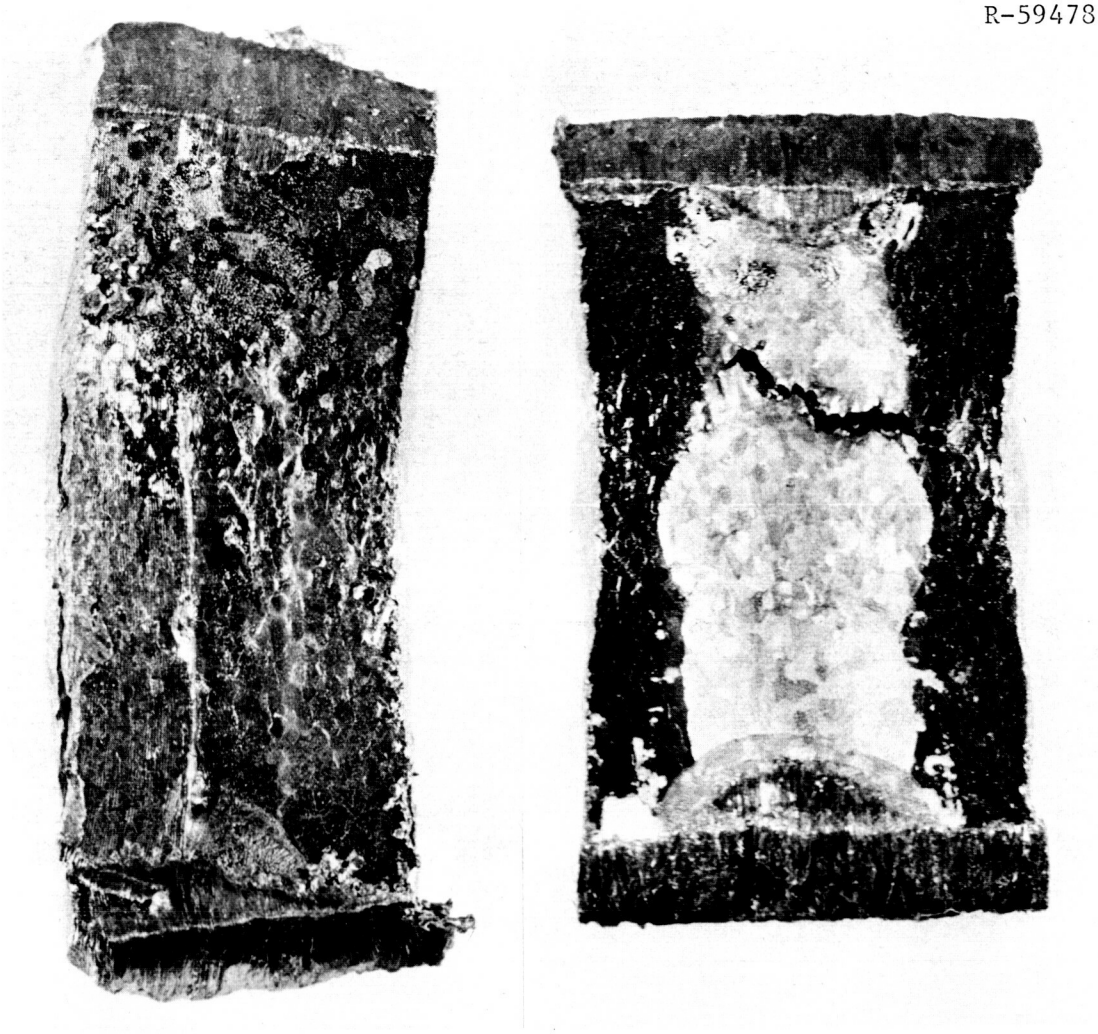

Fig. 40. Inner Surfaces of Fabrication Welds 9 (1eft) and 10 After Crush Tests. 5×.

Table 9. Results from Crush Testing and Chemical Analysis of Field and Fabrication Welds

Weld	Type	Approximate Operating Temperature (°C)	Results of Crush Test	Interstitial Content, ppm		
				H	O	N
4	Field	1255	Cracked	6	600	33
5	Field	1200	Ductile	1	84	15
9	Fabrication	1350	Ductile	1	23	3
10	Fabrication	1200	Cracked	5	55	20

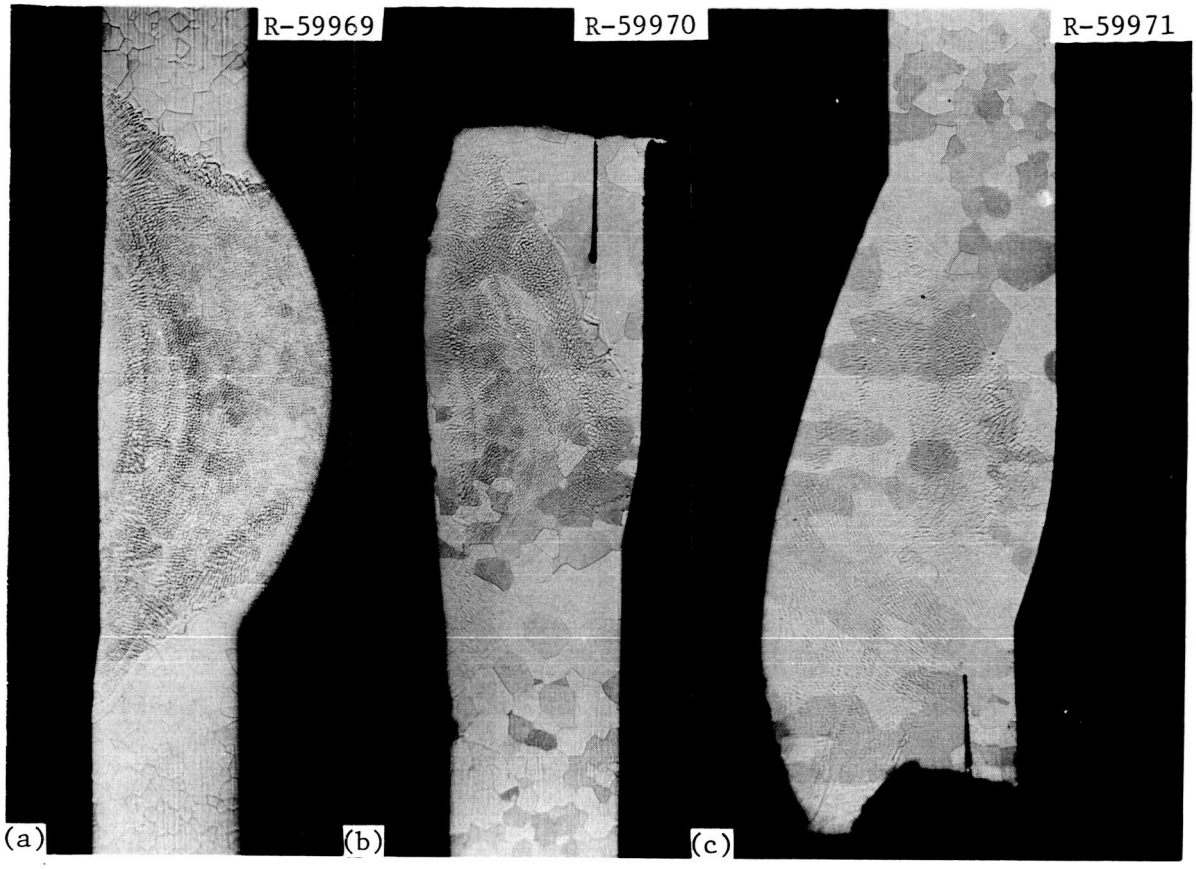

Fig. 41. Longitudinal Sections Made Through Fabrication Welds. 12×. (a) Weld 10. (b) Weld 9. (c) Weld 9, 180° from area shown in (b). The irregular edges on the top of (b) and bottom of (c) is the result of sawing through the weld to sever it from the loop.

chemical analyses are given in Table 9. Typical sections through the metallographic specimens from welds 4 and 5 are shown in Fig. 43. As can be seen in the preceding figure, one section through weld 5 showed the weldment to be slightly misaligned, and only 65% penetration was achieved. A small blowhole was present near the root of the weld in the other section through weld 5 [Fig. 43(b)]. A separation of grain boundaries in the heat-affected zone is noticeable at the root of these welds, extending in some cases into the backing ring. In view of the relatively high oxygen content in the weld area (Table 9), the separations were probably caused by lithium penetration along grain boundaries where oxygen had segregated during welding. Oxygen contamination was apparently concentrated in the crevice between the backing ring and the inner tube surface, where the heaviest intergranular penetration occurred. Although both field welds showed this effect, only the one with highest oxygen content (600 ppm) cracked when flattened at room temperature (Fig. 42).

R-59479

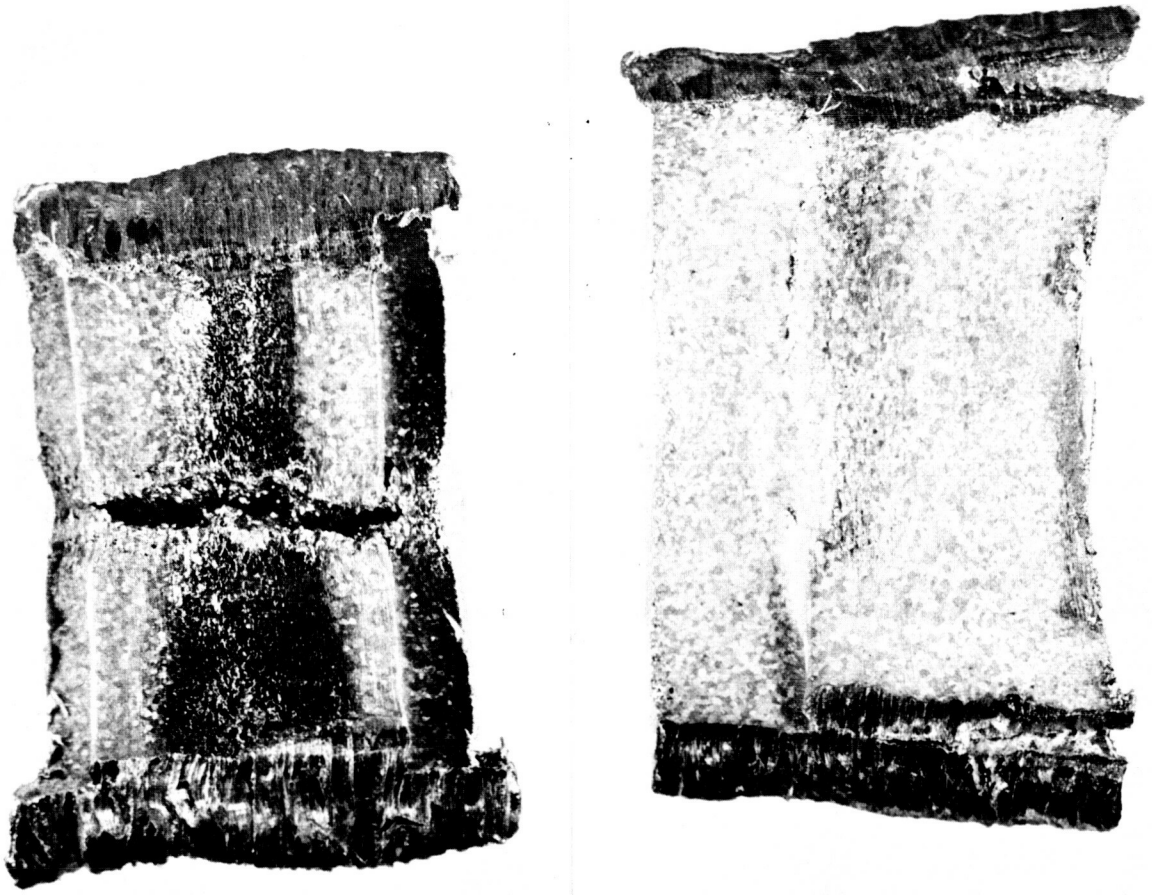

Fig. 42. Inner Surfaces of Field Welds 4 (left) and 5 after Crush Test. 5×.

Transition Welds of Nb—1% Zr with Stainless Steel

The transition between T-111 and type 316 stainless steel was accomplished by joining the stainless steel to a section of Nb—1% Zr tubing, which in turn was welded to the T-111 tubing. Weld 1 was sectioned longitudinally to include the two transitions between the three materials for metallographic evaluation. The microstructural details of the bond of type 316 stainless steel to Nb—1% Zr are shown in Fig. 44. A sound metallurgical bond was evident, with no evidence of selective corrosion. The microstructure of the weldment between the Nb—1% Zr and the T-111 tubing is shown in Fig. 45; complete fusion of this weldment is apparent, with no indication of potential failure. Nondispersive x-ray analysis of the inner surface of the T-111 tubing in the vicinity of the transition joint showed no evidence of iron, chromium, or nickel that could have come from the stainless steel.

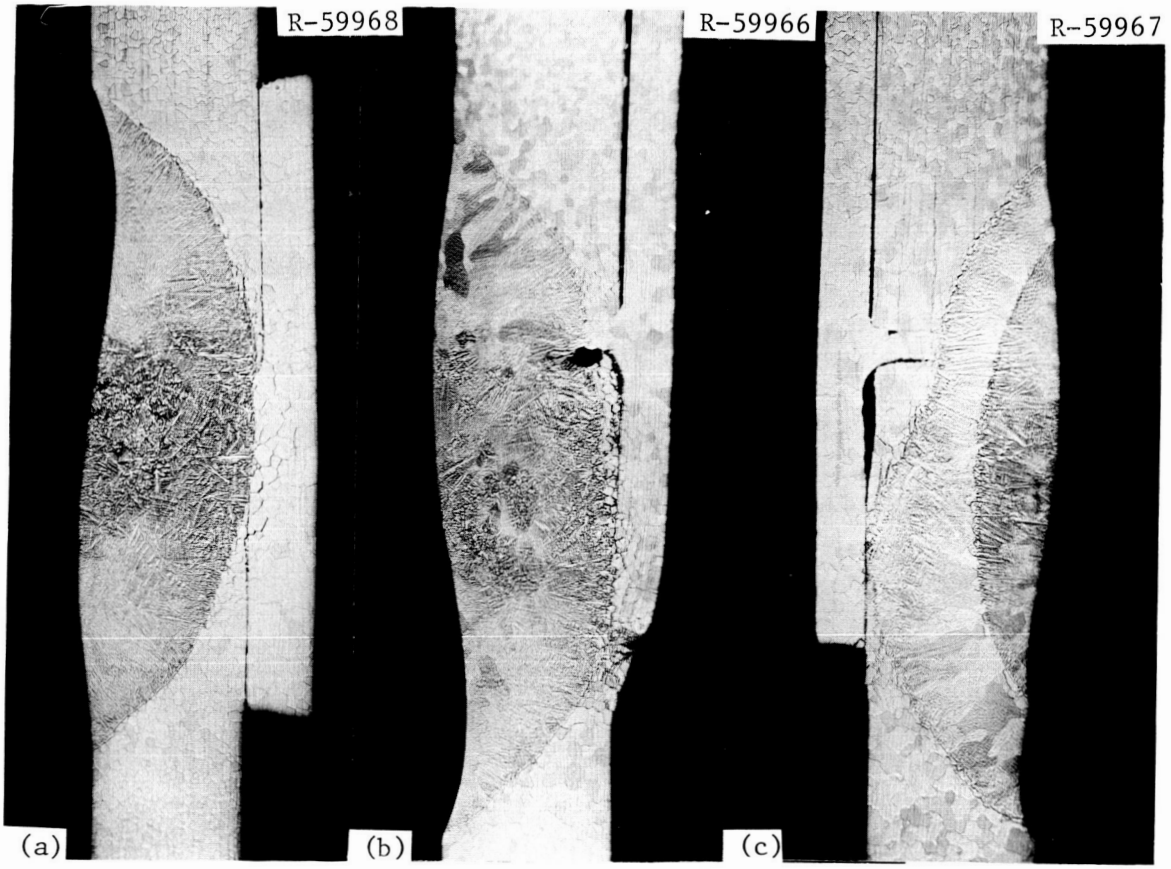

Fig. 43. Typical Sections Through Field Welds. 12×. (a) Weld 4. (b) Weld 5. (c) Weld 5, 180° from area shown in (b).

Repair Welds

Weld 8 was a repair weld that involved removing a vent line that leaked after 1735 hr of operation. (Figure 14, p. 21, shows the arrangement of this repair weld.) After the vent line was cut off, a T-111 plug was welded in place. A T-111 cup was then placed over the plugged vent line and welded in place with the Nb—1% Zr alloy. Figure 46 shows a section made through the repair-weld assembly. Examination at higher magnification showed that the Nb—1% Zr braze had been pulled up into the crevice between the cap and tube stub (Fig. 47). Figure 48 shows the bond area between the original T-111 weld and the Nb—1% Zr brazement.

Weld 6 was a repair of a tack weld that cracked before the loop operated. The leak was located a few inches from the economizer outlet and was repaired by puddling Nb—1% Zr alloy on the defect region. The appearance of the repair weld region after cutting from the loop is shown in Fig. 49. The metallographic section was mounted so as to show the Nb—1% Zr weldment and the cross section of the T-111 tubing.

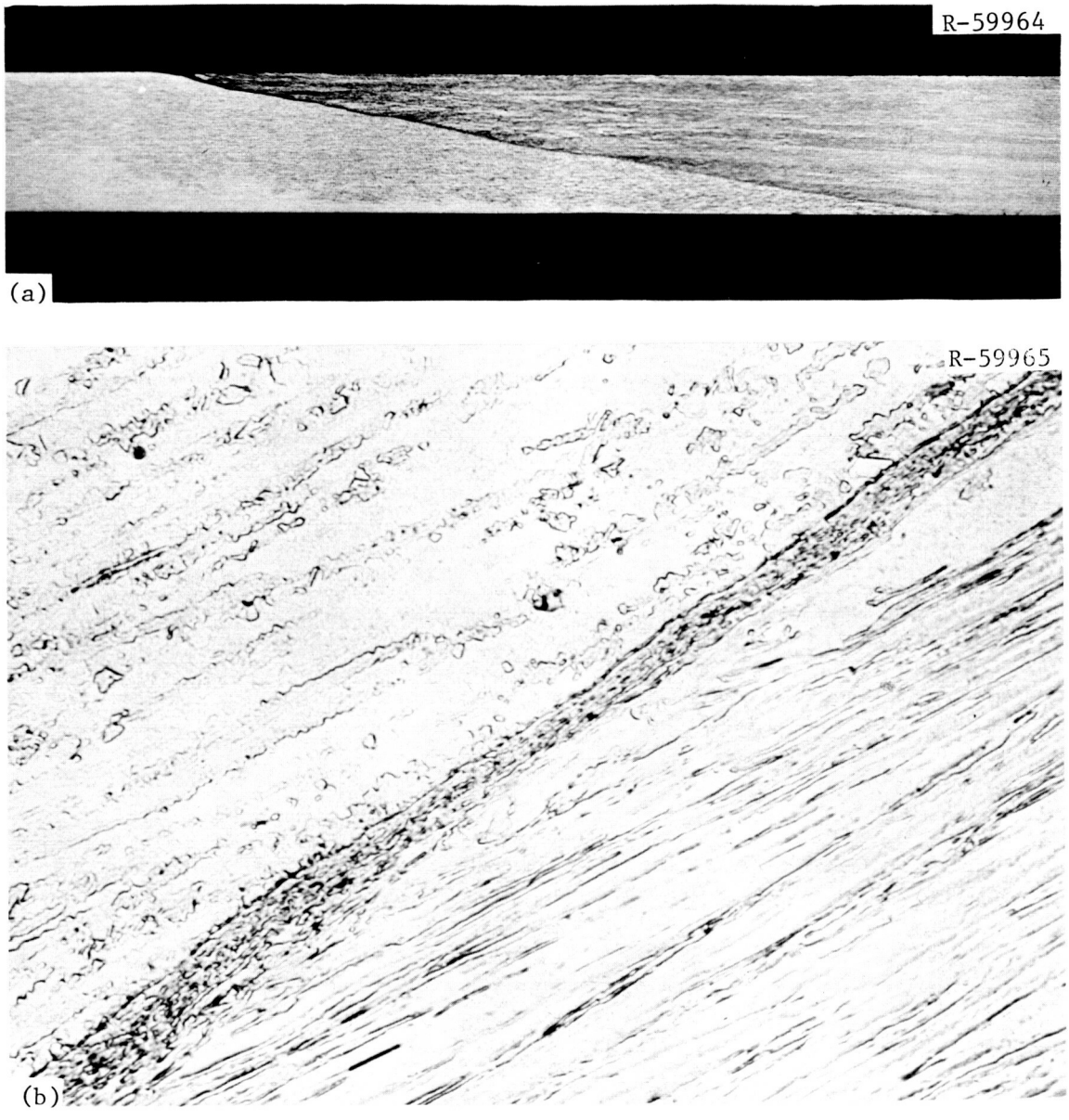

Fig. 44. Longitudinal Section Through the Transition Joint Between Type 316 Stainless Steel and Nb—1% Zr in Weld 1. Etched. (a) 12×. (b) 500×.

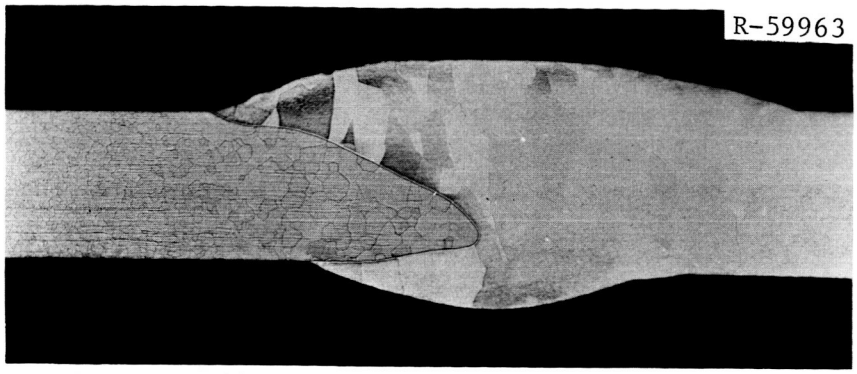

Fig. 45. Weldment Joining Nb—1% Zr and T-111 Tubing from Weld 1. Etched, 12×.

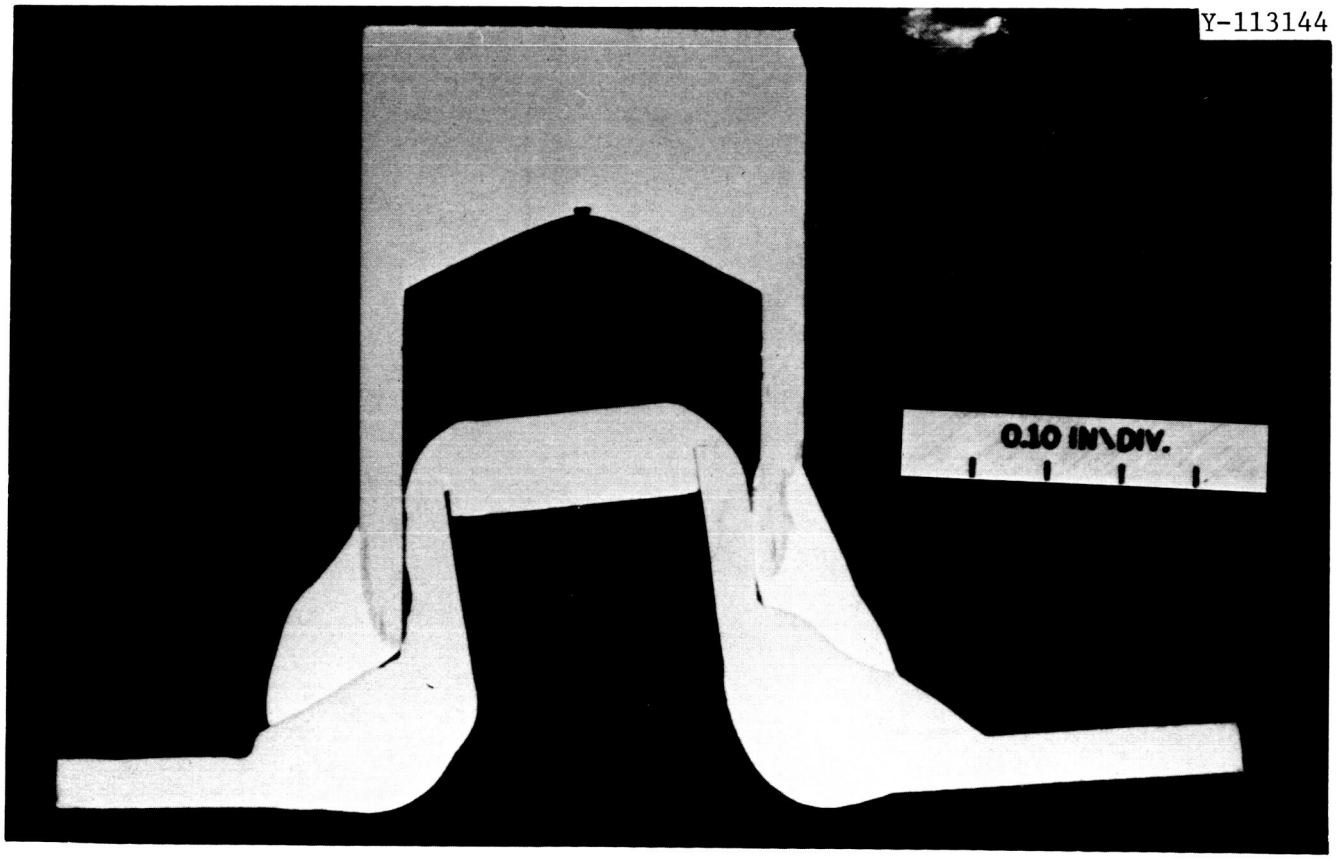

Fig. 46. Section through the Repair Weld Made on the Vent Line. 3.8×. Scale is 2.5 mm/division.

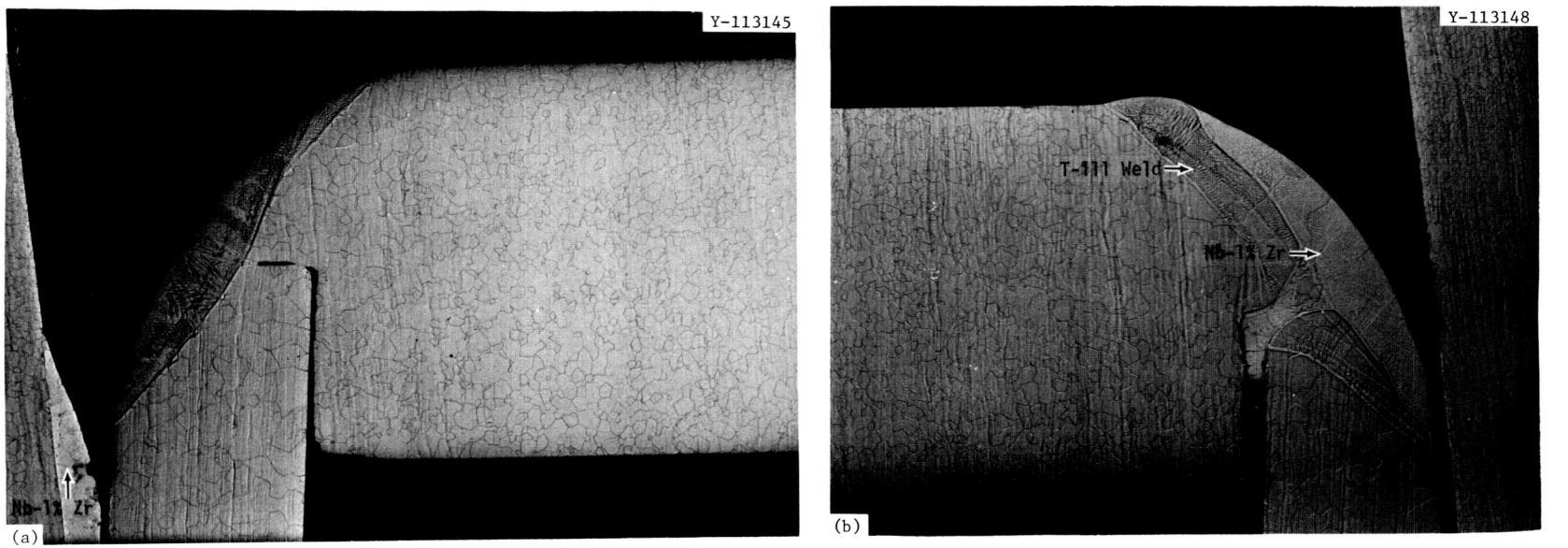

Fig. 47. Metallographic Sections Through (a) The T-111 Vent Line and (b) T-111 Seal Plug Weld. 25× (reduced 32%). Note the presence of the Nb—1% Zr alloy on the inner surface of the T-111 cap in (a) and in the T-111 seal-plug-to-vent-line weld in (b).

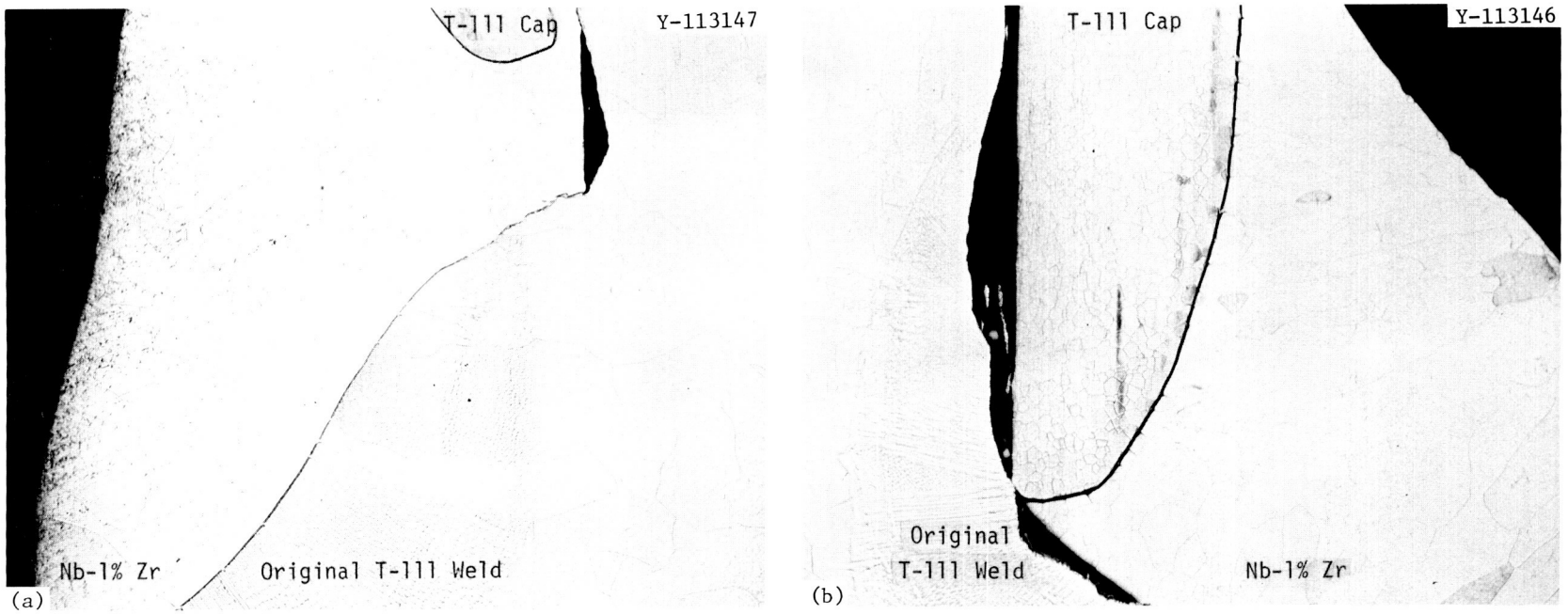

Fig. 48. Typical Areas from the Metallographic Section Made Through the Nb—1% Zr. Weldment that attached the T-111 cap to the original T-111 weld. 25×. Reduced 16%.

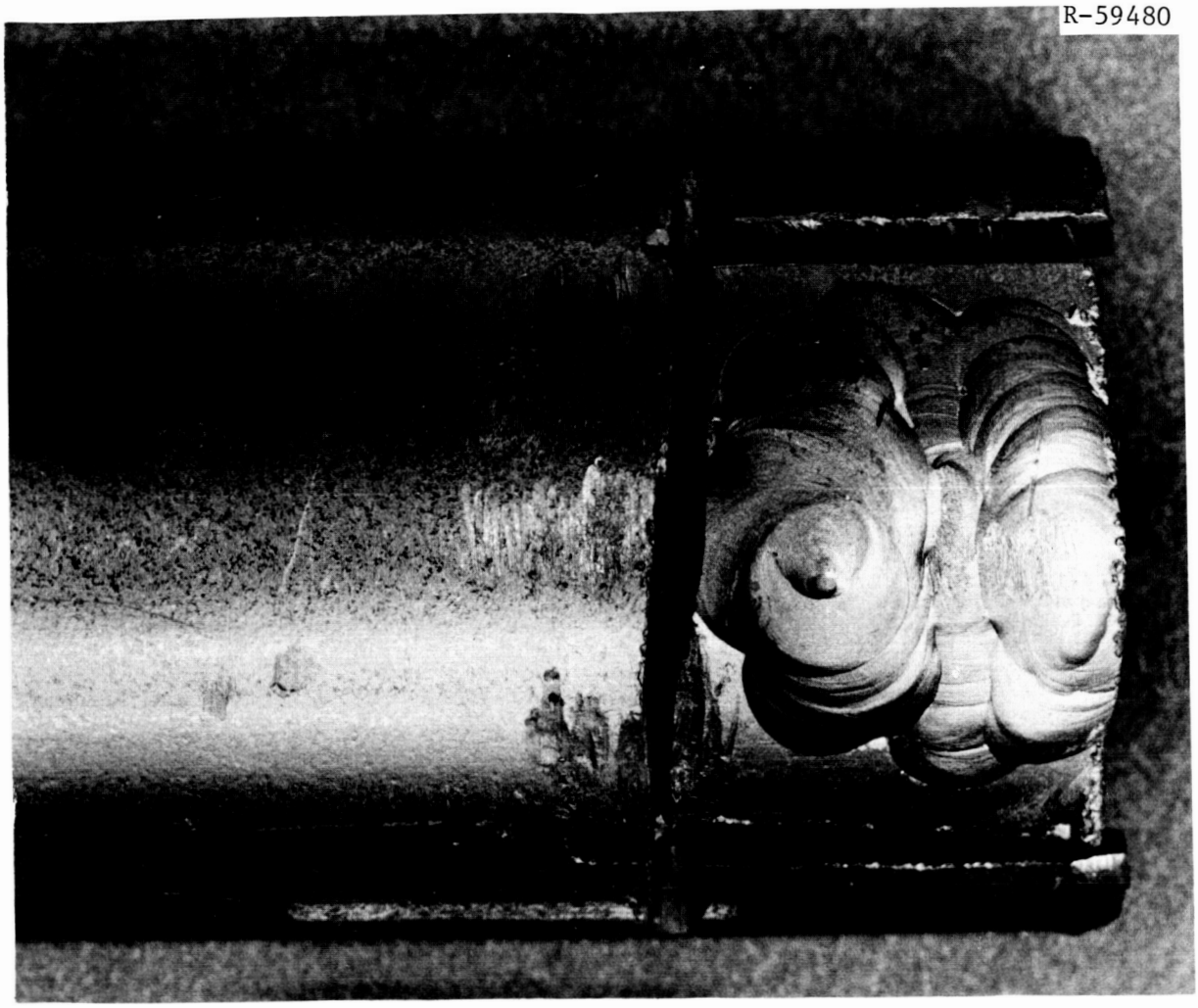

Fig. 49. Section of T-111 Tubing that Contained Nb—1% Zr Overlay to Repair Crack Near Tack Weld. 5×.

A small crack was noted on the inner surface of the T-111 tubing before mounting for metallographic examination. The metallographic mount was polished serially to reveal a succession of elevations through the specimen. Two planes of polish are shown in Fig. 50. The plane in Fig. 50(b) is shown at higher magnification in Fig. 51. The crack was both intergranular and transgranular, and numerous small voids decorated along and around grain boundaries in the vicinity of the crack. Although the Nb—1% Zr formed a metallurgical bond with the outer surface of the T-111 tubing, it did not penetrate the crack.

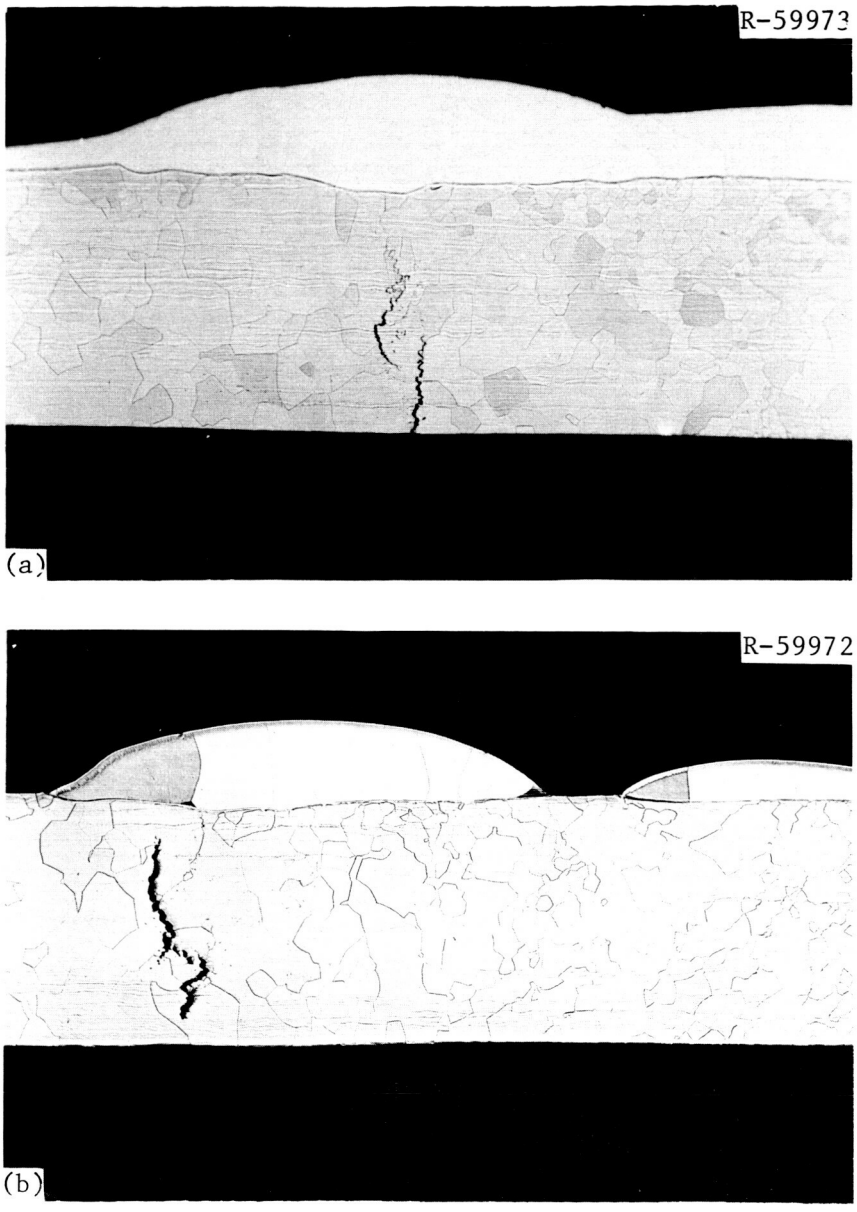

Fig. 50. Two Metallographic Sections Through the T-111 Tubing That Contained Repair Weld 6. These two planes of polish were about 0.38 mm (0.015 in.) apart. Etched, 20×.

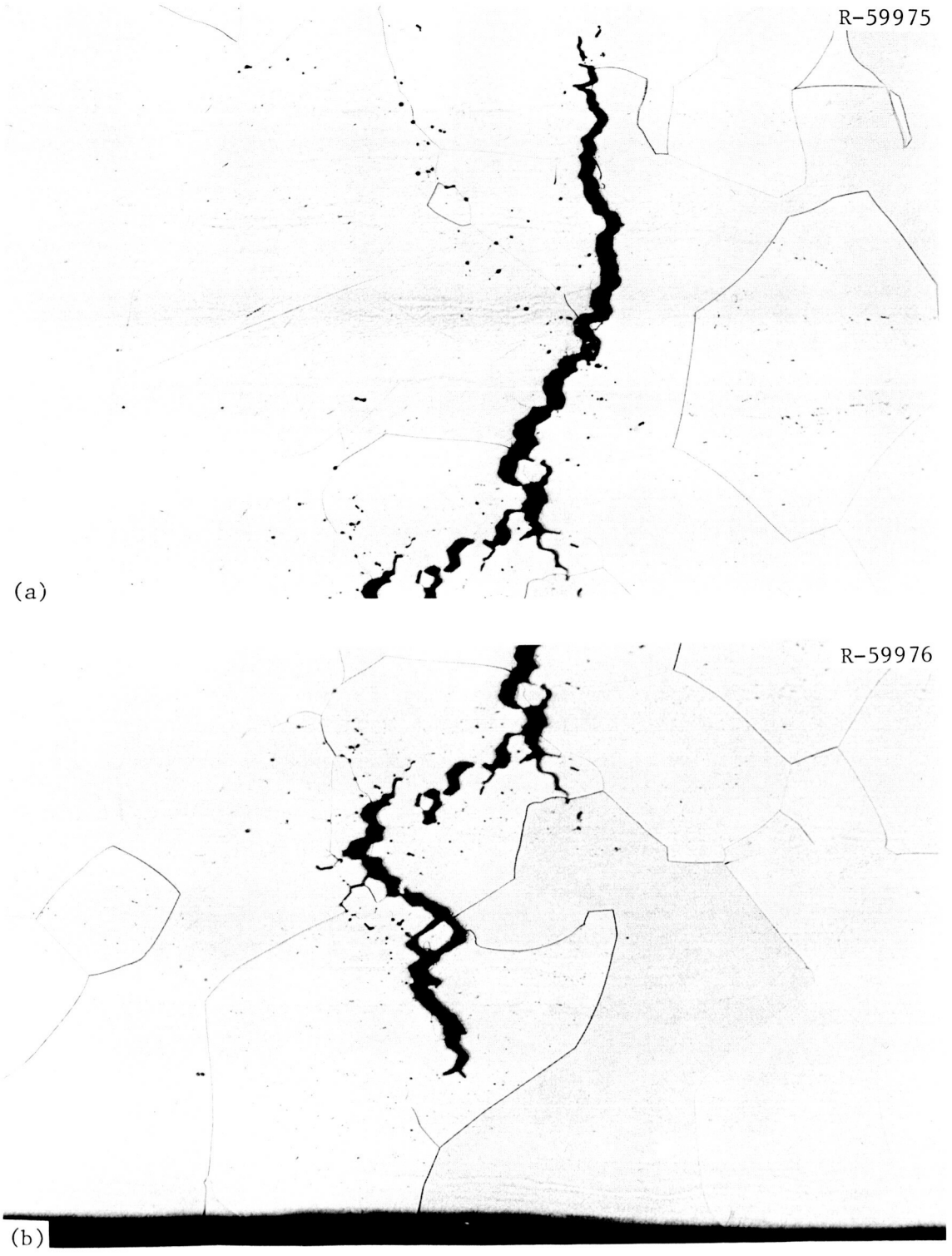

Fig. 51. Crack in T-111 Tubing that Contained the Tack Weld Failure and Repair Weld 6. Etched, 100×. This is a higher magnification view of the plane of polish shown in Fig. 50(b).

Chemical Analyses of Loop Components

Analysis of T-111 for Tungsten and Hafnium

Insert tab specimens from zones in the loop that showed relatively high weight changes were submitted for spectroscopic analysis for tungsten and hafnium. We also analyzed T-111 tubing samples from the same position as that of the tab specimens or close to it. Tubing samples were considerably thicker than the tabs — 1.65 vs 0.86 mm (0.065 vs 0.030 in.) — and were corroded on only one surface, while the tabs were exposed on all sides. The analyses, together with those of as-received or control specimens, are given in Table 10. There is no discernable trend in the tungsten concentration as a function of loop position for either the insert or tubing samples. The insert specimen at the coldest loop position (13-4) shows an increase in hafnium content, while the insert specimen at the hottest position (4-6) has lost hafnium. An increase in hafnium is also apparent in the case of tubing specimen 13 from the coldest position, but the hottest tubing specimen does not show a measurable hafnium decrease.

Later discussions of electron microprobe scans will show that the hotter tubing samples did undergo hafnium depletion, but the losses were apparently too small to be reflected in the bulk analysis of the relatively thick (1.65-mm) tubing.

Interstitial Content of T-111

The leading and trailing edges of one tab specimen per holder were analyzed by vacuum fusion to determine changes in interstitial concentrations (C, O, H, and N). Oxygen, carbon, and nitrogen values are plotted against loop position in Fig. 52. Oxygen had been depleted at all positions. The carbon and nitrogen profiles follow the same pattern as the weight change profile (Fig. 20, p. 29) although nitrogen mass transferred to a much greater extent than carbon. The hydrogen content of the tabs did not exceed 3 ppm.

Also analyzed were samples of the T-111 loop tubing that surrounded the tab specimens and the leading and trailing edges from annular specimens 52B, 55B, and 87, The results for the annular and tubing specimens are given in Table 11. These specimens show the same general trends as the insert tabs, although the oxygen contents of colder specimens tend to be a little higher than in tabs from corresponding locations.

Within the precision of the analyses, no consistent differences in interstitial content appear between the leading and trailing edges of either the tab or annular inserts.

Table 11 also shows the interstitial contents of the control specimens exposed to the vacuum chamber atmosphere for 1735 hr. They show a slight uptake of oxygen, similar to that observed for tubing specimens from the colder regions of the loop.

Table 10. Tungsten and Hafnium Concentrations in Specimens from Loop

Specimen	Distance from Pump Outlet		Approximate Temperature (°C)	Content, wt %	
	(m)	(in.)		W	Hf
	0.76-mm-thick Insert Tab Specimens				
13-4	2.21	87	1200	7.9	2.10
14-15	3.30	130	1230	7.9	1.95
15-23	4.40	173 1/4	1270	8.2	1.90
16-27	5.24	206 1/2	1301	7.9	2.05
1-37	5.73	225 1/2	1329	8.1	1.95
4-56	8.58	337 3/4	1365	7.9	1.80
6-72	10.81	425 3/4	1309	8.2	1.93
7-79	11.79	464 1/4	1274	7.9	1.87
As received				8.0	1.93
Control			1370	7.8	1.98
Control			1205	8.2	2.02
	13-mm-diam Tubing				
13	2.21	87	1200	7.1	2.4
15	4.40	173 1/4	1270	7.7	2.1
16	5.24	206 1/2	1301	7.9	2.0
3[a]	8.08	318 1/4	1365	7.5	2.1
As received				7.9	2.1
	22-mm-diam Tubing				
6	10.81	425 3/4	1309	7.5	2.3
7	11.79	464 1/4	1274	7.5	2.2

[a]Annular specimen 52B was also in this location.

Table 11. Interstitial Contents of T-111 Tubing Samples and Annular Specimens

Specimen	Distance from Pump Outlet		Interstitial Content (ppm)			
	(m)	(in.)	C	H	O	N
	Tubing Specimens					
13	2.03	80	10	<1	98	18
14	3.05	120	20	3	20	12
15	4.19	165	20	2	17	6
16	4.95	195	30	2	20	2
1	6.22	245	20	<1	12	2
3[a]	7.87	310	20	<1	19	2
4[a]	8.26	325	20	<1	19	2
6	10.54	415	<10	4	42	4
7	11.43	450	10	<1	20	5
8[a]	20.32	800	20	2	42	18
	Annular Insert Specimens					
52B-L	7.87	310	20	2	16	3
-T	7.87	310	20	4	21	4
55B-L	8.26	325	20	4	29	3
-T	8.26	325	20	4	22	2
87B-L	20.32	800	20	4	32	22
-T	20.32	800	30	5	120	23
	Control Specimens					
1204°C Anneal			60	<1	90	18
1370°C Anneal			60	2	170	20
As received			60	<1	70	15

[a]The annular specimens tested were contained by these sections of tubing.

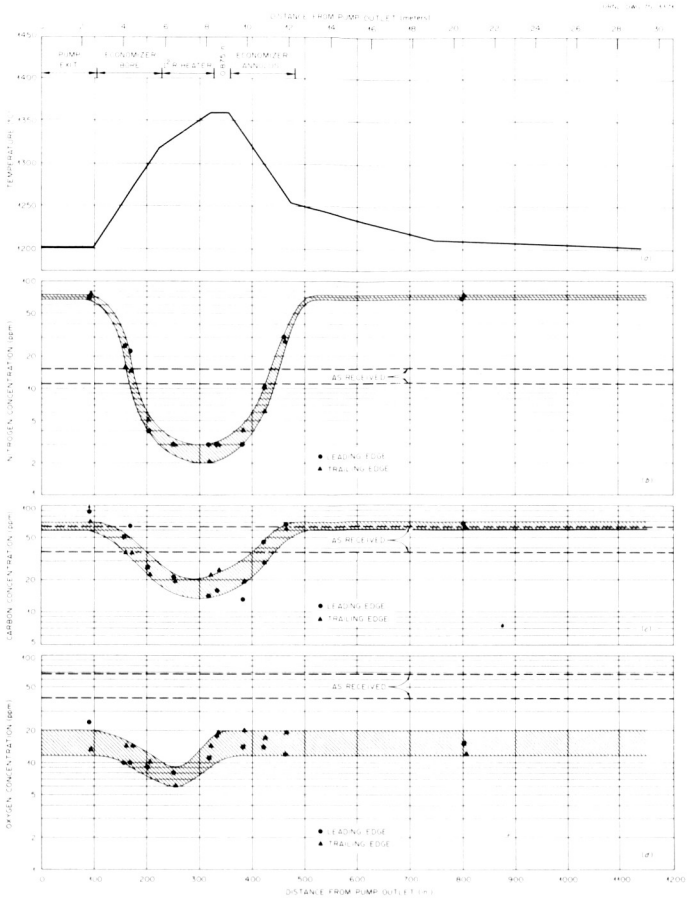

Fig. 52. Oxygen, Carbon, and Nitrogen Contents of T-111 Insert Tab Specimens at Various Loop Positions.

X-Ray Fluorescence Analysis

The surfaces of the insert tab specimens were analyzed by x-ray fluorescence for hafnium, tantalum, and tungsten to establish a concentration profile around the loop. The results of these analyses are shown in Fig. 53 along with the results from an as-received T-111 specimen. The analyses provide a relative measure of the surface concentration of the designated metal atom but are qualitative since the x-ray beam used in the analysis penetrates a small distance below the surface. The apparent loss of tungsten and tantalum in the cooler regions of the loop is caused by the partial masking of the base metal from x rays by a hafnium-rich surface deposit. For more quantitative values see the next section on electron-microprobe analysis of the insert tab specimens.

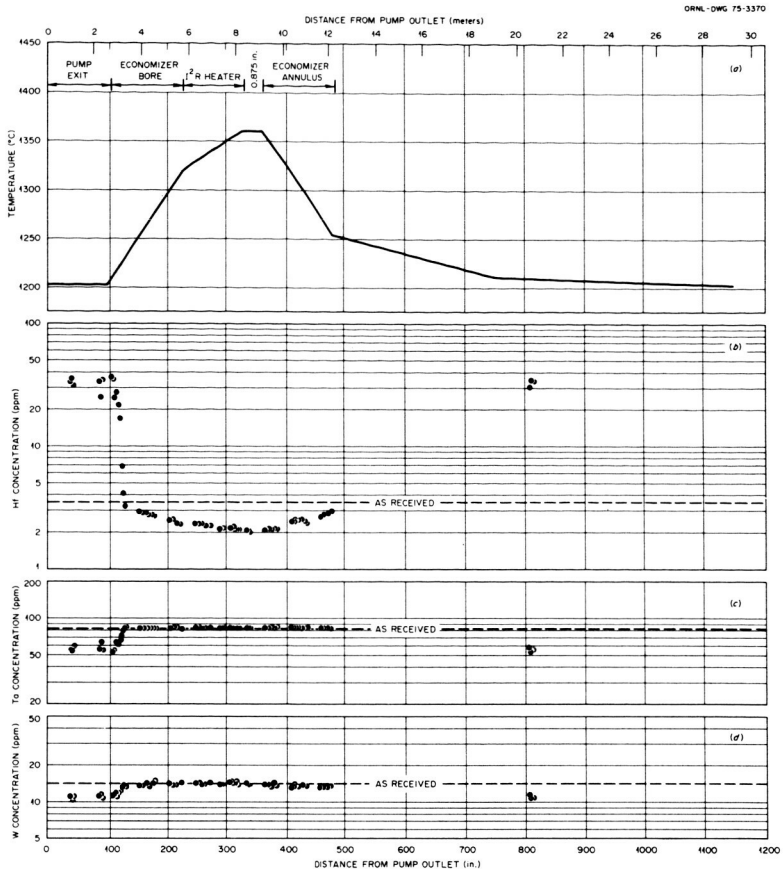

Fig. 53. Apparent Hafnium, Tungsten, and Tantalum Profiles Around the Loop, as Determined by X-Ray Fluorescence of the Surfaces of the T-111 Insert Tab Specimens.

The losses and gains in hafnium concentration around the loop (Fig. 54) showed a direct correspondence with the magnitude and sign of the weight change (Fig. 20, p. 29) and also the nitrogen change (Fig. 52). The temperature dependence of the surface hafnium concentration shown in Fig. 53 was also similar to the weight change temperature dependence (Fig. 21, p. 29). However, weight change differences apparent between tab specimens at similar temperature positions in the heater and economizer did not carry over to the surface hafnium concentration; that is, economizer and heater specimens at equivalent temperatures underwent the same change in hafnium content at the surface, despite differences in lithium flow rate.

Electron-Microprobe Analysis

Insert tab specimens were selected from various positions around the loop for electron-microprobe analyses. The probe beam impinged directly on the tab surfaces to determine surface hafnium concentrations, and then a polished cross section of the same tab was traversed to

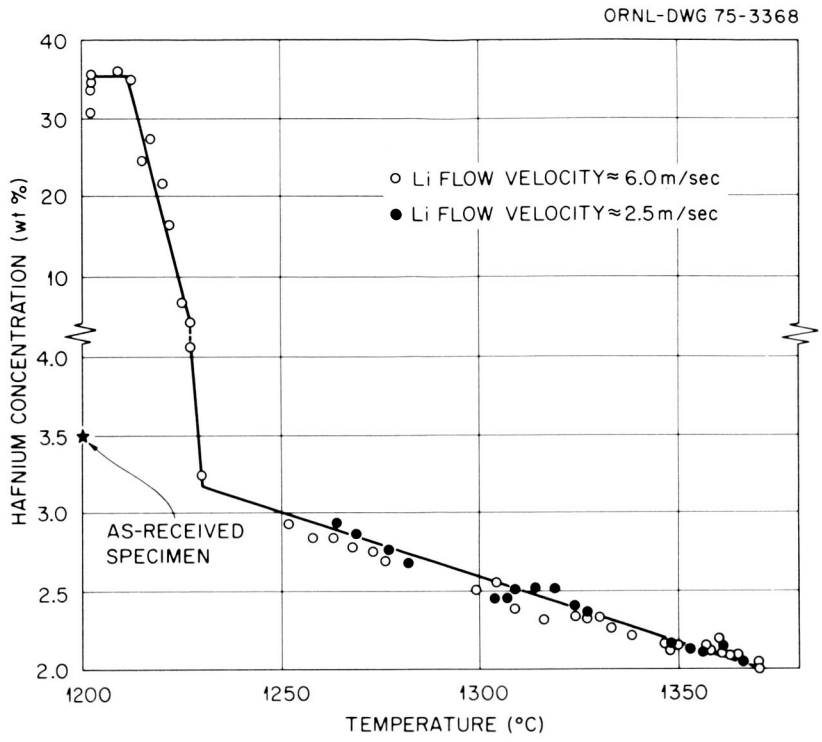

Fig. 54. Temperature Dependence of Surface Hafnium Concentration.

determine the hafnium gradient. In one case the tungsten gradient was also measured. The specimens selected and the results of the surface analysis are given in Table 12. The hafnium gradients on the polished cross sections of seven tab specimens are plotted in Appendix F. The hafnium and tungsten gradients for tab specimen 3-52, which was in the maximum temperature region of the loop (1365°C), are shown in Fig. 55. The hafnium concentration of this specimen was depleted to about 60 μm below the surface of the specimen, whereas no change in the tungsten content was detectable. The average concentration of hafnium in the interior of the specimen is 1.87 wt % and at the surface is 0.79 wt %. The "surface" values indicated in the microprobe analyses of the polished sections are actually the values obtained from an estimated effective hemispherical volume of about 20 μm^3 that was excited by the electron beam; the outer limits of this hemisphere crossed the edge of the cross section for near-surface measurements. For example, excellent agreement exists for specimen 3-52 between the surface analysis shown in Table 12 and the "surface" analysis as determined from the polished cross section, 0.81 and 0.79 wt %, respectively. Conversely, what appears to be a discrepancy between the two types of surface analyses for specimens 13-6 and 8-87 (Table 12 and Appendix F) is really the influence of the composition of the T-111 just below the hafnium-rich deposit on the surface of the tab specimen.

Table 12. Electron-Microprobe Analyses of the Surfaces of Insert T-111 Specimens From the FCLLL-1 Loop

Specimen	Position in Loop[a]		Approximate Temperature (°C)	Hafnium Concentration, wt %	
	(m)	(in.)		Range	Average[b]
13-6	2.35	92 1/2	1200	88[c]	
15-18	4.05	159 1/2	1258	1.46–1.71	1.55
15-22	4.33	170 1/2	1268	1.34–1.64	1.42
16-26	5.17	203 3/4	1299	1.06–1.34	1.17
3-52	8.08	318 1/4	1365	0.77–0.94	0.81
4-55	8.51	335	1370	0.47–0.88	0.75
5-64	9.72	382 3/4	1348	0.88–0.96	0.91
6-71	10.74	423	1312	1.11–1.36	1.21
7-77	11.72	461 1/2	1277	1.16–1.44	1.34
8-87	20.39	802 3/4	1205	80[c]	
Control			1204	0.76–1.21	1.04
Control			1370	1.54–1.68	1.58
As received				1.62–1.93	1.87

[a]Distance from pump outlet to center of tab specimen.

[b]Average based on five analyses per specimen.

[c]Only maximum values reported.

In addition to the tab specimens described above, polished cross sections of T-111 tubing that had contained specimen holders 13, 15, 3, 6, and 8 (Fig. 15, p. 22) were submitted for electron microprobe analysis to determine hafnium gradients near the inner surface of the tubing. Detailed results are given in Appendix F. Tubing from holder positions 15, 3, and 6 showed a loss of hafnium to a depth of about 80 μm from the inner surface. The holder 3 position showed the greatest loss of hafnium, in accord with tab specimen results. The average interior concentration of hafnium was 1.98 wt %, and the average surface value was 0.90 wt %. We analyzed both the exterior and interior near-surface regions on tubing from positions 15 and 8. There was no indication of loss of hafnium from the outer surface region of tubing specimen 8, which has been exposed to vacuum. However, there was a loss of hafnium from both the outer and inner surface regions of tubing specimen 15 from the economizer section. The average concentration of hafnium was 2.11 wt % in the interior of specimen 15 and had decreased to a surface value of 1.56 wt %.

Metallographic examination of the tubing specimens in the as-polished condition disclosed the presence of a precipitate along the grain boundaries in the tubing specimen that contained holder 6. The results of microprobe analysis showed the grain boundary precipitate to be hafnium rich.

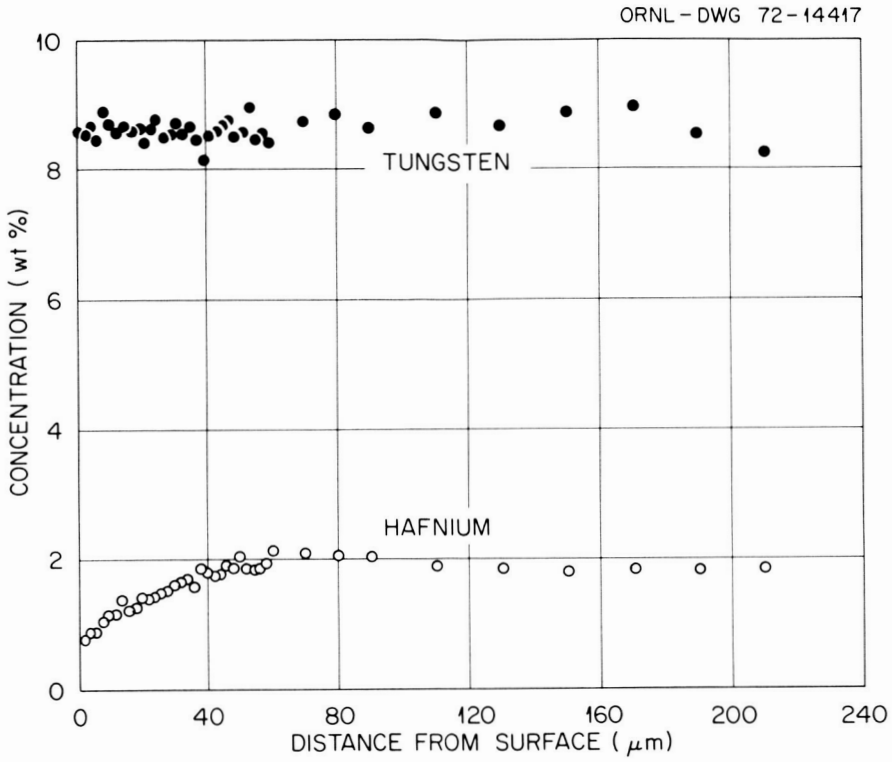

Fig. 55. Results from Simultaneous Electron Microprobe Analyses for Tungsten and Hafnium in a Polished Section Through a T-111 Insert Tab Specimen from the Highest Operating Temperature Region (1365°C) in the Loop.

Mechanical Properties

Bend and Tensile Tests

Fifteen T-111 tab specimens were selected for bend testing. They included tab inserts from various positions around the loop together with as-received and control specimens. The bend tests were intended to determine the ductility, springback, and relative strength of the tab specimens. The bends were made with a table-model Instron machine and in accordance with the procedure as outlined in Appendix G. The results are compiled in Table 13. None of the bend specimens failed or developed cracks as a result of testing; the appearance of representative specimens is shown in Fig. 56.

Subsequently, 16 miniature sheet tensile specimens were machined from the insert tab specimens that represented conditions around the loop. In addition, tensile specimens were machined from as-received and control tab specimens. A schematic of the miniature sheet tensile specimen is shown in Fig. 57. The resultant room-temperature mechanical properties are compared with operating temperatures in Fig. 58. Both

Table 13. Results of Bend Tests[a] Made on As-Received, Control, and Insert Tab Specimens

Tab Specimen	Operating Temperature (°C)	Bend Angle, deg		Springback (deg)	Strength, GPa(ksi)	
		Under Load	No Load		Ultimate	Yield[b]
As received		135	112	23	1.28(186)	0.93(135)
As received		140	112	28	1.31(190)	0.98(142)
Control	1204	135	112	23	1.29(187)	0.88(128)
Control	1371	135	112	23	1.15(167)	0.80(116)
13-6	1204	133	110	23	1.12(163)	0.79(114)
15-18	1259	135	113	22	1.13(164)	0.78(113)
15-22	1272	135	114	21	1.10(159)	0.74(108)
16-26	1301	135	113	22	1.07(155)	0.70(102)
1-36	1337	135	112	23	0.99(144)	0.68(98)
3-52	1367	135	114	21	1.08(156)	0.73(106)
4-55	1371	135	112	23	1.02(148)	0.72(105)
5-64	1358	135	112	23	1.08(157)	0.72(105)
6-71	1306	135	112	23	1.14(165)	0.77(112)
7-77	1264	135	112	23	1.18(171)	0.81(118)
8-87	1214	135	112	23	1.19(172)	0.83(120)

[a]Testing speed of 85 μm/sec (0.2 in./min) at room temperature.

[b]Commonly referred to as "modulus of rupture" in bend tests.

R-59979

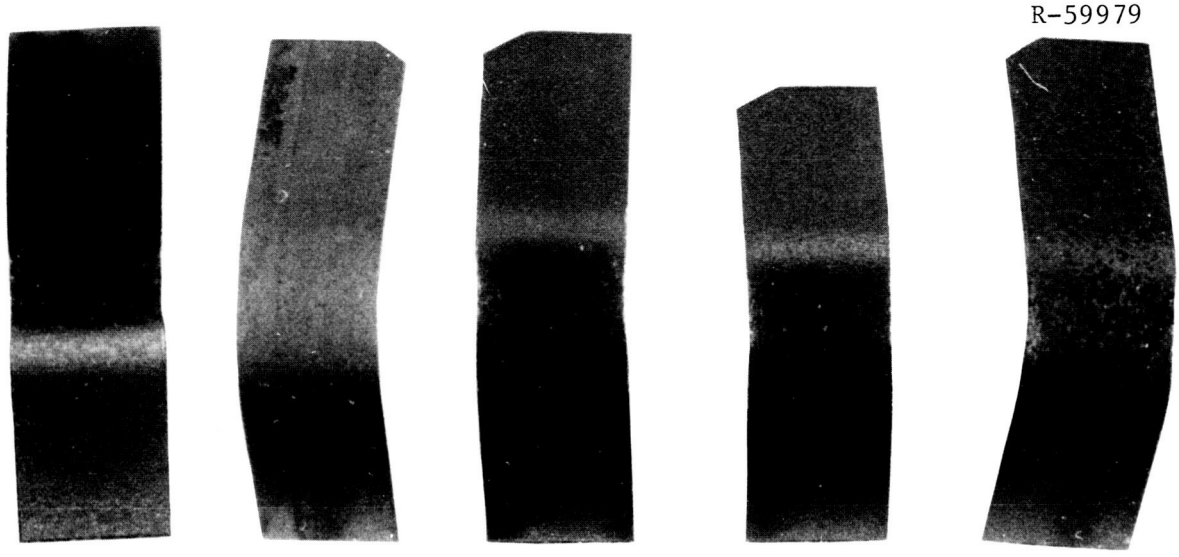

Fig. 56. Appearance of Representative T-111 Tab Specimens After Bend Testing. 3×. Left to right: As Received, 13-6, 15-18, 16-26, and 4-55.

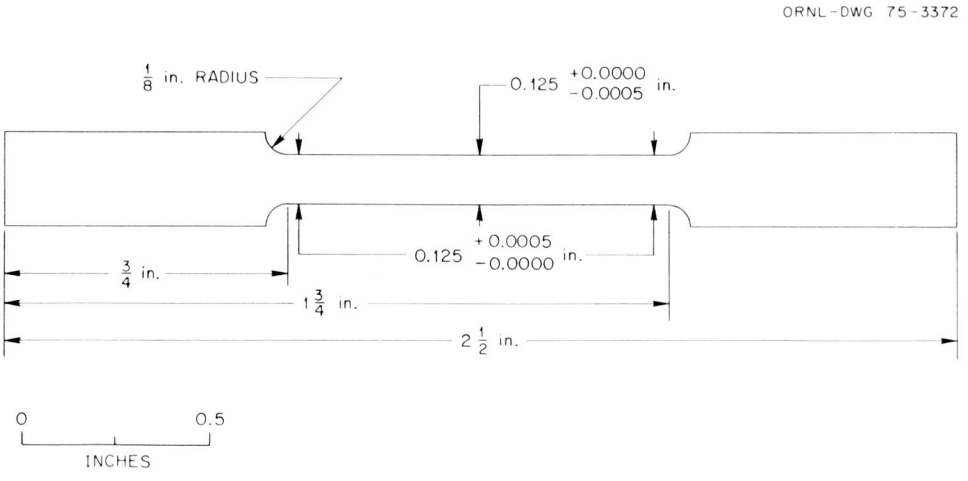

Fig. 57. Schematic of Miniature Sheet Tensile Specimens Machined From T-111 Insert Tab Specimens. Original dimensions of tab specimens were 0.76 × 3.2 × 64 mm (0.030 × 1/4 × 2 1/2 in.). 1 in. = 25.4 mm.

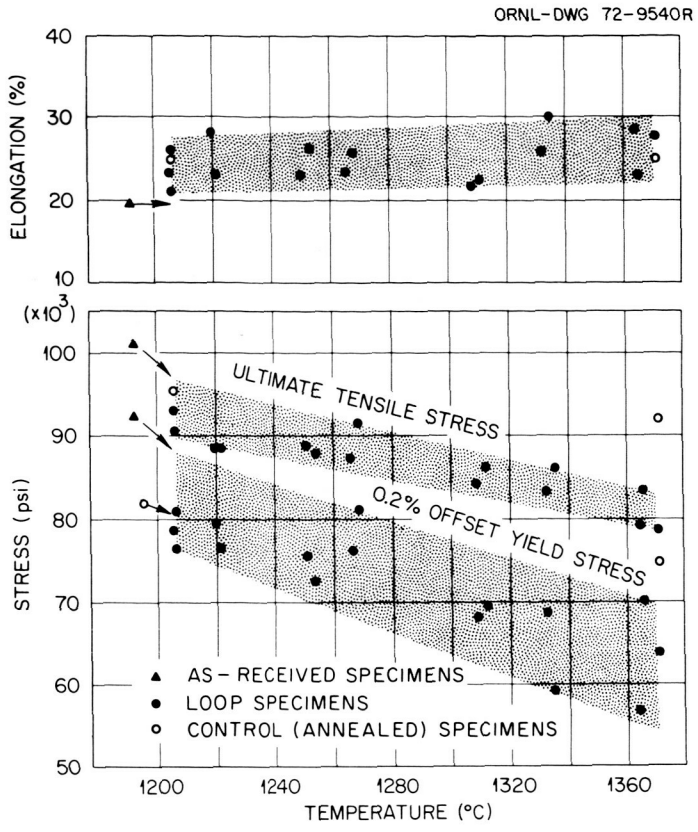

Fig. 58. Effect of Operating Temperature on the Room-Temperature Elongation, Ultimate Strength, and 0.2% Offset Yield Strength of the T-111 Miniature Tensile Specimens from the Forced-Circulation Lithium Loop. 1000 psi = 6.895 MPa.

the control (vacuum-annealed) and lithium-exposed specimens decreased in ultimate and 0.2% offset yield strengths as compared with as-received material, while the elongation remained essentially unchanged. Specimens annealed at 1204 and 1370°C had nearly the same tensile properties at room temperature. The specimens exposed to lithium at 1204°C had properties comparable with the thermally aged control specimens, but lithium-exposed specimens at 1370°C were noticeably weaker than the annealed specimens. This weakening is not unexpected in view of the large grain size and interstitial depletion of the latter specimens.

To determine if the T-111 tubing had developed a sensitivity to low-temperature cracking, ring-shaped sections of the loop tubing were crushed in a vise at room temperature. None of the tubing sections cracked during the crush test. The identity of the T-111 tubing sections and appearance after crush testing are shown in Fig. 59.

Fig. 59. Sections of T-111 Loop Tubing After Crush Testing, Exact size. Left to right: Edge view of sections 6, 3, 16, 15, and 13; frontal view of sections 6, 3, 16, 15, and 13. The numbers refer to the tubing sample positions identified in Table 7, p. 32.

Microhardness Measurements

We determined the room-temperature microhardness of four T-111 tab specimens that covered the full range of ultimate and yield strengths as determined from mechanical property testing. Two of the tab specimens came from the maximum and minimum temperature regions of the loop; one was an as-received specimen; the fourth specimen was a control specimen thermally aged at 1204°C. Since tantalum and tantalum-base alloys are subject to work hardening, microhardness tests were made with loads that ranged from 0.1 to 1.0 kg to see what influence localized strain in the region of the indentation might have on diamond pyramid hardness (DPH). The results from these tests are given in Table 14. The individual DPH value given for each specimen represents an average of at least four indentations. Since there was no obvious trend in DPH with load, the average values listed at the right of the table were used for comparison with the ultimate and yield strengths in Table 15. As can be seen, there is no significant difference in the variation of DPH values with the variation in mechanical properties.

Table 14. Microhardness Values (DPH) for T-111 Tab Insert Specimens

Specimen	Exposure Temperature (°C)	Microhardness, DPH at Given Indenter Loads (kg)					
		1.0	0.6	0.4	0.2	0.1	av
As received		239	268	267	265	284	265
Control	1204	252	264	261	277	267	267
14-14	1227	251	251	237	247	248	256
4-55	1370	256	259	268	267	261	262

Table 15. Comparison of Ultimate and Yield Strengths of T-111 Tab Insert Specimens with Microhardness Values

Tab Insert Specimen	Stress, ksi		Average Hardness (DPH)
	Ultimate	Yield 0.2% Offset	
4-55	81.5	63.5	262
14-14	90.5	78.0	256
1204°C Control	94.2	81.0	267
As received	101.0	92.5	265

DISCUSSION

It is informative to compare the present forced-circulation lithium loop (FCLLL) results with the results of a much smaller tantalum-alloy thermal-convection loop, which circulated lithium for 3000 hr at a maximum temperature of 1350°C. The latter loop was composed of the alloy T-222, which is similar in composition to T-111, as shown below:

Alloy	Nominal Composition, wt %			
	Hf	W	C	Ta
T-111	2	8	0.01	Bal
T-222	2.5	9.5	0.01	Bal

The loop geometry and test procedures were the same as reported earlier for niobium alloy loops.[6,7] The loop was constructed of 25-mm-OD by 1.05-mm-wall (1 by 0.015-in.) tubing and was 1.65 m (65 in.) in overall length. The lithium velocity was approximately 36 mm/sec (7 ft/min).

The temperature profile and weight changes for the thermal-convection loop test are given in Fig. 60. The weight change profile correlated closely with the migration patterns for hafnium and interstitial impurities, which are shown in Figs. 60(c) and 61, respectively.

---

[6] J. H. DeVan and C. E. Sessions, "Mass Transfer of Niobium-Base Alloys in Flowing Nonisothermal Lithium," *Nucl. Appl.* 3: 102–09 (1967).

[7] C. E. Sessions and J. H. DeVan, "Thermal Convection Loop Tests of Nb–1% Zr Alloy in Lithium at 1200 and 1300°C," *Nucl. Appl.* 9: 250–59 (1970).

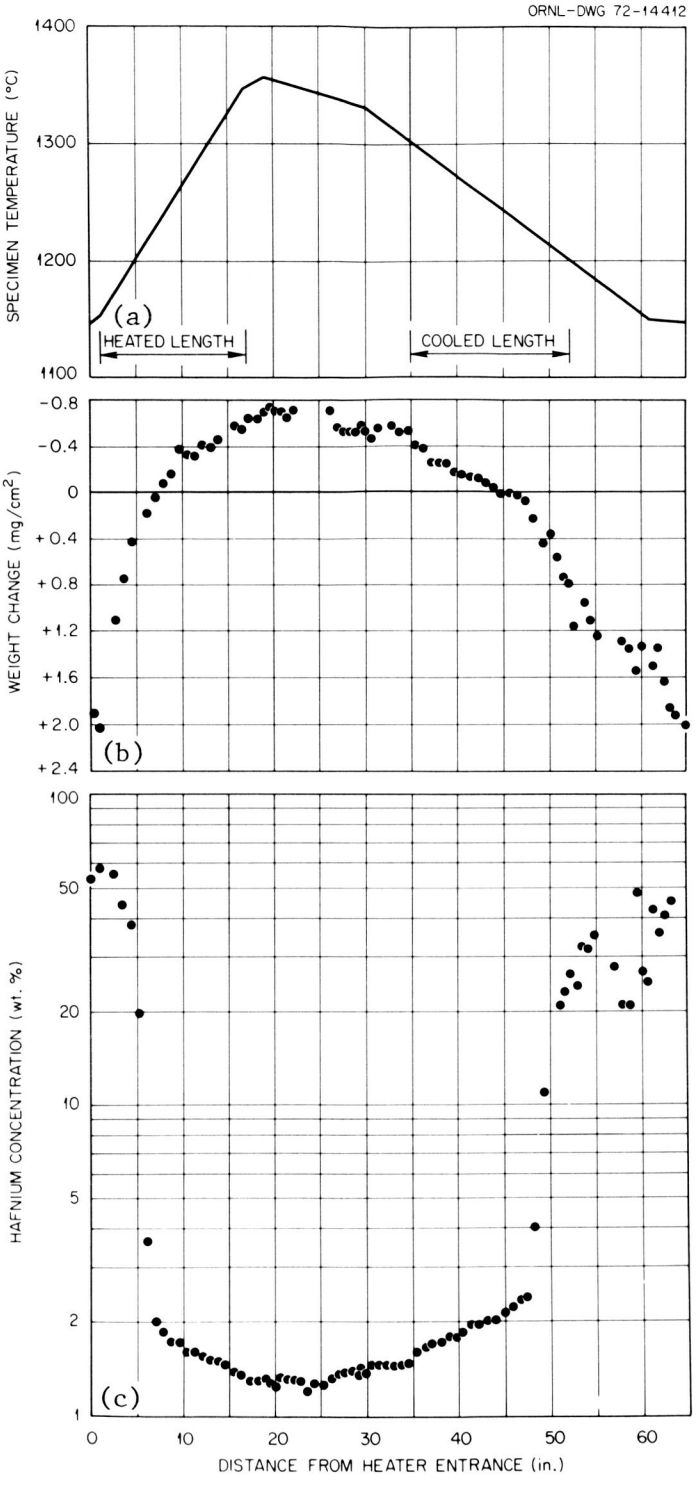

Fig. 60. Weight and Composition Changes Occurring as a Function of Loop Position in Lithium T-222 Thermal-Convection Loop. (a) Loop temperature profile; (b) weight change profile; (c) after-test concentration of hafnium at specimen surfaces.

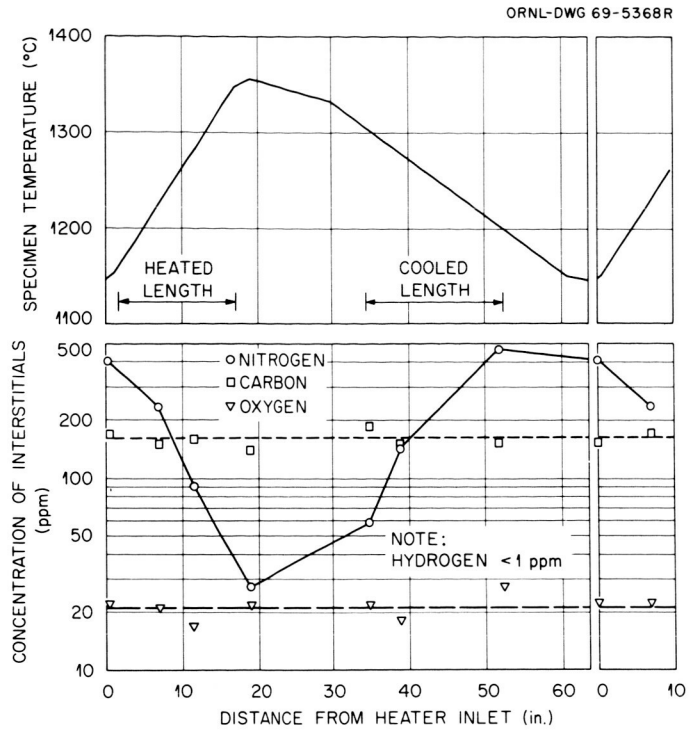

Fig. 61. Changes in Concentration of Interstitial Impurities in Insert Specimens from T-222 Thermal-Convection Loop.

The latter show strong similarities to the hafnium and interstitial concentration patterns observed in the higher velocity FCLLL test (Figs. 52 and 53).

The test data for insert specimens contained at the hottest and coldest positions of the respective loops can be compared in Table 16. The maximum weight losses were essentially the same between the two loop types; however, the thermal-convection loop showed a higher specific weight gain. It is evident from Table 16 that hafnium and nitrogen migration accounted for a higher fraction of the overall weight change in the case of the thermal-convection loop than the higher velocity loop. Also the thermal-convection loop apparently had a higher total concentration of nitrogen in the system (most likely as an impurity in the lithium) at the onset of test, and this probably caused the higher hafnium migration in that test.

In view of the differences in hafnium depletion, the similarity in weight loss between the two loops indicates that there was more mass transport of tantalum and/or tungsten in the higher velocity loop. Another indication of tantalum mass transport in the forced-flow loop (FCLLL) was evidenced by changes in the corrosion rate as a function of lithium velocity in the latter loop. Although the depletion of hafnium at a given temperature in FCLLL was the same at lithium velocities of 6.0 and 2.5 m/sec, respectively (Fig. 54), the weight loss at a given temperature was higher at the higher velocity (Fig. 21, p. 29). The weight loss difference obviously reflects tantalum and tungsten.

Table 16. Chemical and Weight Changes Incurred by Insert Specimens in Thermal-Convection Loop (TCL) and Forced-Convection Loop (FCLLL)

Loop System	Specimen Temperature (°C)	Weight Change (mg/cm^2)	Hafnium Surface Concentration,[a] %		Nitrogen Concentration, ppm	
			Before Test	After Test	Before Test	After Test
TCL	1350	−0.70	3.0	1.3	17	24
FCLLL	1370	−0.72	3.5	2.0	15	3
TCL	1150	+2.02	3.0	58.9	17	460
FCLLL	1200	+0.71	3.5	35.6	15	760

[a]Determined by x-ray fluorescence.

Hafnium transport in these systems shows a close parallel with zirconium transport in Nb–1% Zr loop systems tested with lithium at 1200 and 1300°C. Note, for example, the similarity in the zirconium surface concentrations measured in Nb–1% Zr thermal convection loops,[6,7] shown in Fig. 62, and the hafnium surface concentrations in Figs. 54 and 60(c). Furthermore, the zirconium concentration changes, coupled with interstitial impurity migration, accounted for the bulk of the weight changes occurring in Nb–1% Zr systems, and transport of niobium was almost negligible. An earlier report[7] discussed the kinetics of zirconium transport in Nb–1% Zr systems containing lithium, and these same kinetic models appear to describe the transport of hafnium in our tantalum loops. The models also predict hafnium transport to be independent of the lithium velocity, in accord with our loop results.

Buzzard and Sheffler[8] investigated the effect of high-temperature lithium and vacuum on the tensile properties of T-111 at temperatures similar to the present investigation. Although their lithium tests were conducted in static capsules, the results were surprisingly similar to those that we obtained under dynamic flow conditions. For example, the room-temperature ultimate and yield strengths of T-111 specimens exposed to lithium for 5000 hr at 1315°C in static capsules were 538 and 462 MPa (78 and 67 ksi), respectively. These compare with ultimate and yield strengths of 558 and 428 MPa (81 and 62 ksi), respectively, under forced flow conditions for 3000 hr at 1370°C. Similarly, the tensile elongations were 28 and 26% for the capsule and loop, respectively. Exposures to static lithium at 1315°C also resulted in about the same grain growth in the T-111 as observed at a comparable temperature in our test loop.

[8]R. J. Buzzard and K. D. Sheffler, *Effect of Long-Time, Elevated-Temperature Exposures to Vacuum and Lithium on the Properties of a Tantalum Alloy, T-111*, NASA-TN-D-7548 (1974).

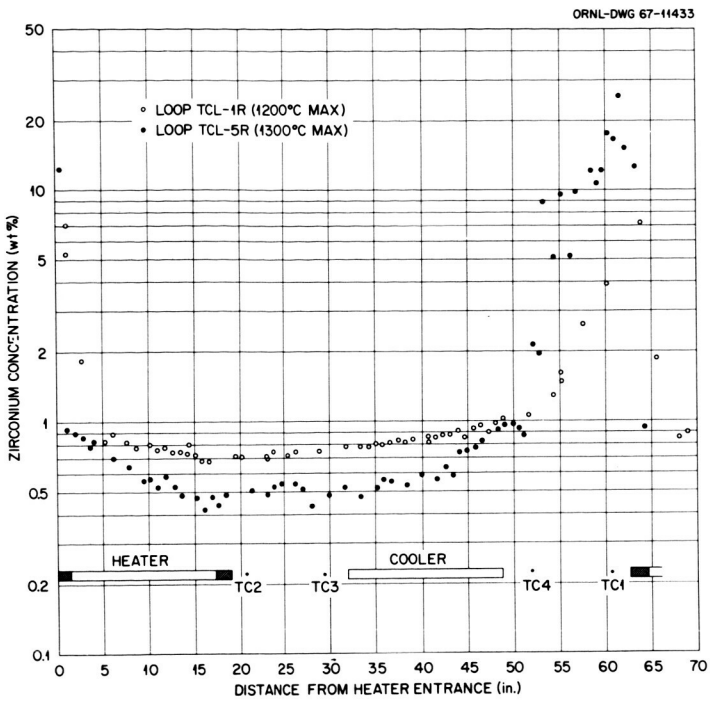

Fig. 62. Zirconium Surface Concentrations of Nb—1% Zr Loops Operated with Lithium. 1 in. = 25.4 mm.

Buzzard and Sheffler ascribe the strength reduction in lithium to a depletion of oxygen in solid solution, which suppresses an otherwise operative strain aging effect. Our test provides further support for this conclusion, since the only effect common between the respective tests was the depletion of oxygen from the T-111. In particular, carbon and nitrogen were depleted from the higher temperature specimens in our loop test but not in the static capsule test. Hence, these latter elements appear to have less effect on tensile properties than does oxygen.

One significant difference between the results of Buzzard and Sheffler and our own concerns the vacuum exposures. Specimens exposed by the former at 1315°C were slightly deoxidized, while our specimens exposed at 1315 to 1370°C did not change in oxygen. This deoxidation resulted in a larger grain size and greater decrease in tensile strength in the former tests than occurred for our vacuum-exposed specimens.

Thermal aging can strongly affect the ductility response of T-111 to small amounts of interstitial impurities. For example,[9] T-111 is extremely sensitive to hydrogen embrittlement during handling after long-term aging at 1040°C (1900°F). Although this problem is apparently less severe for specimens aged in the FCLLL temperature range (1200—1370°C), we were

---

[9]G. K. Watson and J. R. Stephens, *Effect of Aging at 1040°C (1900°F) on the Ductility and Structure of a Tantalum Alloy, T-111*, NASA-TN-D-6988 (October 1972).

nevertheless concerned whether small amounts of hydrogen would be introduced into the metal by the stripping technique used to remove residual lithium after test. Earlier problems of hydrogen embrittlement were actually encountered in lithium capsule tests of T-111 in which residual lithium had been removed by chilled alcohol.[10] According to the tensile and bend test results for inserts and loop tubing, the anhydrous ammonia dissolution technique adopted for FCLLL appears to have obviated the hydrogen problem, at least under the aging conditions of the test.

Another cause of embrittlement of T-111 is the introduction of small amounts of oxygen at temperatures in the range 800 to 1000°C. In tests of Inouye and Liu,[11] the addition of as little as 300 ppm O to T-111 at 825°C reduced the tensile elongation to only 1.6% at room temperature. Subsequent aging at 1093°C did not noticeably increase the elongation; however, aging at 1200°C or above restored the ductility to that of an uncontaminated alloy. The colder sections of our loop tubing, where the external surface was exposed directly to vacuum, increased in oxygen content to as high as 98 ppm (Table 11, p. 64). However, all these sections operated at a temperature of 1200°C and remained ductile in flattening tests (Fig. 59).

Four butt welds joining various tubing sections of FCLLL were sectioned after test, and in two cases the fusion zone of these welds showed limited ductility in flattening tests at room temperature (Figs. 40 and 42, pp. 50 and 52). The ductility response of these welds appeared to be controlled by the level of interstitial impurities, and the effect of service temperature was not discernable from the samples selected. The two FCLLL welds that survived the flattening test contained less than 100 ppm O and essentially no hydrogen. The welds that cracked showed an abnormally high hydrogen concentration (5–6 ppm) and, in one case, an abnormally high oxygen concentration (600 ppm).

Two of the welds selected for examination were final assembly welds and did not receive a postweld heat treatment. Although the heat treatment did not appear to have been a factor in the after-test ductility of the welds, its ommission may have affected the resistance of the welds to lithium attack. There were grain boundary separations in the heat-affected zone near the root of both field welds (Fig. 43, p. 53). The separations were possibly produced by shrinkage stresses during welding. However, the increase in oxygen content during welding (Table 9, p. 50) would definitely have "sensitized" the welds to lithium attack without the postweld treatment.[12] Although the field welds were adequate for the service requirements in this loop test, the welding procedure obviously needs

---

[10]C. E. Sessions and J. H. DeVan, *Effect of Oxygen, Heat Treatment, and Test Temperature on the Compatibility of Several Advanced Refractory Alloys with Lithium*, ORNL-4430 (April 1971).

[11]H. Inouye and C. T. Liu, *Low Pressure Oxidation of T-111 and Effect on Tensile Properties*, ORNL-TM-4621 (August 1974).

[12]E. E. Hoffman, *Effects of Oxygen and Nitrogen on the Corrosion Resistance of Columbium to Lithium at Elevated Temperatures*, ORNL-2675 (January 1959).

further development. The arc position must be better stabilized to avoid the misalignment evident in Fig. 43(c). Also a higher degree of purity must be established in the inert purge gas, particularly in the crevice between the backing ring and the inner tube wall.

CONCLUSIONS

Corrosion of the tantalum alloy T-111 by flowing lithium was evaluated in a pumped loop operated for 3000 hr at a maximum temperature of 1370°C. The major findings were:

1. The mass transport rates of T-111 were relatively small under the test conditions as judged from the weight changes of sleeve and tabular insert specimens. In terms of uniform wall thinning, the maximum dissolution rate was less than 1.3 μm/year.

2. Hafnium was preferentially removed from the hotter T-111 loop surfaces and was deposited on the colder surfaces. Microprobe examination showed that the loss of hafnium from the highest temperature region was confined to a depth less than 60 μm below the exposed surface. Nitrogen and, to a less extent, carbon also migrated from the high-temperature to the low-temperature loop regions. A thin hafnium carbonitride deposit was visible where the deposition of these components was heaviest. All insert specimens were depleted of oxygen.

3. Metallographic examination showed no microstructural changes in the inserts or loop tubing other than grain growth at exposure temperatures above 1300°C. Control specimens annealed in vacuum at 1370°C exhibited little or no grain growth. Accordingly the grain size increase of lithium-exposed specimens was related more to the depletion of interstitial impurities than to the test temperature *per se*.

4. The corrosion behavior of T-111 under the present forced-convection test conditions was not substantially different from that obtained previously under slower flow, thermally convecting conditions. Hafnium and nitrogen were the major elements mass transferred under both flow conditions, although the transfer of tantalum and tungsten did increase as a function of lithium velocity.

5. The transfer of hafnium in the T-111-lithium system appears to be a close analog of the transfer of zirconium in the Nb–1% Zr-lithium system. The transfer rate of both these elements appears to be controlled by the initial concentration of nitrogen in the system and by the solid-state diffusion rates of the elements in the respective alloys.

6. The room-temperature tensile strength of T-111 specimens exposed at the highest loop temperature was significantly lowered compared with control specimens exposed to vacuum at an equivalent temperature. The decrease in strength appeared to be related to the increased grain size and changes in interstitial impurity concentration produced by the lithium. Comparison with results obtained in static lithium showed that the major cause of the grain growth and associated room-temperature strength loss was a decrease in oxygen concentration, and that additional decreases in nitrogen and carbon concentrations had little added effect.

ACKNOWLEDGMENT

David L. Clark and W. R. Huntley (Reactor Division) were in charge of the overall design and fabrication of the experiment. Bertram Fleisher and R. E. McDonald (Metals and Ceramics Division) were responsible for the specification, procurement, and fabrication of the T-111 material and for all metallurgical and control specimens.

G. W. Greene (Instrument and Controls Division) was responsible for the instrumentation of the loop and was assisted by W. W. Johnston, Jr., on temperature measurement problems.

APPENDIX A

REPORT OF TRIP TO KOKOMO, INDIANA, FOR ANNEALING OF T-111 ASSEMBLIES

B. Fleischer and J. B. Phillips

INTRODUCTION

The T-111 assemblies discussed in this report are portions of a refractory metal forced circulation loop that will contain lithium to 2500°F. These assemblies were fabricated using many weld joints. It has been shown by various researchers that welds severely contaminated with oxygen will fail rapidly when exposed to lithium. It has also been demonstrated that annealing for several hours at 2400°F will completely eliminate the adverse corrosion behavior of contaminated welds. Even though the welds made in assembling these parts were performed under clean, inert, dry-box conditions, the possibility of undiscovered weld contamination makes it prudent to insure against this possibility by annealing. The cost of this insurance is inconsequential compared to the cost of materials and labor already invested in the assemblies.

PROCEDURE

A requisition was issued to the Purchasing Department on July 2, 1968, to arrange for annealing of T-111 assemblies. After appropriate bidding procedures conducted by AEC, the contract was awarded on August 28, 1968, to Union Carbide, Materials Systems Division, Kokomo, Indiana. The basic cost was to be $1800 per furnace run plus overtime at $30/hr for the furnace operator as required. Their annealing furnace is described in Appendix A.

During the week of Septmeber 9 to 13, 1968, the assemblies were prepared for annealing. The outer surfaces were wiped with lint-free cloths soaked in alcohol and then wrapped spirally at about 3/4-in. pitch with 0.060-in.-diam Tantalum wire. Tantalum foil 0.001-in.-thick by 2-in.-wide was wrapped at half lap over the wire. The wire serves as a spacer to prevent welding of the foil to the parts. The foil acts as a mechanical barrier to minimize environmental contamination.

After wrapping, the assemblies were placed in plastic bags, sealed, crated in wooden boxes, and placed in a station wagon owned by the government.

On Sunday, September 15, we transported the parts to Kokomo. The following day was used for fixturing the assemblies on the holder. On

Tuesday morning, we placed thermocouples at two probable heat lag positions on the parts. The holder containing the parts was then lowered onto the furnace floor, and the free ends of the thermocouples were threaded up through the furnace lid and through the ceramic compaction fittings. The thermocouples, prepared by Materials Systems Division, were 15-ft-long Pt-6% Rh vs Pt-30% Rh beaded with Al_2O_3. The hot junctions were wrapped in Ta foil to avoid contamination or interaction of the Al_2O_3 beads with the parts.

The furnace was sealed at about 10:30 am, and pumping was initiated. At 11:30 am, the leakup rate was about 6 μ/hr. At about 12:30 pm, the leakup rate was down to 2 μ/hr, and furnace heatup was started. The furnace was programmed to heat at a rate not to exceed 25°F/min and not to exceed a pressure of 5×10^{-5} torr. Holding periods were incorporated at 500°F intervals to reduce thermal gradients. A complete history of the annealing operation is presented in Table 1.

RESULTS AND DISCUSSION

During annealing, the vacuum pressure indicated by the meter readout differed from the recorder readout. Both instruments receive their signals from the same sensor. At a pressure of about 1×10^{-5} torr indicated by the recorder, the meter was reading 2×10^{-5}. At 5×10^{-5} torr on the recorder, the meter indicated 1×10^{-4} torr. The source of this discrepancy was not detected. Control was keyed to the recording instrument. Only during the heatup from 2000 to 2400°F did the meter readout exceed 5×10^{-5} torr. The period of time above this level was less than 15 minutes, as indicated by the meter.

On Wednesday morning, the parts were removed from the furnace. All foil was still bright. An unprotected T-111 sheet specimen, which also remained bright, was bent without any evidence of cracking. By 10:00 am, the parts and the thermocouples were removed from the holder and packed in the station wagon for transport back to Oak Ridge.

After returning to Oak Ridge, several 0.030-in.-thick T-111 coupons exposed during the anneal were analyzed. The results reported in Table 2 show that there was no contamination. Even the specimens that did not have a protective wrap showed no contamination.

Table 1. History of Annealing Operation

Time	Description of Operation	Furnace Temperature (°F)	Part Temperature (°F)	Part Temperature (°F)	Vacuum Pressure (torr)
12:30 pm	Start heatup				20.00×10^{-6}
1:00 pm	Start 500°F hold	500			27.00×10^{-6}
1:25 pm	End 500°F hold	500			8.00×10^{-6}
1:35 pm		600			29.00×10^{-6}
2:10 pm	Start 1000°F hold	1000	580	650	12.00×10^{-6}
2:35 pm	End 1000°F hold	1000	790	830	4.40×10^{-6}
3:00 pm		1300			33.00×10^{-6}
3:15 pm	Start 1500°F hold	1500	1240	1300	17.00×10^{-6}
3:30 pm	End 1500°F hold	1500	1400	1440	7.30×10^{-6}
3:40 pm	Realign vacuum instruments	1600			9.00×10^{-6}
		1600			19.00×10^{-6}
4:05 pm	Start 2000°F hold	2000	1850	1890	32.00×10^{-6}
4:20 pm	End 2000°F hold	2000	1940	1960	21.00×10^{-6}
4:35 pm		2400	2280	2320	65.00×10^{-6}
4:45 pm	Start 2 hr anneal	2420	2350	2375	54.00×10^{-6}
5:05 pm		2420	2385	2395	23.00×10^{-6}
6:45 pm	End 2 hr anneal (start controlled cool down)	2420	2385	2395	6.30×10^{-6}
7:20 pm	Cut off all furnace power	1500	1580	1580	0.75×10^{-6}
7:35 pm		1000			0.56×10^{-6}
8:35 pm		500			0.50×10^{-6}
11:55 pm		200			0.67×10^{-6}

Table 2. Interstitial Element Concentration (ppm)

Specimen Description	Unwrapped				Wrapped[a]			
	Carbon	Oxygen	Nitrogen	Hydrogen	Carbon	Oxygen	Nitrogen	Hydrogen
Unexposed control specimen	90	140	12	3	70	140	7	4
Exposed at top of furnace	80	150	7	12	70	140	8	1
Exposed at bottom of furnace	70	140	10	7	70	140	13	1

[a]These specimens were wrapped with two layers of 0.001-in.-thick Tantalum foil.

As indicated by the foregoing data and information, the entire annealing operation was quite successful and smooth. The cooperation of the Kokomo staff and the excellent equipment commend this facility for future use.

For future reference, a summary of the costs associated with this anneal are presented in Table 3.

Polaroid pictures of the fixtures and furnace are available at Bert Fleischer's office, Building 9201-3, Y-12 Area (Ext. 3-7689). The thermocouples are also available for future use.

Table 3. Summary of Costs Associated with Annealing

Preparation of Assemblies	
Labor (~ 40 man hours)	$ 600
Tantalum foil and wire (4 lb at $60 per lb)	240
Furnace Operation	
One run at $1800 per hr	$ 1800
3 1/2 hrs of operator overtime at $30 per hr	105
Thermocouples	
Two 15-ft Pt-6% vs Pt-30% Ph Al_2O_3 beaded thermocouples at $15 per ft	$ 450
Labor for assembling couples	45
Total Cost[a]	$ 3240

[a]This does not include transportation and follow-up by ORNL technical and technician manpower, which would add about $1500.

APPENDIX A

Description of Large Vacuum Annealing Furnace at Materials Systems Division, Haynes Stellite Works, Kokomo, Indiana

Manufacturer: R. D. Brew Company

Furnace Construction: ~40-in.-diam by 120-in.-long working zone

1. Cold wall with Tantalum heaters and Tantalum reflective insulation.
2. Top loading with load support platform on bottom and hanger type support structure on top.
3. Three zones of heaters each monitored with a W-Re thermocouple. Central zone thermocouple is the controller couple.
4. Lid contains Conax type fitting to accommodate 10 auxiliary thermocouples.

Capability:

1. Maximum leakup rate 3 μ/hr.
2. 5×10^{-7} torr vacuum obtainable at room temperature.
3. 5×10^{-5} torr or better during heatup to 2400°F.
4. Can operate up to 3300°F.
5. Heatup rate can be programmed to vacuum specification.

APPENDIX B

THERMAL CYCLES OF DRAIN LINE DURING CAVITATION TESTS

INTRA-LABORATORY CORRESPONDENCE

OAK RIDGE NATIONAL LABORATORY

April 1, 1971

TC: J. H. DeVan

SUBJECT: Thermal cycles of Drain Line on FCLLL-1 During Cavitation Tests

We have reviewed the FCLLL-1 test data in an attempt to determine the number and magnitude of thermal cycles that occurred on the drain line as a result of pump cavitation tests during the final 1300 hr run. This drain line failed at a point located 4 1/2 inches from the tee on the 2200°F pump discharge line and the point of failure is estimated to have been at 1200°F during normal operation due to heat losses from this static, uninsulated line. During pump cavitation tests, vapor bubbles were created in the loop and these bubbles expelled 2200°F lithium out the drain line with resultant thermal cycling. The maximum temperature cycling at the failure area would have been 2200-1200 or 1000°F. Nine cavitation tests were run during the final weeks of operation as we were nearing our 3000 hr goal. These cavitation tests were made with the loop at design conditions and the temperature profile in the circulating portions of the loop was not disturbed. However, the on-set of caviation could be noted by pressure fluctuations and by the temperature changes in the static drain line as 2200°F liquid was expelled from the loop. A review of the strip chart recordings of TR-4, pt 2 (TE 34, TS-2B) during the period June 2 to June 19, 1970, gave general confirmation that about nine thermal cycles occurred in the line during that time.

The temperature of the drain line was measured by TE 34 (reference flow-sheet I-10436-QG-001-E-3) at the dissimilar metal transition joint which was normally operated at 500-600°F. The transition joint was located about two feet from the tee at the 2200°F pump discharge line. During cavitation testing TE 34 indicated temperature changes as liquid lithium moved within the line. TE 34 temperature recordings do not necessarily represent the maximum temperature occurring at the transition joint because this temperature was not recorded continuously but instead was recorded on a multipoint (16) recorder. However, typical maximum recorded temperatures may be of interest so they are shown in Table 1 for information. The fact that only seven major temperature excursions of the drain line were found for nine cavitation tests is believed due to the thermocouple selector switch (TS-2 on TR-4) which may not have been set on TE-34 during all cavitation testing.

Dick Huntley

W. R. Huntley

WRH:bks

Enclosure - Table 1

cc: C. W. Cunningham
B. Fleischer
Ron Kleih
J. W. Koger
R. E. MacPherson

Table 1. Maximum Recorded Temperature of Transition Joint During Cavitation Testing.

Date	Time	Max. Temp. TE 54 on TR-4 (PT TS-2B) °F
6-9-70	1045	1545
6-15-70	1119	1590
6-18-70	1113	1260
6-19-70	0925	1050
6-19-70	0943	1620
6-19-70	0958	1320
6-19-70	1115	1770

APPENDIX C

ELECTRON-MICROPROBE EXAMINATION RELATED TO LEAK AFTER 1735 HR

INTRA-LABORATORY CORRESPONDENCE

OAK RIDGE NATIONAL LABORATORY

Metallography Report No. 659

To: Bertram Fleischer

From: R. S. Crouse, H. Mateer, T. J. Henson

Subject: Electron Microprobe Examination of T-111-Li Forced Circulation Loop (FCLLL-1)

cc: J. H. DeVan
J. R. Weir
R. J. Gray - Met. File
H. Mateer
R. S. Crouse (2) - FC

A forced circulation loop (FCLLL-1) of T-111 and containing lithium was operated at 2200-25 0°F for 1700 hr. A leak occurred and metallographic specimens from the area were examined. These examinations led to a request for microprobe examination.

The first request was for a scanning picture and qualitative x-ray examination of the inside surface of a small section of loop tubing. In this section were small areas that had the cancerous appearance of molten metal spatter. Figure 1 shows the section with a backscattered electron picture at 200X. Using an accelerating voltage of 20 kv and 0.01 μa sample current, the La x-rays of Ta, W, and Hf were displayed and photographed. There are also in Fig. 1. This particular area is Hf-rich.

After the above determination, the macro section was mounted and polished through one of the areas (M-441, Met. 68345). Metallographic examination showed it to be a deposit. An x-ray spectral scan revealed the presence of Zr in addition to Hf in the deposit. This is not surprising since the two elements occur naturally together and are very difficult to separate.

Figure 2 shows the x-ray displays of Ta, W, Hf, and Zr indicating that the deposit is quite rich in Hf and Zr and poor in Ta and W. A step scan for W and Hf was made in the direction indicated by the arrow and the semi-quantitative results plotted in Fig. 3.

The steps of the scan were 10μm apart and were taken into the base metal for 180 μm to check for composition gradients and inhomogeneities in Hf and W. The break in the trace in the deposit is due to a hole. A gradient in the Hf of about 30 μm under the deposit was detected, but no inhomogeneity beyond that in the base metal. A step scan across the edge in an area adjacent to the deposit showed no variation in Hf x-ray intensity right to the inside surface. I feel that the Hf was truly a deposit since there was no depletion of the element up to 180 μm below the area and the composition at 180 μm was the same as was found in the bulk of the sample.

In addition to the deposit, several areas of severe corrosion on the outside of the loop were probed (M-442, Met. 68121). In general, there appeared to be a loss of Hf in these areas and there were some spots containing some nickel. This Ni concentration was low and localized and did not appear recognizable optically. Figure 4 shows generally how it was distributed. The corroded area was so porous that a quantitative determination would be unreliable. Suffice it so say, there was not much Ni there.

Underneath the corroded areas some bright intergranular material could be seen (M-444, Met. 68380). A spectral scan showed these to be devoid of Hf and containing only Ta and W. No other element was detected. Figure 5 shows the phase.

One sample (M-445, Met. 68381) had some small, dark intergranular phases near the outside surface of the loop. Figure 6 shows this phase at 500X. A spectral scan was attempted with questionable success. The phase particles were generally smaller than the electron beam so some x-rays were being generated in the surrounding matrix. The Hf appeared to be considerably below what one would expect in the matrix, which indicates that the phase is probably poor in Hf.

Some sections of the loop exhibited a thin, continuous layer along the inside surface. The layer was too thin for a semi-quantitative analysis, so an x-ray CRT display was done. Figure 7 shows the results of this part of the analysis. The layer was rich in Hf.

Discussion of Results

The results of this entire examination indicate that Hf is the one element that is somehow most involved, either by its presence of absence. It constitutes the bulk of the material deposited on the inside of the loop in both "spatter" deposit and continous layer. In the corroded areas and adjacent intergranular phases, there seems to be a lack of it. Attempts to analyze small phase particles were generally less than successful, although, once again, Hf seemed to be lacking.

The presence of nickel in the corroded areas may be significant if a low melting eutectic is formed with Ta, W, and/or Hf. The source of the Ni is unknown but its presence is a fact. The amount of Ni is small but it could have been therein greater quantities at one time and been lost as corrosion proceeded.

R. S. Crouse

RSC:mc

H. Mateer

T. J. Henson

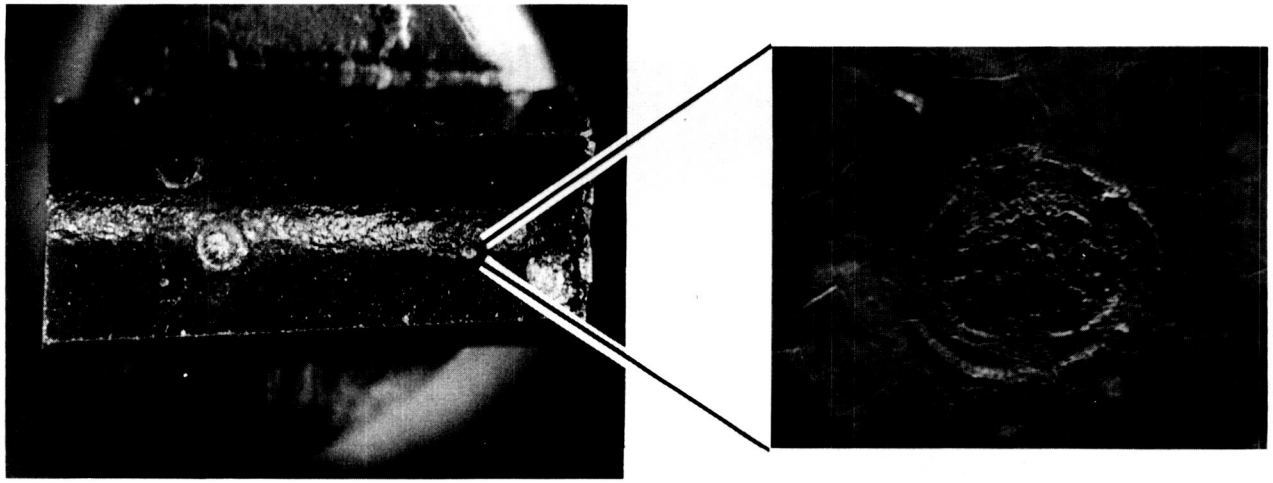

INSIDE SURFACE OF LOOP SECTION. 12.5X

BACKSCATTERED ELECTRONS DISPLAY OF DEPOSIT. 200X

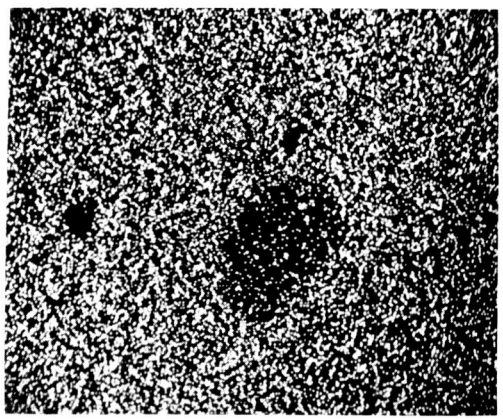

Ta Lα X-RAYS 200X

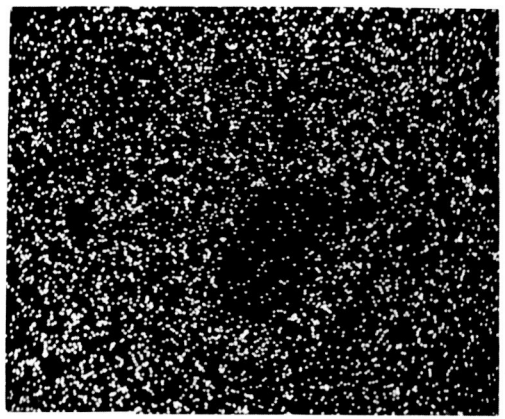

W Lα X-RAYS 200X

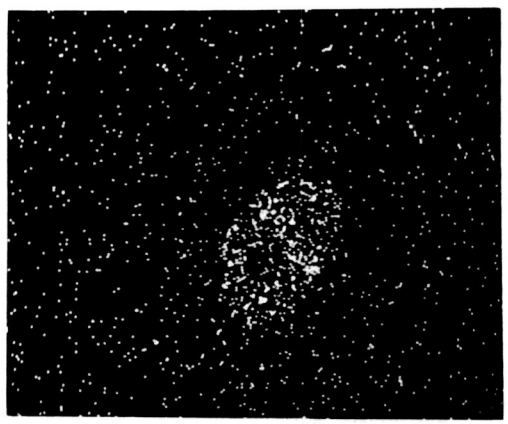

Hf Lα X-RAYS 200X

CHARACTERIZATION OF DEPOSITS IN A T-111 LOOP CONTAINING LITHIUM

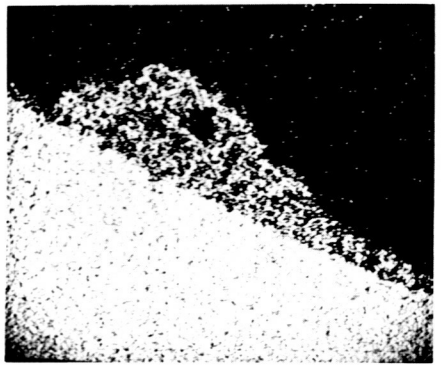

300X

Ta Lα X-RAYS

300X

OPTICAL (Bright Field)

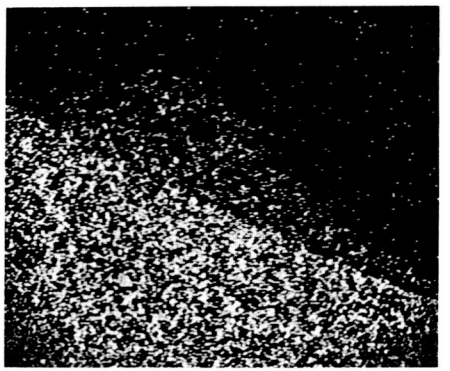

300X

W Lα X-RAYS

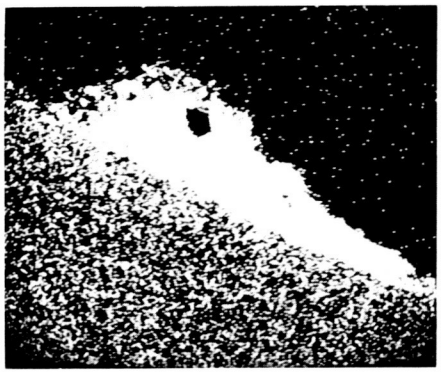

300X

Hf Lα X-RAYS

300X

Zr Lα X-RAYS

ELEMENT DISTRIBUTION IN DEPOSIT CROSS SECTION. T-III LOOP CONTAINING LITHIUM.

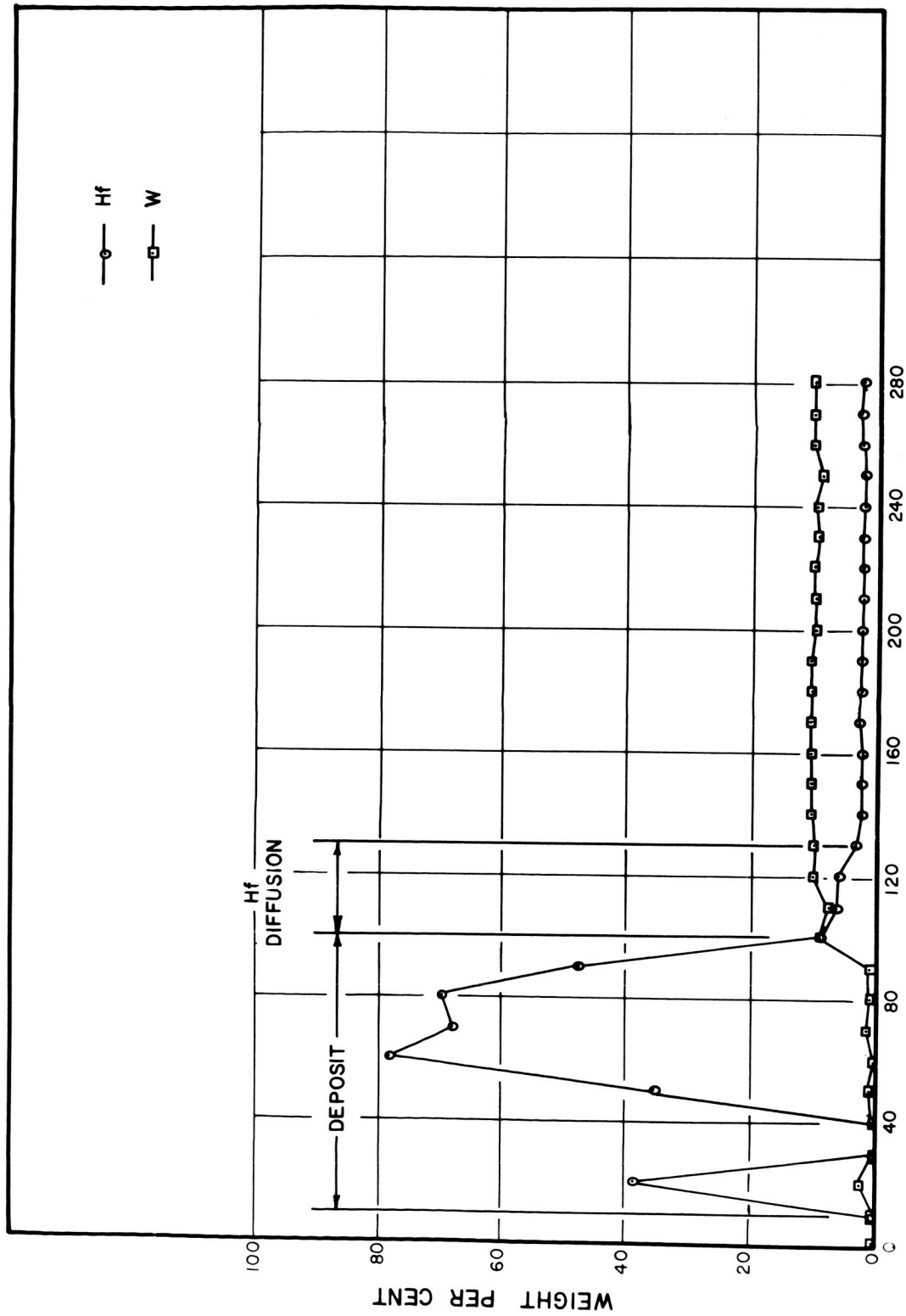

FIG. 3. STEP SCAN ACROSS DEPOSIT INTO BASE METAL

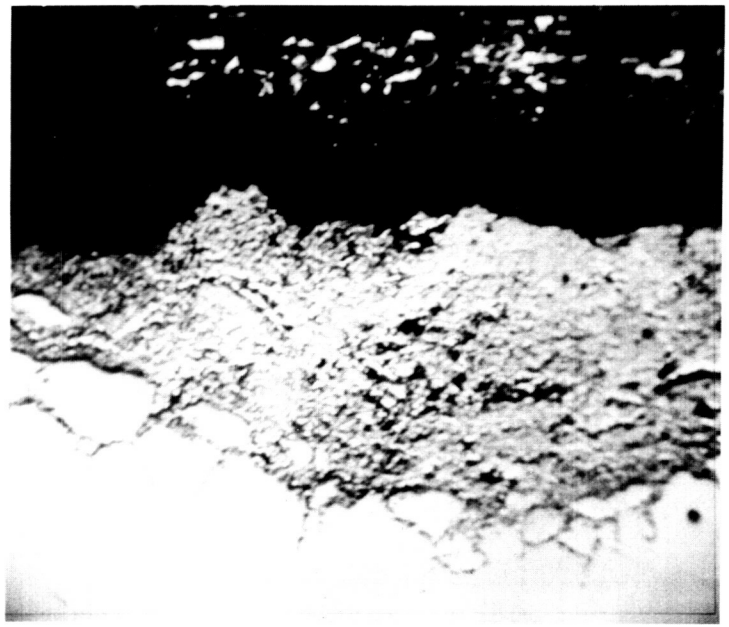

300X

BACKSCATTERED ELECTRONS

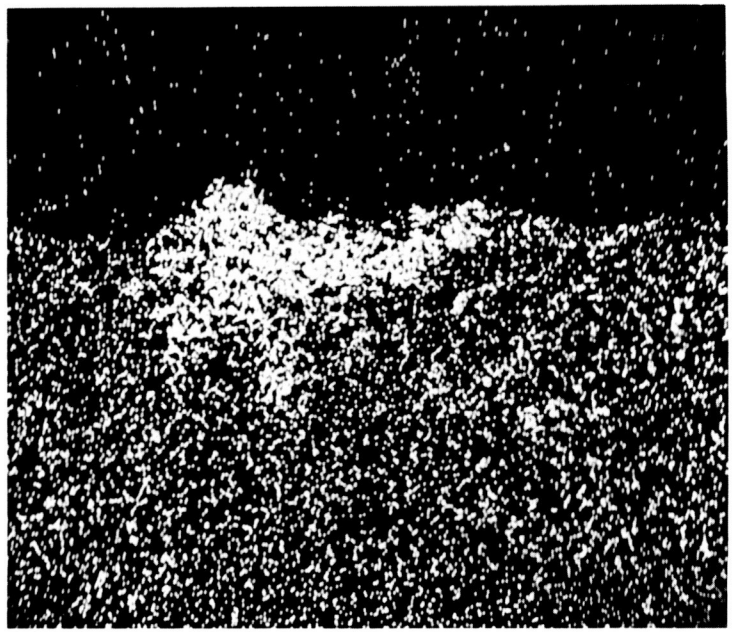

300X

Ni Kα X-RAYS

NICKEL IN CORRODED AREA ON OUTSIDE SURFACE OF LOOP

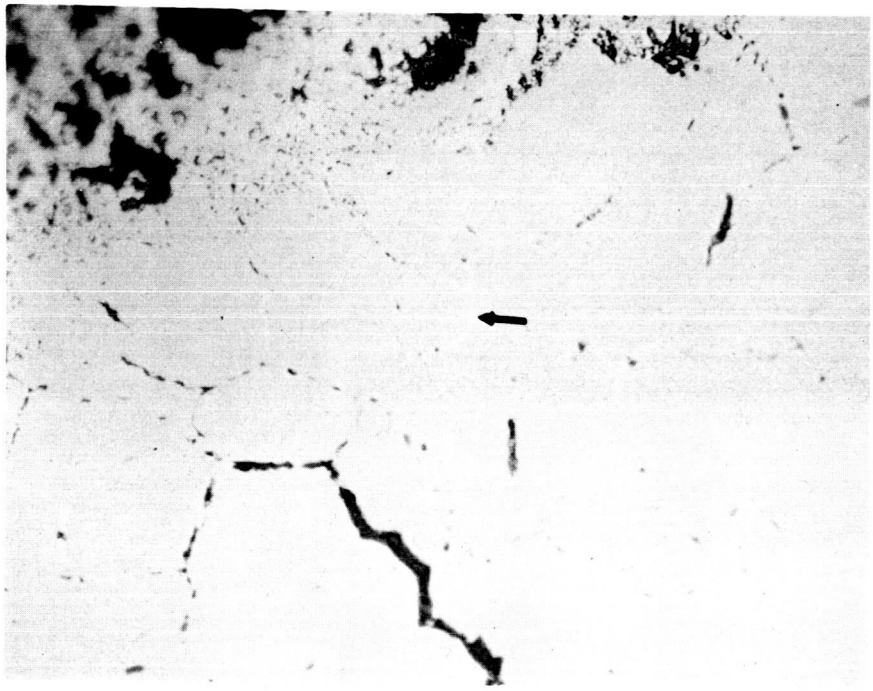

Figure 5. Intergranular Phase Under Corrosion. 500X

Figure 6. Dark Intergranular Phase Near Outside Surface. 500X

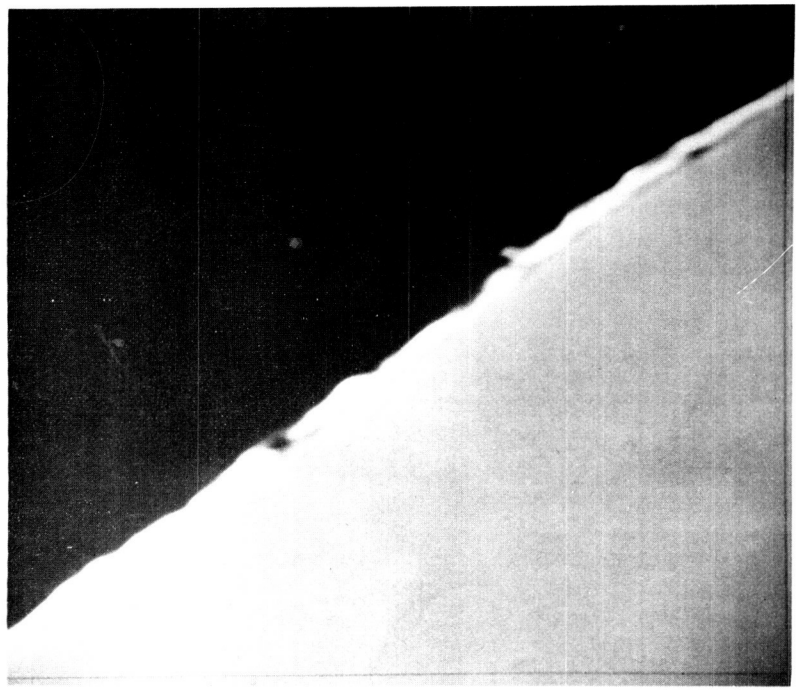

1000X

BACKSCATTERED ELECTRONS

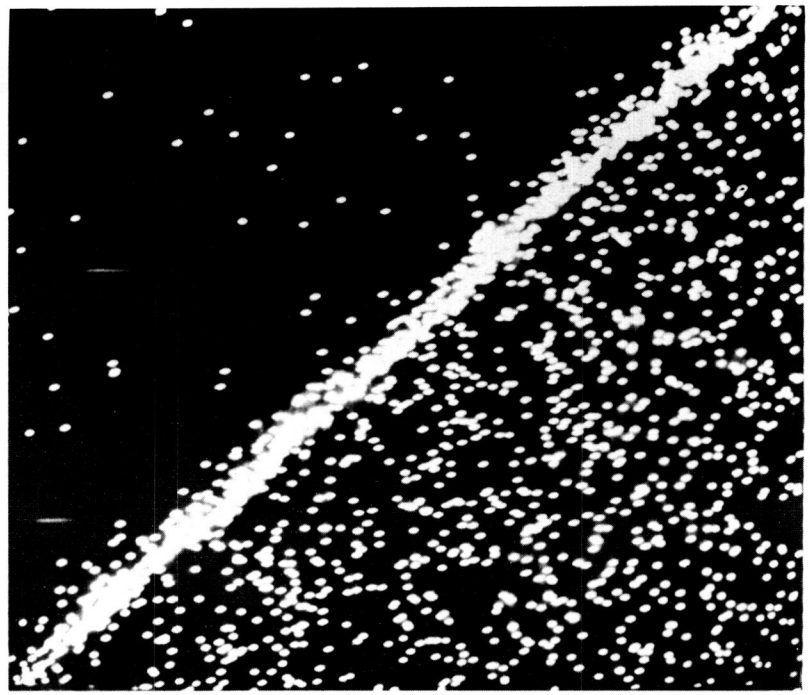

1000X

Hf Lα X-RAYS

IDENTIFICATION OF LAYER ON INSIDE OF T-111 LOOP CIRCULATING LITHIUM

APPENDIX D

MICROPROBE ANALYSIS OF DEPOSITS RELATED TO DRAIN LINE LEAK

INTRA-LABORATORY CORRESPONDENCE

OAK RIDGE NATIONAL LABORATORY

Metallography Report No. 719

To: J. H. DeVan

Date: January 13, 1972

From: H. Mateer, T. J. Henson, R. S. Crouse

Subject: Microprobe Analysis of a T-111 Specimen

cc: R. J. Gray - Met. File
J. R. Weir, Jr.
T. S. Lundy
R. S. Crouse (2)
H. Mateer

A T-111 specimen showing cracking below a thin surface layer was submitted for electron microprobe examination. Analysis of both the surface layer and material found in the crack was requested. Determination of the presence of any Ni, Fe, and Cr. was of interest.

Analysis was performed using a 20 kev electron beam. Sample current was .015 μa.

Figures 1 through 4 display elemental distribution at the surface of the specimen. The following table shows the results of semi-quantitative analysis of the areas of interest. The electron beam was larger than the crack material analyzed. Compositions reported for this material will be somewhat low.

Table 1

	Composition, wt %				
	Fe	Ni	HF	Ta	W
Surface layer	1.9	7.5	49.5	11.4	1.0
Matrix	< 0.5	< 0.5	2.8	92.0	10.5
Crack Material	1.7	23.2	41.2	NA	NA

H. Mateer

HM:mc

Y-107547

Backscattered Electrons

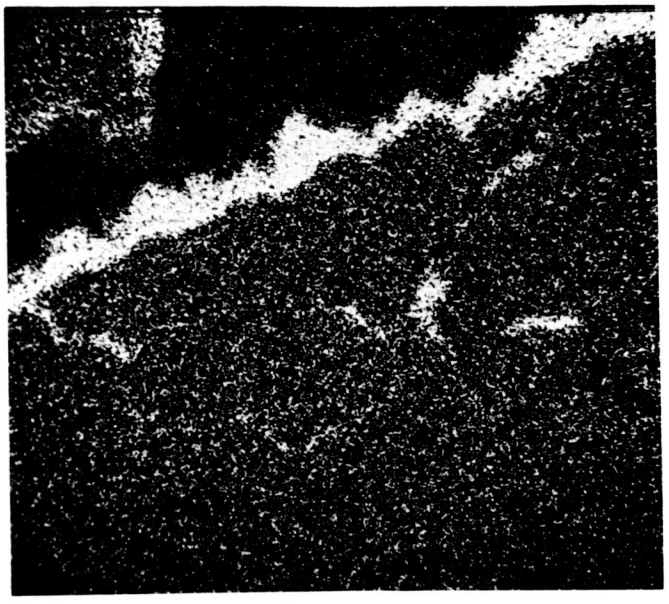

HfLα

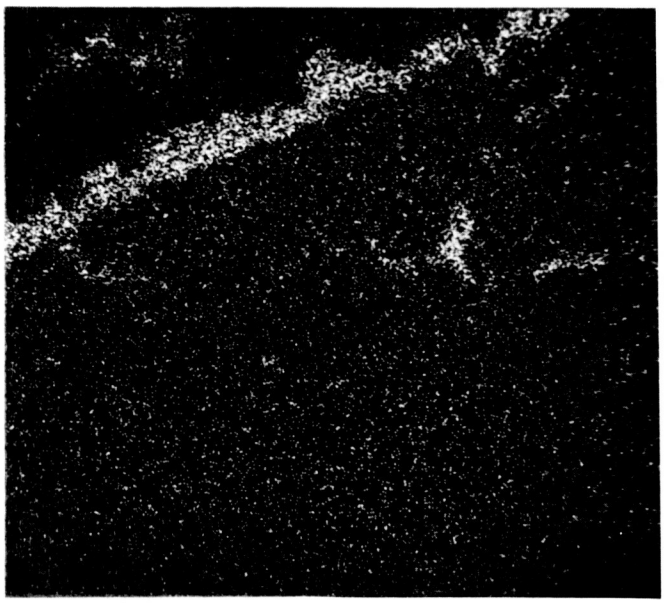

NiKα

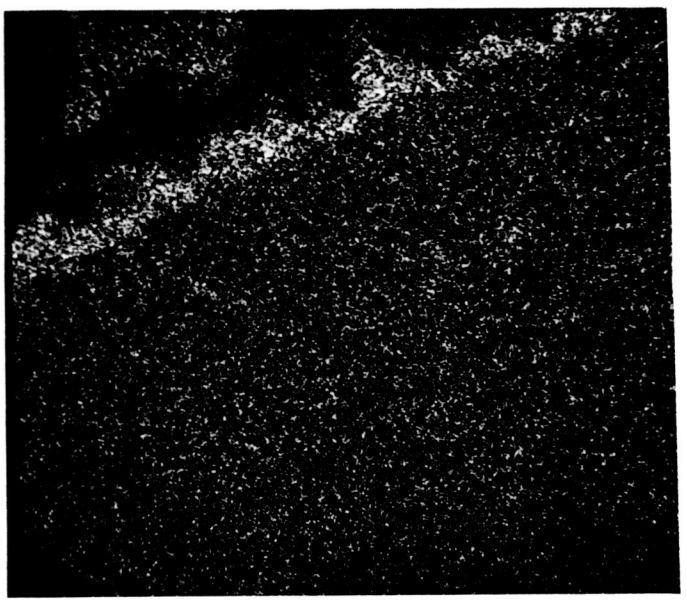

FeKα

Figure 1. Electron Beam Scanning Images of T-111 Specimen (M-531, Met. 71025, 18-3A)

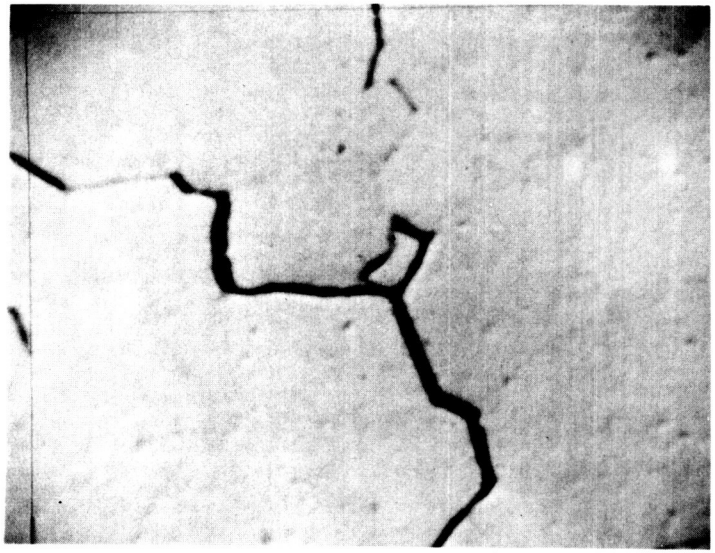

Backscattered Electrons

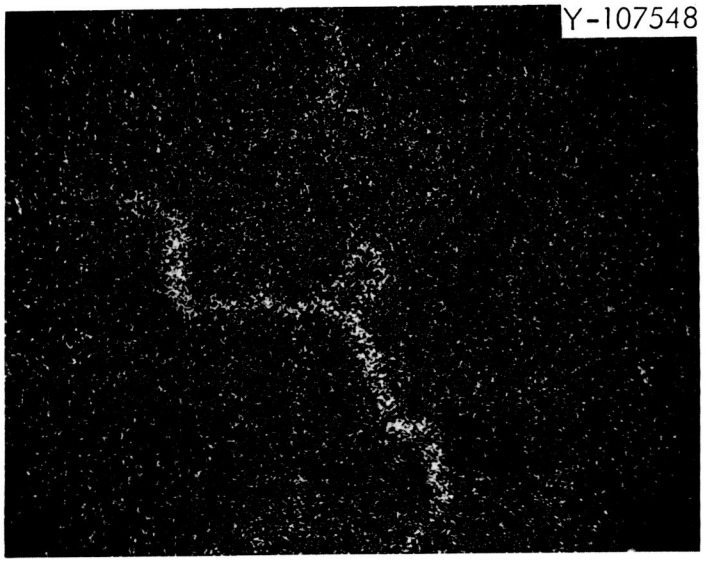

HfLa

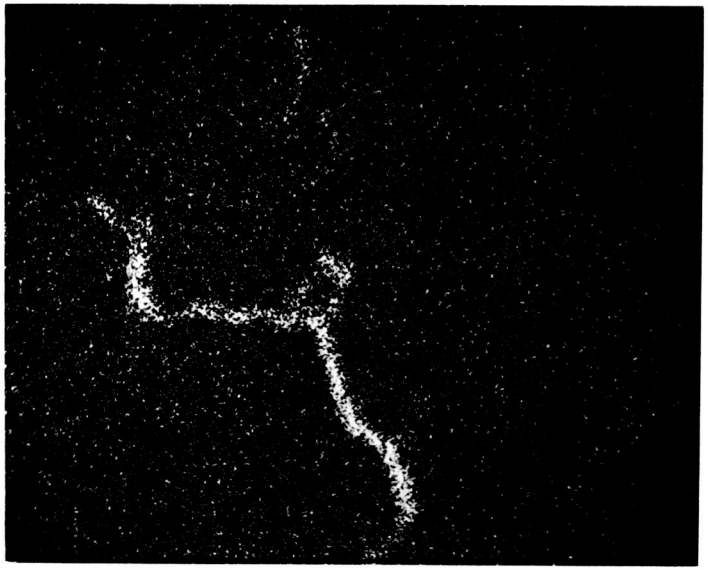

NiKa

Figure 2. Electron Beam Scanning Images of T-111 Specimen.
(M-531, Met. 71025, 18-3A)

Y-107549

Backscattered Electrons

HfLα

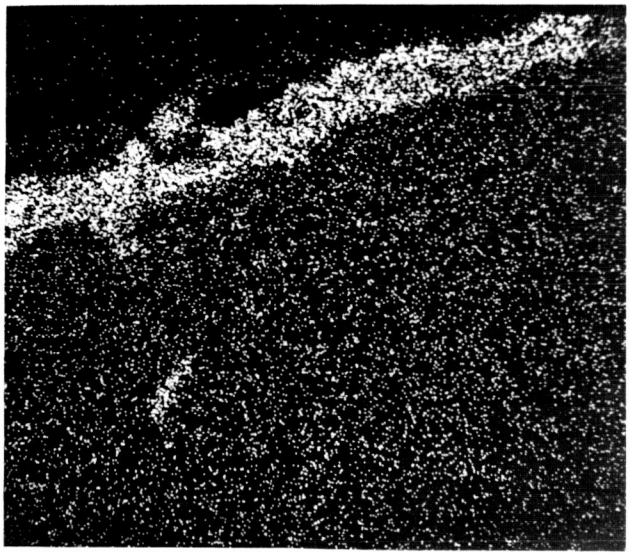

NiKα

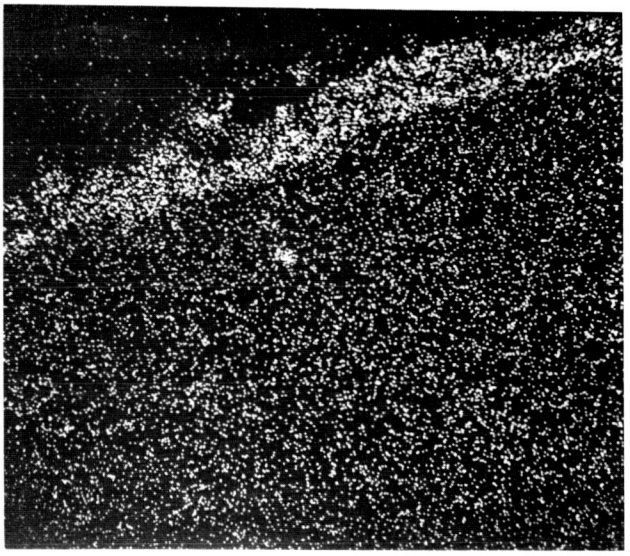

FeKα

Figure 3. Electron Beam Scanning Images of T-111 Specimen (M-531, Met. 71025, 18-3A)

Y-107550

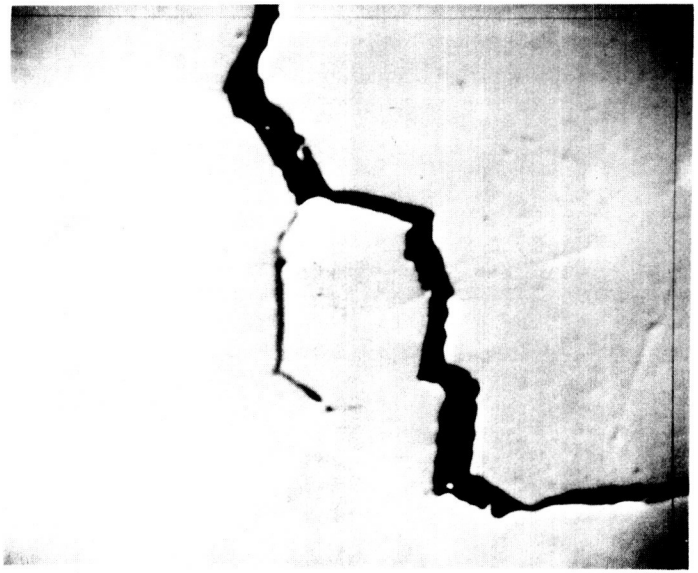

Backscattered Electrons

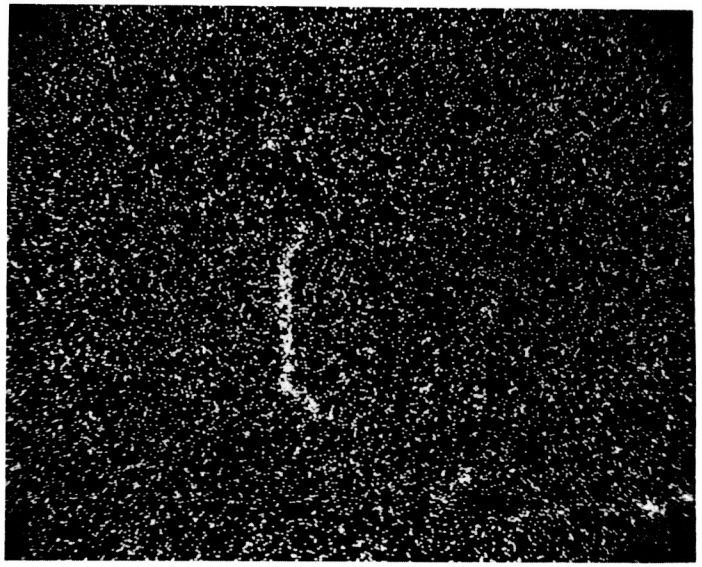

HfLa

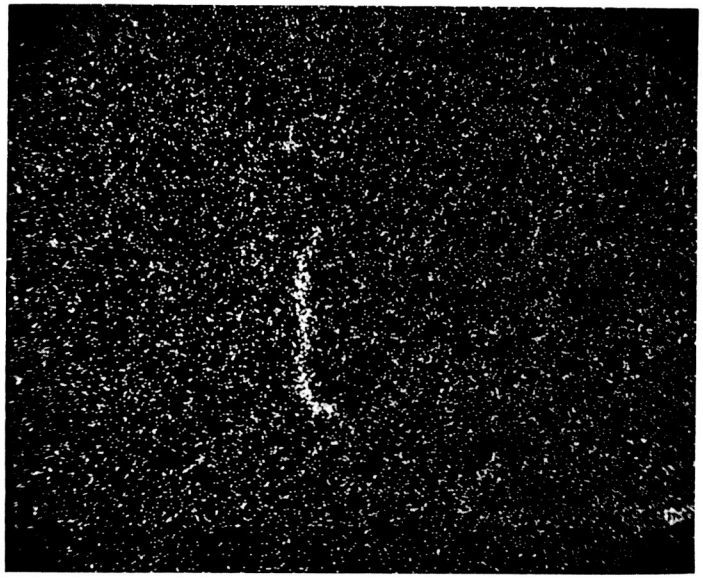

NiKa

Figure 4. Electron Beam Scanning Images of T-111 Specimen.
(M-531, Met. 71025, 18-3A)

APPENDIX E

WEIGHT-CHANGE DATA FOR INSERT SPECIMENS

Table 1.
Weight Change Data for Insert Specimens
in FCLLL-1

Holder No.	Specimen No.	Before (g)	After (g)	Change (mg)	Change/Area mg/cm^2
12	1	4.4808	4.4865	+5.7	+0.631
	2	4.6097	4.6151	+5.4	+0.598
	3	4.3556	4.3609	+5.3	+0.587
13	4	4.5730	4.5790	+6.0	+0.664
	5	4.6172	4.6215	+4.3	+0.476
	6	4.3102	4.3166	+6.4	+0.709
14	7	4.4917	4.4980	+6.3	+0.698
	8	4.5416	4.5476	+6.0	+0.664
	9	4.6288	4.6326	+3.8	+0.421
	10	4.2690	4.2735	+4.5	+0.498
	11	4.6354	4.6387	+3.5	+0.388
	12	4.6078	4.6100	+2.2	+0.244
	13	4.6763	4.6773	+1.0	+0.111
	14	4.5896	4.5894	−0.2	−0.022
	15	4.4098	4.4097	−0.1	−0.011
15	16	4.6656	4.6639	−1.7	−0.188
	17	4.7437	4.7418	−1.9	−0.210
	18	4.9158	4.9136	−2.2	−0.244
	19	4.4071	4.4052	−1.9	−0.210
	20	4.3137	4.3119	−1.8	−0.199
	21	4.8385	4.8363	−2.2	−0.244
	22	4.8693	4.8669	−2.4	−0.266
	23	4.6252	4.6228	−2.4	−0.266
	24	4.7188	4.7164	−2.4	−0.266
	25	4.2903	4.2876	−2.7	−0.299
16	26	4.6339	4.6298	−4.1	−0.454
	27	4.8011	4.7971	−4.0	−0.443
	28	4.6665	4.6627	−3.8	−0.421
	29	4.7848	4.7808	−4.0	−0.443
	30	4.6575	4.6534	−4.1	−0.454
	31	4.7553	4.7511	−4.2	−0.465
	32	4.8353	4.8307	−4.6	−0.509
	33	4.5268	4.5219	−4.9	−0.543

Holder No.	Specimen No.	Before (g)	After (g)	Change (mg)	Change/Area mg/cm^2
1	34	4.5139	4.5089	−5.0	−0.554
	35	4.5087	4.5034	−5.3	−0.587
	36	4.5364	4.5310	−5.4	−0.598
	37	4.5467	4.5414	−5.3	−0.587
	38	4.3986	4.3936	−5.3	−0.587
	39	4.7239	4.7182	−5.7	−0.631
	40	4.6798	4.6743	−5.5	−0.609
	41	4.5048	4.4999	−4.9	−0.543
	42	4.8006	4.7952	−5.4	−0.598
	43	4.2304	4.2252	−5.2	−0.576
2	44	4.7101	4.7044	−5.7	−0.631
	45	4.5122	4.5063	−5.9	−0.653
	46	4.7104	4.7043	−6.1	−0.676
3	47	4.7046	4.6983	−6.3	−0.698
	48	4.5580	4.5515	−6.5	−0.720
	49	4.7228	4.7147	−8.1	−0.897
	50	4.8063	4.7998	−6.5	−0.720
	51	4.7356	4.7290	−6.6	−0.731
	52	4.5820	4.5755	−6.5	−0.720
4	53	4.4476	4.4415	−6.1	−0.676
	55	4.1919	4.1875	−4.4	−0.487
	56	4.6278	4.6231	−4.7	−0.520
5	57	4.8214	4.8162	−5.2	−0.576
	58	4.7607	4.7562	−4.5	−0.498
	59	4.6460	4.6423	−3.7	−0.410
	60	4.7231	4.7192	−3.9	−0.432
	61	4.6882	4.6841	−4.1	−0.454
	62	4.5422	4.5386	−3.6	−0.399
	63	4.3083	4.3053	−3.0	−0.332
	64	4.3237	4.3205	−3.2	−0.354
6	65	4.8118	4.8099	−1.9	−0.210
	66	4.7704	4.7683	−2.1	−0.233
	67	4.5475	4.5458	−1.7	−0.188
	68	4.7666	4.7649	−1.7	−0.188
	69	4.6709	4.6689	−2.0	−0.222
	70	4.6008	4.5989	−1.9	−0.210
	71	4.5433	4.5413	−2.0	−0.222
	72	4.8537	4.8514	−2.3	−0.255
	73	4.5080	4.5056	−2.4	−0.266
	74	4.4315	4.4292	−2.3	−0.255

Holder No.	Specimen No.	Before (g)	After (g)	Change (mg)	Change/Area mg/cm^2
7	75	4.8672	4.8661	−1.1	−0.122
	76	4.7592	4.7589	−0.3	−0.033
	77	4.6481	4.6474	−0.7	−0.078
	79	4.9247	4.9235	−1.2	−0.133
	81	4.6602	4.6594	−0.8	−0.089
	82	4.4052	4.4046	−0.6	−0.066
	83	4.5484	4.5479	−0.5	−0.055
	84	4.6238	4.6233	−0.5	−0.055
8	86	4.8055	4.8114	+5.9	+0.653
	87	4.6707	4.6767	+6.0	+0.664
	88	4.7648	4.7703	+5.5	+0.609

APPENDIX F

MICROPROBE TRAVERSES ACROSS VARIOUS SPECIMENS

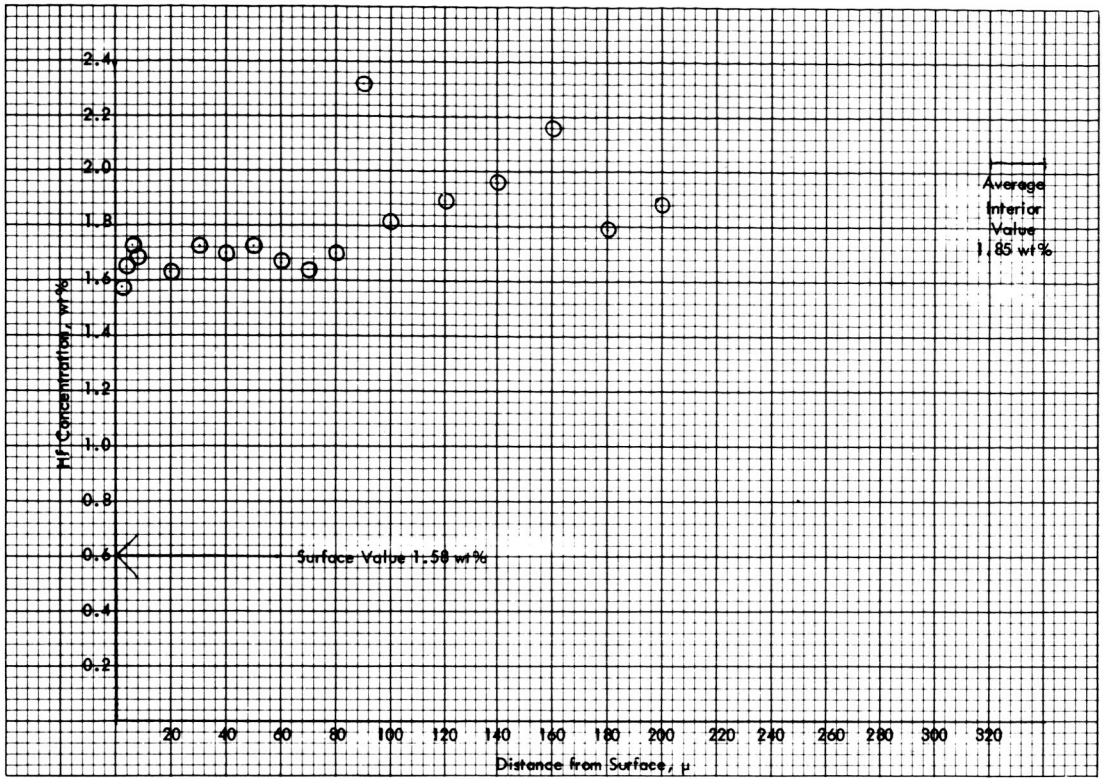

Holder 13, ID, M-607

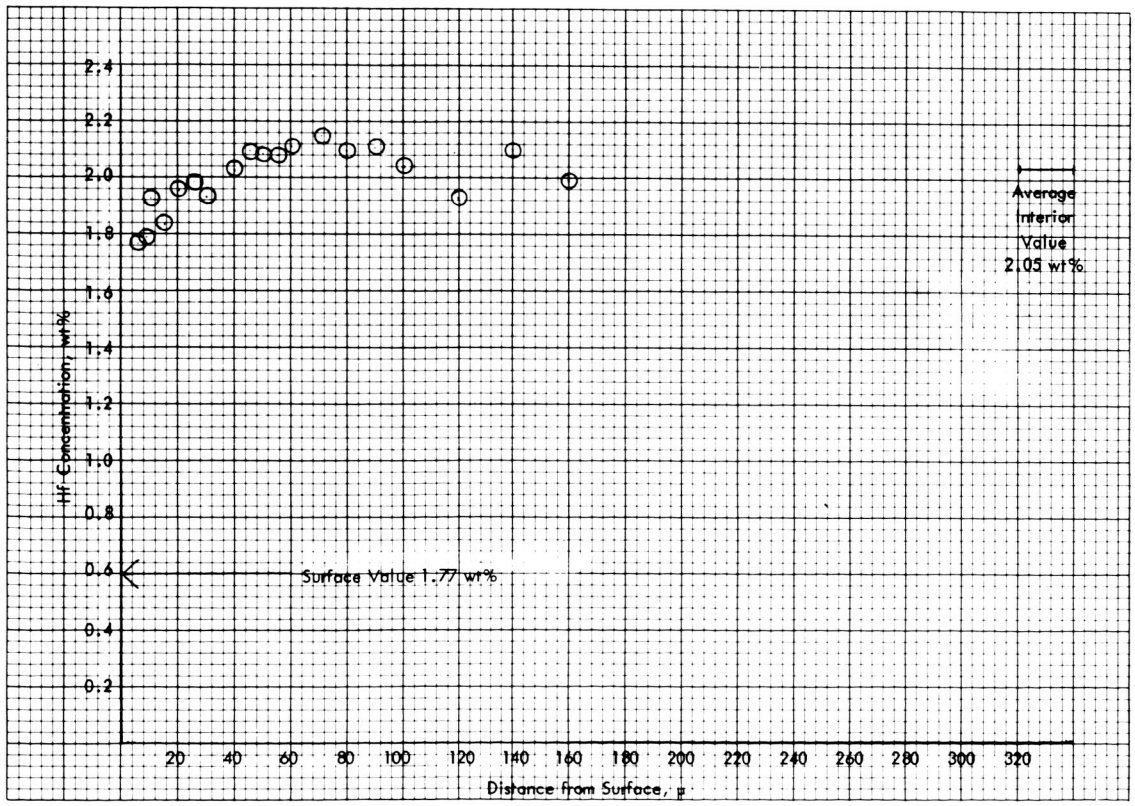

Holder 15, ID, M-606

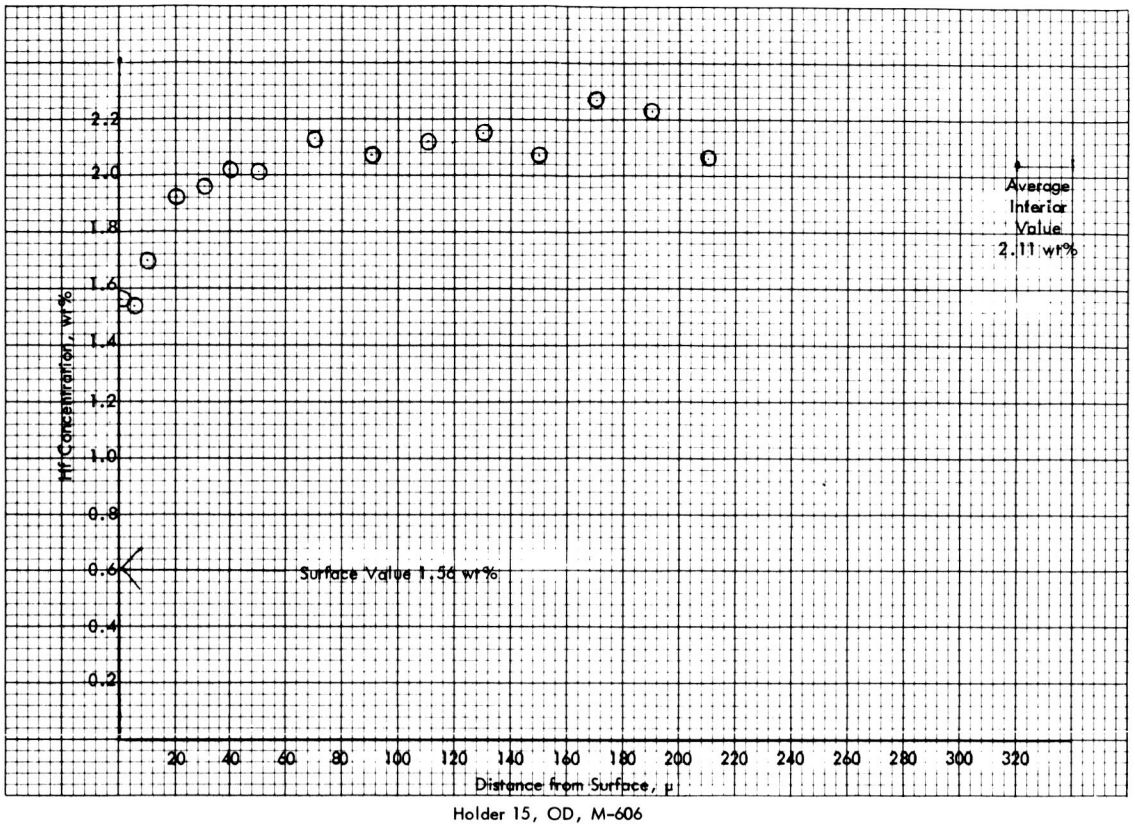

Holder 15, OD, M-606

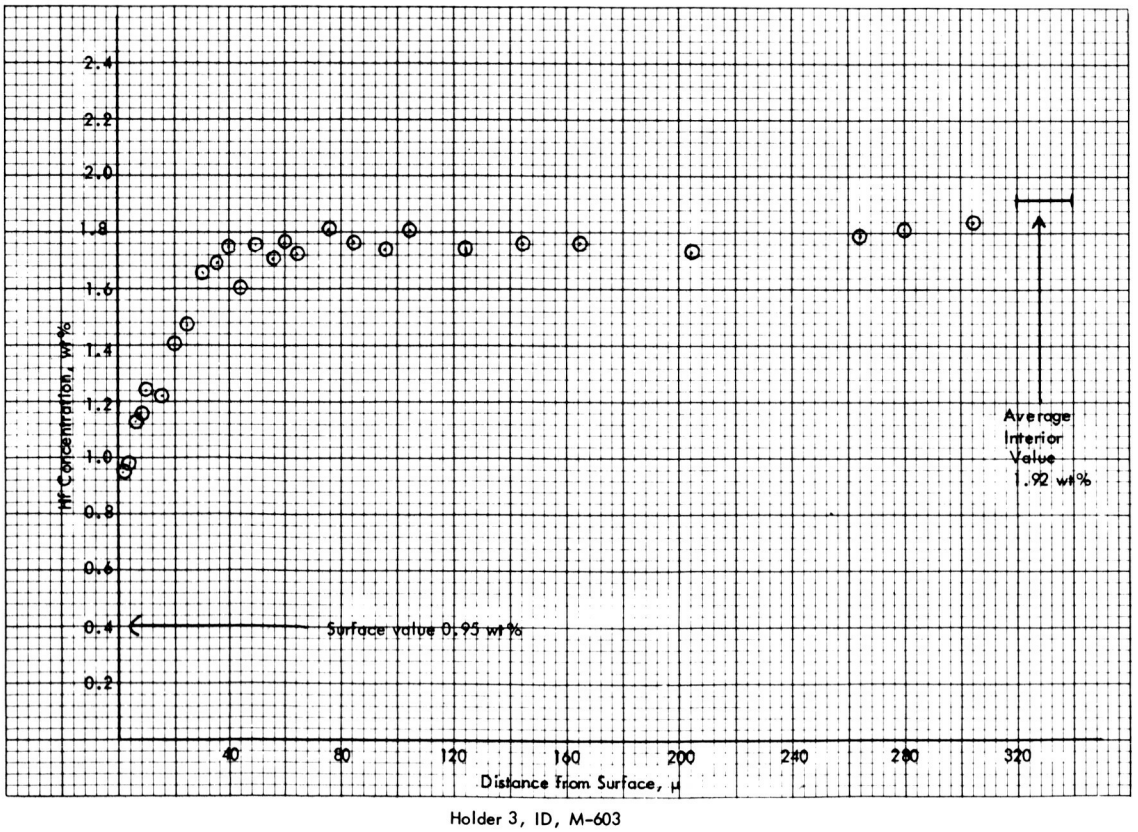

Holder 3, ID, M-603

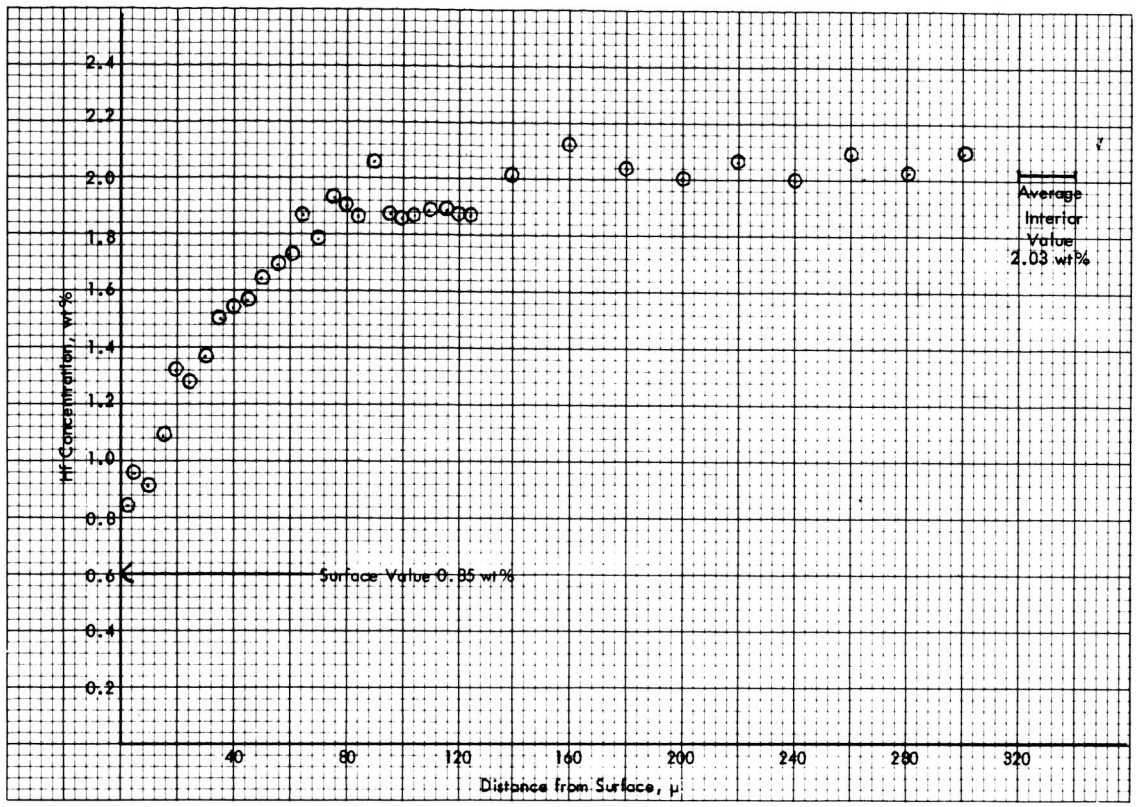

Holder 3, ID, M-603

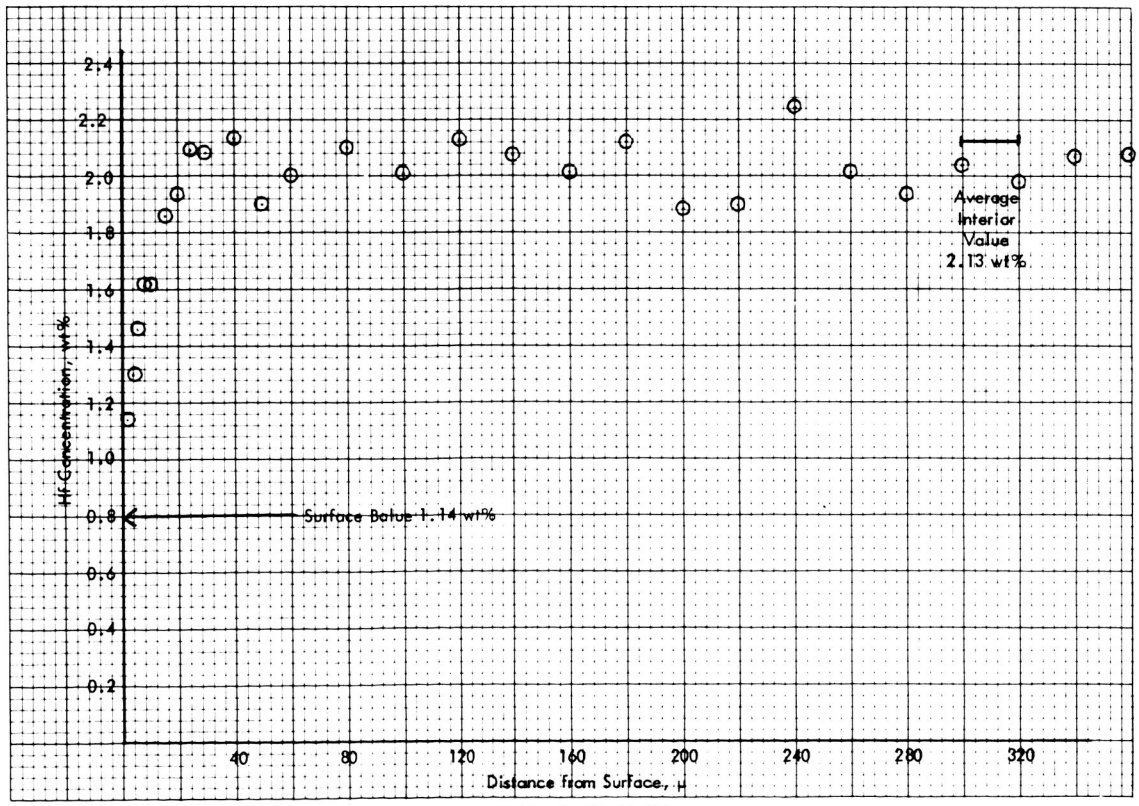

Holder 6, ID, M-604

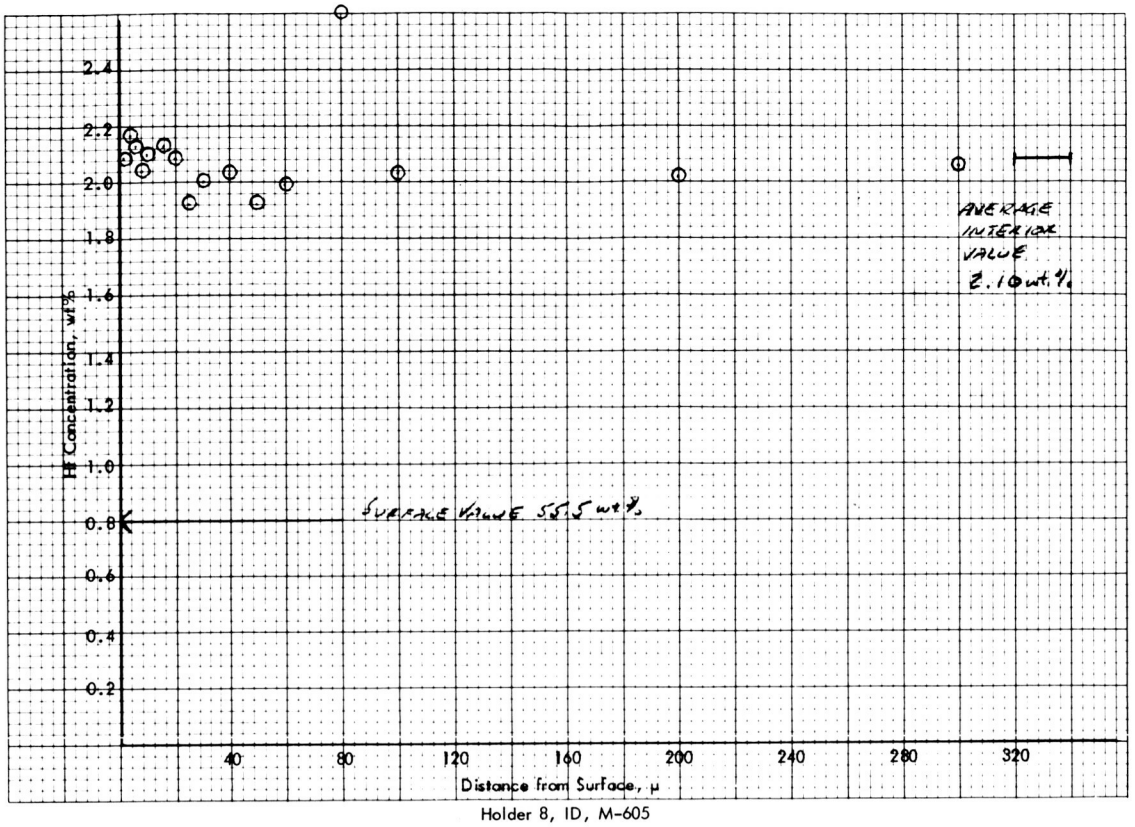

Holder 8, ID, M-605

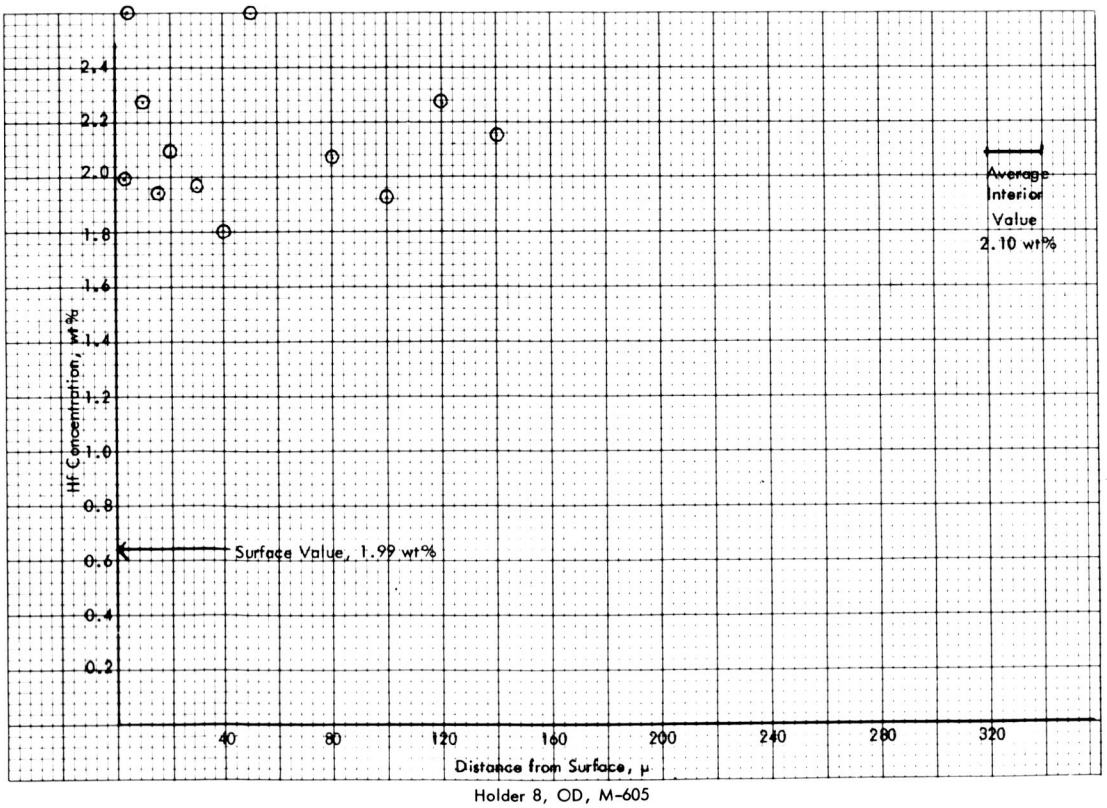

Holder 8, OD, M-605

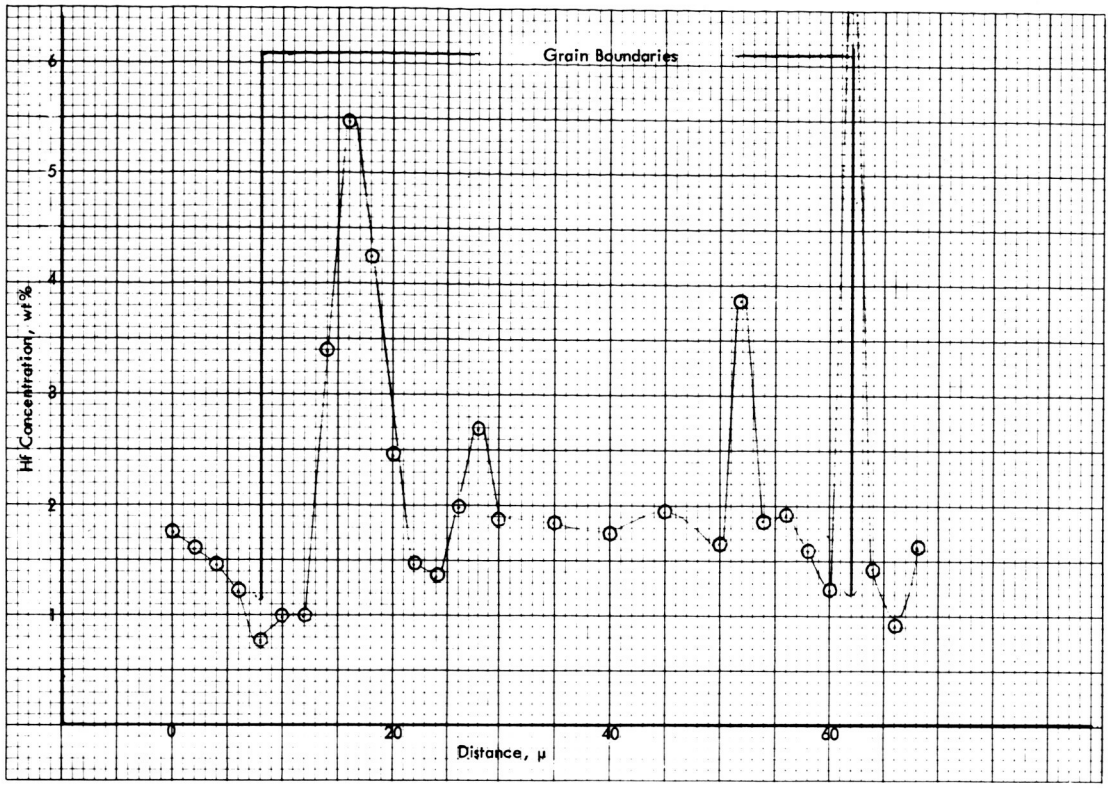

TRAVERSE ACROSS GRAIN
Holder 6, M-604

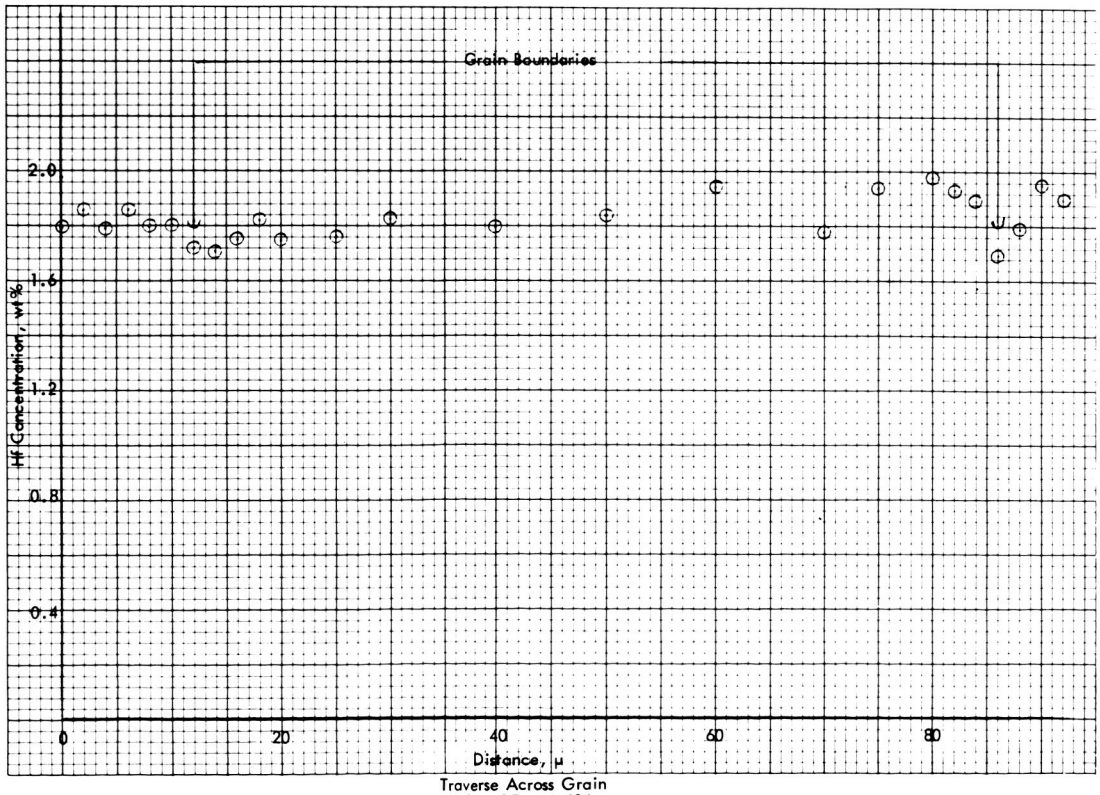

Traverse Across Grain
Holder 15, M-606

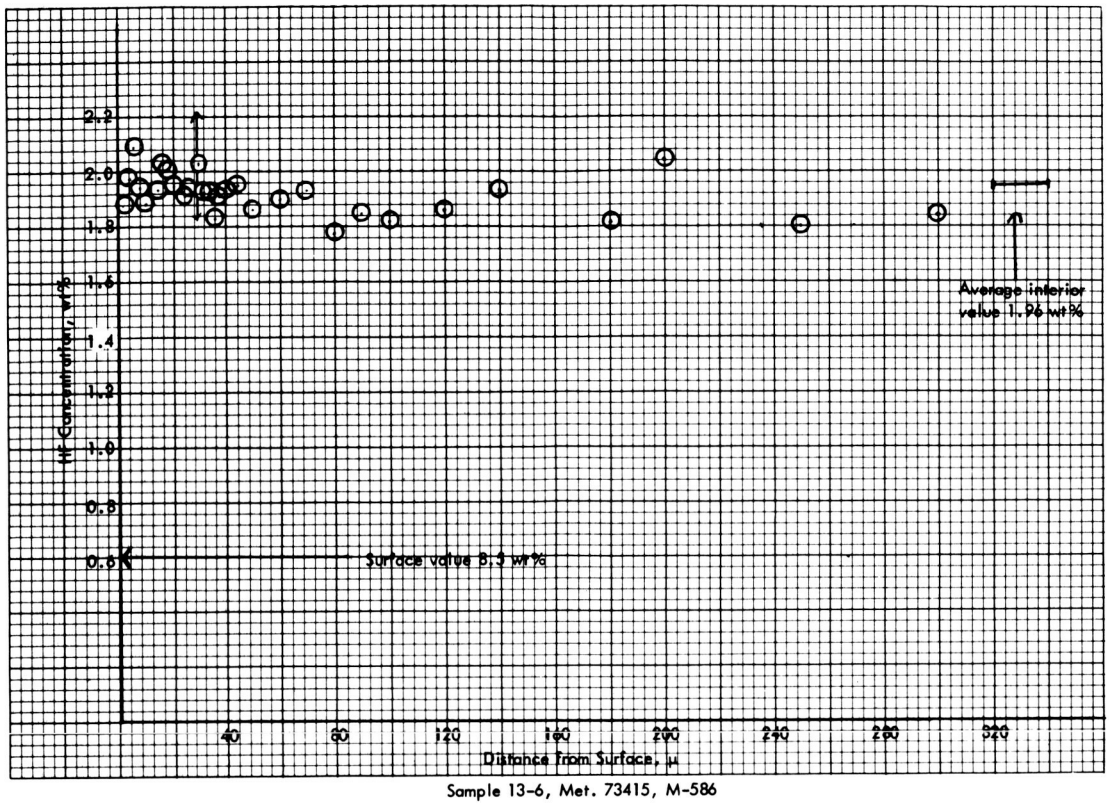

Sample 13-6, Met. 73415, M-586

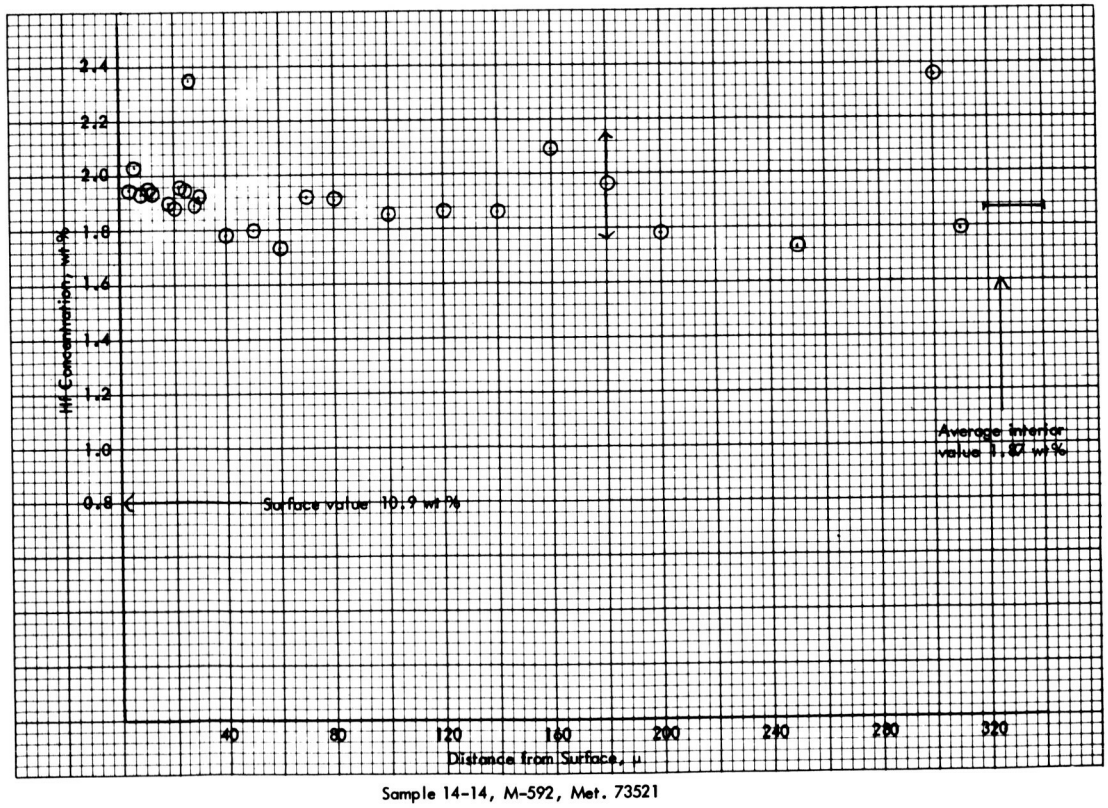

Sample 14-14, M-592, Met. 73521

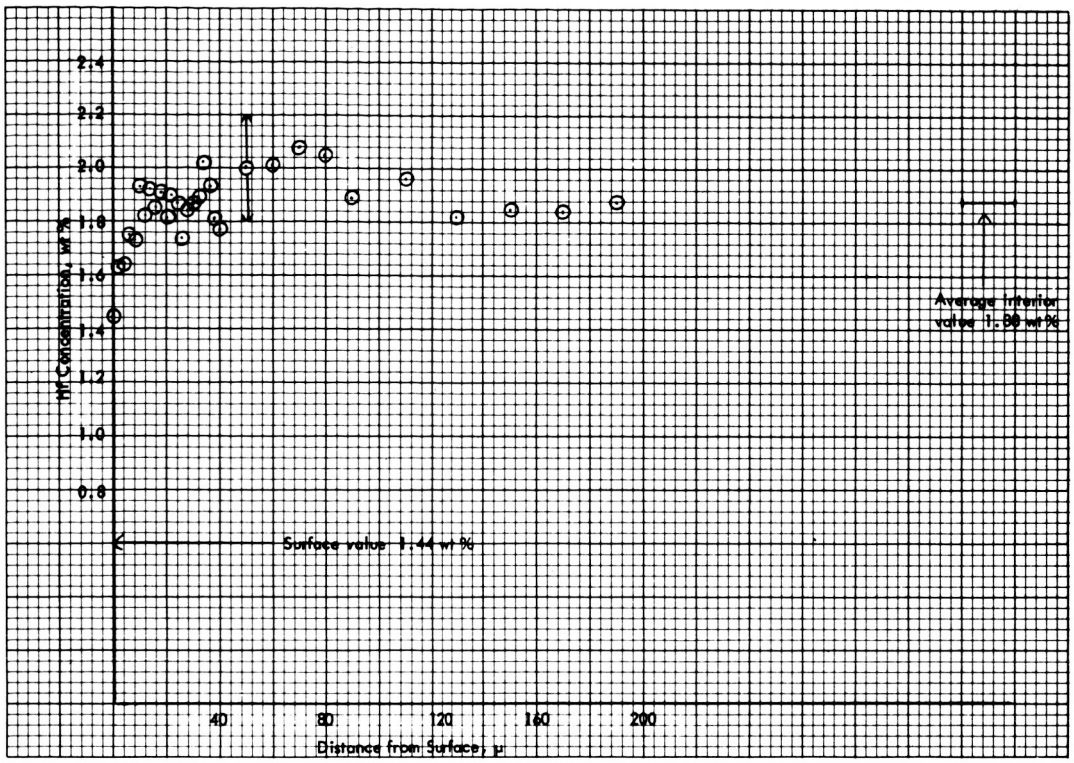

Sample 15-18, M-590, Met. 73416

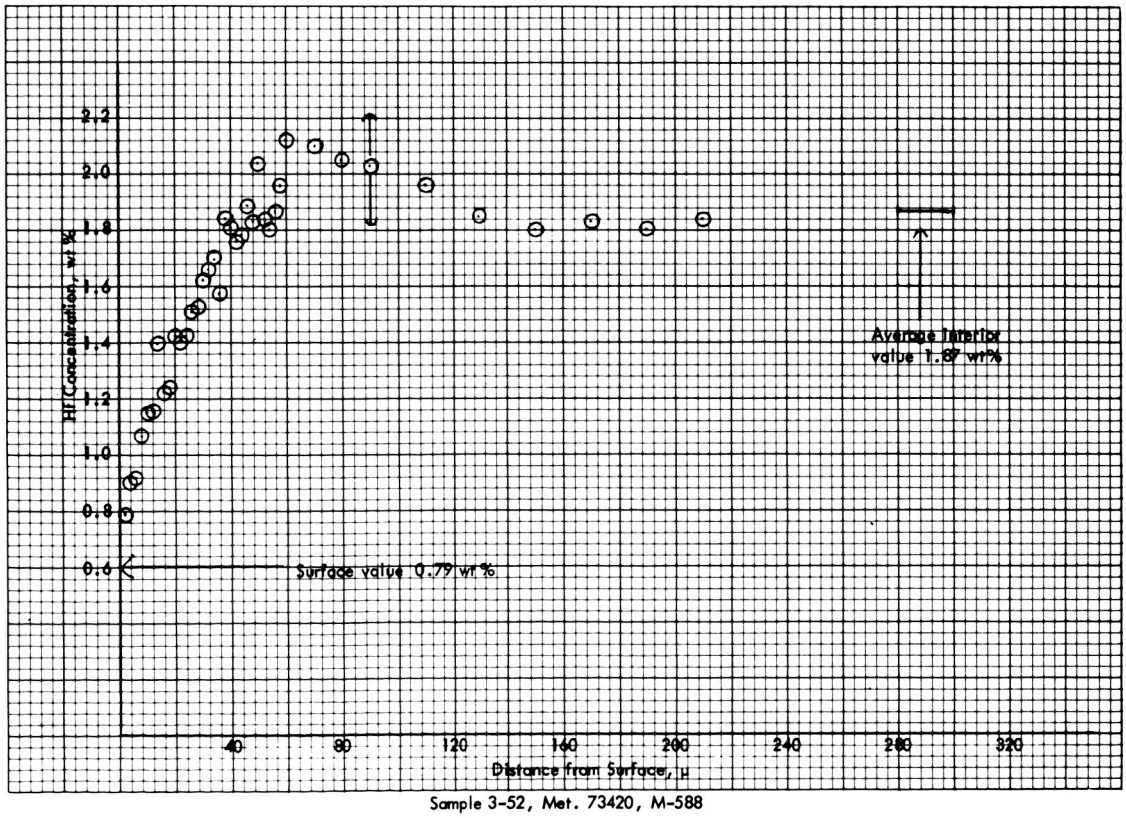

Sample 3-52, Met. 73420, M-588

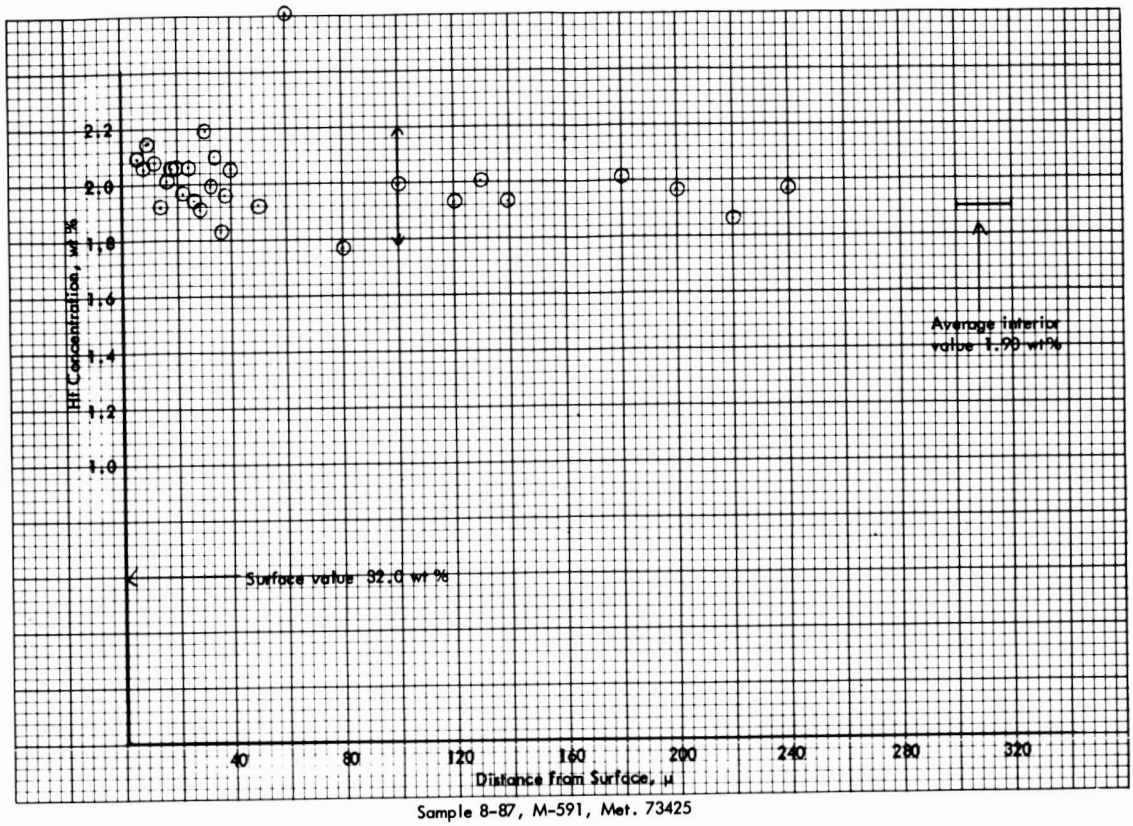

Sample 8-87, M-591, Met. 73425

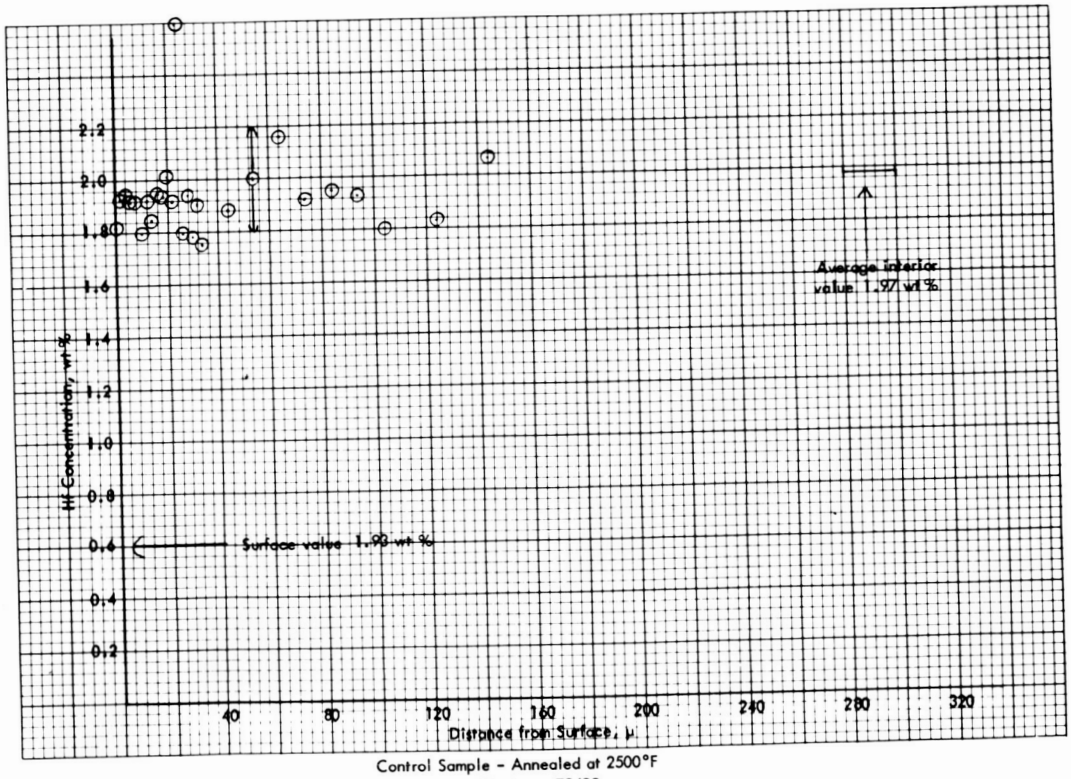

Control Sample - Annealed at 2500°F
M-589, Met. 73429

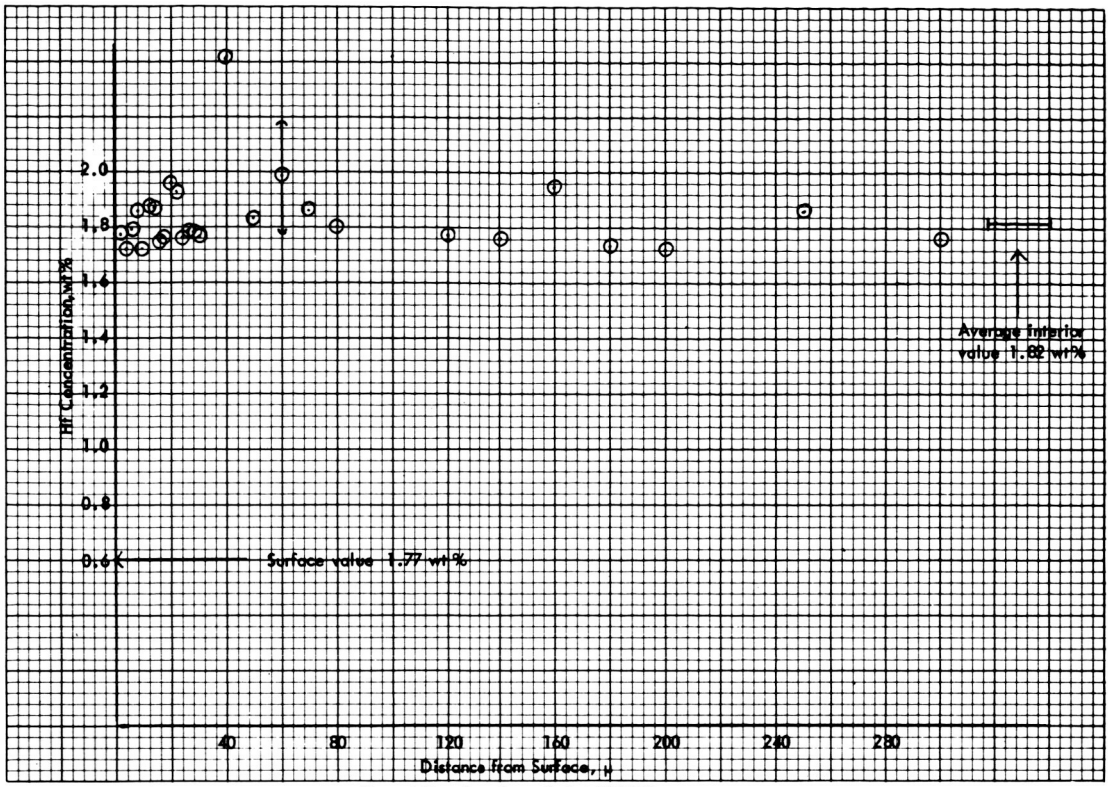

Control Sample - Annealed at 2200°F
M-587, Met. 72428

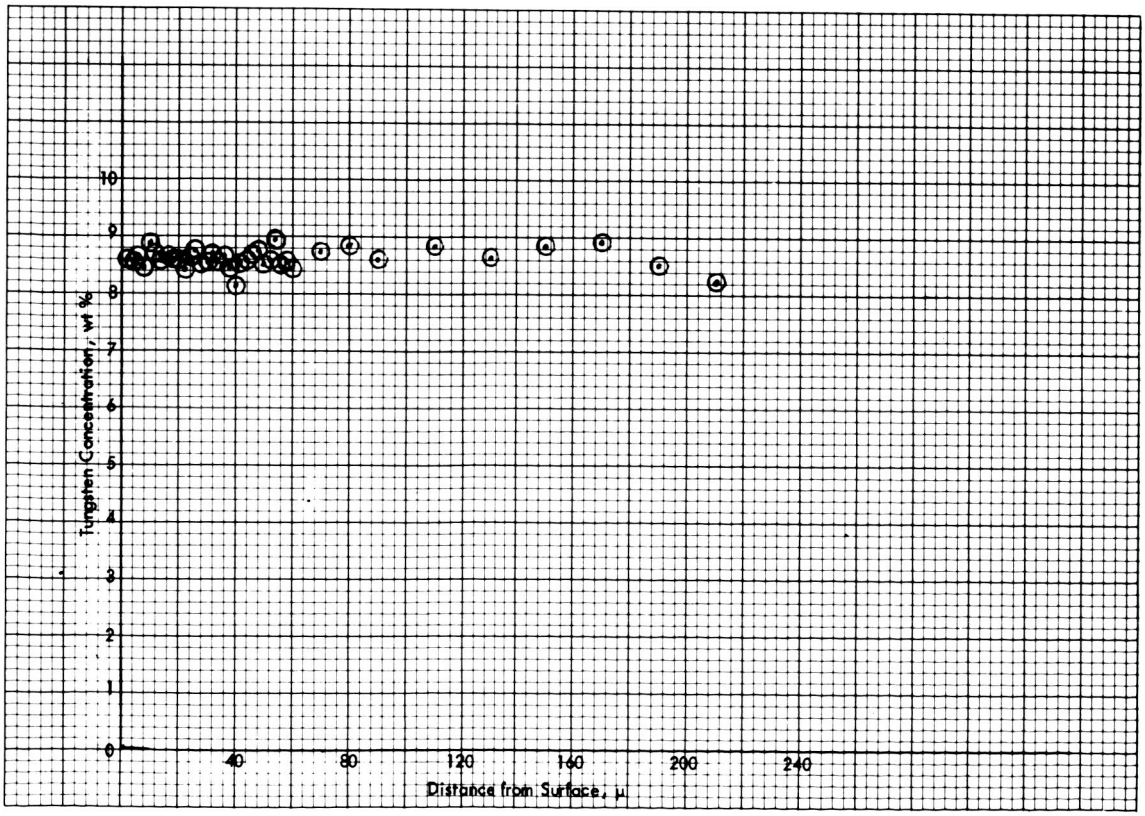

Sample 3-52, M-588, Met. 73420

APPENDIX G

BEND TESTING STANDARD OPERATING PROCEDURE MET-MatP-SOP-60

Powder Metallurgy Product
Development Laboratory

OAK RIDGE NATIONAL
LABORATORY

Oak Ridge, Tennessee

Procedure No. MET-MatP-SOP-60

Revision No. 0

Date December 10, 1971

Page 1 of 3

STANDARD OPERATING PROCEDURE

TITLE: Bend Testing

Prepared by: J. Erwin

Approved by: Supervisor Group Leader

QAC Approval: QAC - Materials 1/5/72

1.0 Purpose

1.1 Bend tests are made to determine the ductility, springback and approximate strength of sheet materials.

2.0 Desired Data

2.1 Minimum bend radius (without cracking) that will permit 90–105° free bend.

2.2 Relaxation from bend under load to free bend.

2.3 Approximate ultimate strength.

3.0 Equipment

3.1 Table model Instron Testing Machine complete with 1000 DR load cell and recorder.

3.2 Bend test rig with support rollers whose diameter is three times ± 0.010 in. the strip thickness, and punch adaptors of the desired diameters for bends to be made.

4.0 References

4.1 Materials Advisory Board suggested Evaluation Procedures for Refractory Metal Sheet Materials - MAB 176-M.

4.2 Operating instructions for Instron table model testing machine.

5.0 Samples

5.1 Minimum sample width = 12 X thickness and length = 24 X thickness.

5.1.1 Sample Preparation - The bend test specimen is supposed to represent the sheet from which it is taken. However, if the alloys being tested are extremely notch sensitive, the surface and edges of all samples are to have all visible imperfections removed by the following procedure:

(1) Polish one surface of all specimens with 600 grit followed by 2/o grit silicon carbide paper to remove all surface imperfections visible when viewed at 20x. All polishing to be parallel to the specimen length.

(2) Remove all effects of specimen cutting from the edges parallel to the length by filing and polishing in the length direction with 400 grit silicon carbide paper.

6.0 Testing Procedure

6.1 Preparation of Instron Machine and Bending Rig

6.1.1 Turn on power to allow 15 minutes minimum warm up prior to use.

6.1.2 Place "AX" gears on chart drive to make chart travel at ten in. per minute. (Gears on drive and high speed spindles.)

6.1.3 Place 1000 lb "DR" load cell on bottom of machine for compression. Connect to recorder.

6.1.4 Check zero and calibration of recorder (15 minute warm up required).

6.1.5 Check speed of testing machine drive to operate at 0.2 in. per minute on the low "A" setting.

6.1.6 Place the proper support rollers (diam = three times specimen thickness) in the bending jig and check roll separation (center distance = 15 times specimen thickness).

6.1.7 Install bending rig on Instron tester and adjust specimen support to "center" with the pressure blade.

6.1.8 Adjust "balance" on recorder to "tare weight" bending rig to zero on the right hand side of recorder.

7.0 Sample Testing

7.1 Attach the desired pin for bending radius to the bottom of the pressure blade.

7.2 Record number, thickness, length, and width of specimen on data sheet.

7.3 Check specimen and bending rolls to make sure they are clean and free of any grit.

7.4 Place specimen, polished side down, on support and adjust to "center" under punch.

7.5 With the "B" speed, bring the punch to within about 1/16 in. of the specimen.

7.6 Check to make certain instrument pen drive is "on".

7.7 With the "A" speed, bring the punch to within about 0.010 in. of the specimen. Stop motor drive and by hand continue depression until contact is made with specimen (Contact is made when recorder pen begins to move).

7.8 Set the fine graduation gage length dials to "0".

7.9 Start the chart drive followed by the "A Down" on the machine.

7.10 Allow the machine to proceed to a gage length reading equal to 1/2 (distance between supports + 0.020) and then stop. Stop chart drive motor. Record gage length reading.

7.11 Activate "A Up" and stop when recorder reaches "zero". Record gage length reading.

7.12 Label recorder paper with sample number and intended bend radius.

BEND TEST DATA

Date _____

Sample No. _____ Alloy _____ Heat Treatment _____

Thickness _____ Width _____ Length _____

Punch Diameter _____

Maximum gage length (depth under load) _____

No load gage depth _____

Max load from chart _____

Specimen deflection at maximum load _____

If failure, at what deflection (chart) _____

Calculated-----(a) Bend angle under load _____

(b) Bend angle no load _____

(c) Spring back _____

(d) Part radius _____

(e) Ultimate strength _____

_____

Signature

NASA CR-134745

NASA DISTRIBUTION

NASA
Washington, D.C. 20546
Attn: George C. Deutsch (RW)
J. Gangler (RWM)

NASA Scientific & Tech. Info. Facility
P.O. Box 33
College Park, Maryland 20740
Attn: Acquisitions Branch (SQT-34054)
(10 copies)

NASA
Goddard Space Flight Center
Greenbelt, Maryland 20771
Attn: Librarian

NASA
Langley Research Center
Hampton, Virginia 23365
Attn: Librarian

NASA
Lewis Research Center
21000 Brookpark Road
Cleveland, Ohio 44135
Attn: Librarian, MS 60-3
R. L. Davies, MS 106-1 (2)
Maxine Sabala, MS 3-19
N.T. Saunders, MS 105-1
Report Control Office, MS 5-5
V. Hlavin, MS 3-14
Terry Gulko MS 49-3
R. English, MS 500-201
G. Ault 3-13
G. Watson 105-1 (2)
R. W. Hall MS 49-1

NASA
Geroge C. Marshall Space FLight Center
Huntsville, Alabama 35812
Attn: Librarian

Jet Propulsion Laboratory
California Institute of Technology
4800 Oak Grove Drive
Pasadena, California 91103
Attn: Librarian

National Bureau of Standards
Washington, D.C. 20224
Attn: Librarian

Air Force Aero Propulsion Lab
Wright Patterson AFB, Ohio 45433
Attn: Librarian

Army Ordnance Frankford Arsenal
Bridgesburg Station
Philadelphia, Pennsylvania 19137

Bureau of Mines
Albany, Orgeon
Attn: Librarian

Bureau of Ships
Department of the Navy
Washington, D.C.
Attn: Librarian

U.S. Energy Research and Development
Administration
Technical Reports Library
Washington, D.C. 20545

U.S. Energy Research and Development
Administration
Germantown, Maryland 20767
Attn: K. E. Horton
E. E. Hoffman
A. VanEcho

Office of Naval Research
Power Division
Washington, D.C. 20225
Attn: Librarian

U.S. Naval Research Laboratory
Washington, D.C. 20225
Attn: Librarian

Aerojet-General Corporation
P.O. Box 209
Azusa, California 91702
Attn: Librarian

AiResearch Manufacturing Company
Sky Harbor Airport
402 South 36th Street
Phoenix, Arizona 85034
Attn: Librarian

AiResearch Manufacturing Company
9851-9951 Sepulveda Boulevard
Los Angeles, California 90045
Attn: Librarian

Atomics International
8900 DeSoto Avenue
Canoga Park, California 91303
Attn: T. A. Moss

Avco
Research & Advanced Development Dept.
201 Lowell Street
Wilmington, Massachusetts 01800
Attn: Librarian

Battelle Memorial Institute
505 King Avenue
Columbus, Ohio 43201
Attn: Librarian
Dr. E. M. Simmons

Battelle-Northwest Labs
P.O. Box 999
Richland, Washington 99352

The Bendix Company
Research Laboratories Division
Southfield, Michigan
Attn: Librarian

The Boeing Company
Seattle, Washington 98100
Attn: Librarian

Brookhaven National Laboratory
Upton, Long Island, New York 11973
Attn: Librarian

Chance Vought Aircraft, Inc.
P.O. Box 5907
Dallas, Texas 75222
Attn: Librarian

Clevite Corporation
Mechanical Research Division
540 East 105th Street
Cleveland, Ohio 44108
Attn: N. C. Beerli
Project Administrator

Curtis-Wright Corporation
Wright-Aeronautical Division
Woodridge, New Jersey 07075
Attn: S. Lombardo

Ford Motor Company
Aeronautronics
Newport Beach, California 92660
Attn: Librarian

General Atomic
John Jay Hopkins Laboratory
P.O. Box 608
San Diego, California 92112
Attn: Librarian

General Electric Company
Atomic Power Equipment Division
P.O. Box 1131
San Jose, California

General Electric Company
Missile & Space Division
P.O. Box 8555
Philadelphia, Pennsylvania 19114
Attn: Librarian

General Electric Company
Vallecitos Atomic Lab
Pleasanton, California 94566
Attn: Librarian

General Dynamics/Fort Worth
P.O. Box 748
Fort Worth, Texas 76100
Attn: Librarian

General Motors Corporation
Allison Division
Indianapolis, Indiana 46206
Attn: Librarian

Hamilton Standard
Division of United Aircraft Corp.
Windsor Locks, Connecticut
Attn: Librarian

Hughes Aircraft Company
Engineering Division
Culver City, California 90230-2
Attn: Librarian

IIT Research Institute
10 West 35th Street
Chicago, Illinois 60616
Attn: Librarian

Lockheed Missiles and Space Division
Lockheed Aircraft Corporation
Sunnyvale, California
Attn: Librarian

Marquardt Aircraft Company
P.O. Box 2013
Van Nuys, California
Attn: Librarian

Teledyne Isotopes
Nuclear Systems Division
110 West Timonium Road
Timonium, Maryland 21093

Materials Research & Development
Manlabs, Incorporated
21 Erie Street
Cambridge, Massachusetts 02139

Materials Research Corporation
Orangeburg, New York
Attn: Librarian

McDonnel-Douglas Aircraft Co.
St. Louis, Missouri 63100
Attn: Librarian

Union Carbide Metals
Niagara Falls, New York 14300
Attn: Librarian

United Aircraft Corporation
Pratt & Whitney Division
400 West Main Street
Hartford, Connecticut 06108
Attn: Librarian

United Nuclear Corporation
Research and Engineering Center
Grassland Road
Elmsford, New York 10523
Attn: Librarian

Union Carbide Corporation
Parma Research Center
P.O. Box 6115
Cleveland, Ohio 44101
Attn: Technical Info. Services

Southwest Research Institute
8500 Culebra Road
San Antonio, Texas 78206
Attn: Librarian

Superior Tube Company
Norristown, Pennsylvania
Attn: A. Bound

Sylvania Electrics Products, Inc.
Chemical & Metallurgical
Towanda, Pennsylvania
Attn: Librarian

TRW, Inc.
Caldwell Research Center
23444 Euclid Avenue
Cleveland, Ohio 44117
Attn: Librarian

Cabot Industries
Stellite Division
Kokomo, Indiana
Attn: Librarian

Union Carbide Nuclear Company
P.O. Box X
Oak Ridge, Tennessee 37831
Attn: X-10 Laboratory
Records Department (2)
J. Scott
J. H. DeVan

National Research Corporation
405 Industrial Place
Newton, Massachusetts
Attn: Librarian

NASA
Manned Spacecraft Center
Houston, Texas 77001
Attn: Librarian

Los Alamos Scientific Laboratory
University of California
Los Alamos, New Mexico
Attn: Librarian

Lockheed Georgia Company
Division, Lockheed Aircraft Company
Marietta, Georgia
Attn: Librarian

TRW Inc.
TRW Systems Group
One Space Park
Redondo Beach, California 90278
Attn: Dr. H. P. Silverman

Sandia Corporation
Aerospace Nuclear Safety Division
Sandia Base
Albuquerque, New Mexico 87115
Attn: Librarian

Rockwell International
Rocketdyne
Canoga Park, California 91303
Attn: Librarian

Engineering Library
Fairchild Hiller
Republic Aviation Corporation
Farmingdale, Long Island, New York
Attn: Librarian

MSA Research Corporation
Callery, Pennsylvania 16024
Attn: Librarian

Climax Molybdenum Company of Michigan
1600 Huron Parkway
Ann Arbor, Michigan 48105
Attn: Librarian
Dr. M. Semchyshen

McDonnell-Douglas Astronautics
Douglas Company, Inc.
Missile and Space Systems Division
3000 Ocean Park Boulevard
Santa Monica, California
Attn: Librarian

Rockwell International
Atomics International Division
P.O. Box 309
Canoga Park, California 91304
Attn: Director, Liquid Metals
Information Center

Allison-General Motors
Energy Conversion Division
Indianapolis, Indiana
Attn: Librarian

Lawrence Radiation Laboratory
Livermore, California
Attn: Librarian (2)

Grumman Aircraft
Bethpage, New York
Attn: Librarian

Wah Chang Corporation
Albany, Oregon
Attn: Librarian

Westinghouse Electric Corporation
Astronuclear Laboratory
P.O. Box 10864
Pittsburgh, Pennsylvania 15236
Attn: Librarian
R. W. Buckman

Westinghouse Electric Corporation
Materials Manufacturing Division
RD #2, Box 25
Blairsville, Pennsylvania
Attn: Librarian

Wyman-Gordon Company
North Grafton, Massachusetts
Attn: Librarian

Westinghouse Electric Corporation
Research & Development Center
Pittsburgh, Pennsylvania 15235
Attn: Librarian
R. T. Begley

Mr. Robert L. Hirsch
Acting Director
Division of Controlled Thermonuclear Research
U. S. Energy Research and Development Administration
Washington, D.C. 20545

INTERNAL DISTRIBUTION

(3) Central Research Library
ORNL — Y-12 Technical Library
Document Reference Section
(10) Laboratory Records
Laboratory Records, ORNL RC
ORNL Patent Office
G. M. Adamson, Jr.
R. G. Alsmiller
C. F. Barnett
S. E. Beall
J. T. Bell
L. A. Berry
E. E. Bloom
D. N. Braski
C. E. Bush
J. L. Cadden
D. Cannon
S. Cantor
R. W. Carpenter
D. L. Clark
J. F. Clarke
R. E. Clausing
R. J. Colchin
W. H. Cook
W. B. Cottrell
F. L. Culler
C. W. Cunningham (K-25)
J. E. Cunningham
R. A. Dandl
(10) J. H. DeVan
J. R. DiStefano
R. G. Donnelly
R. A. Dory
J. I. Federer
L. M. Ferris
B. Fleischer (K-25)
A. P. Fraas
T. A. Gabriel
G. M. Goodwin
W. R. Grimes
A. G. Grindell
Miriam Guthrie
D. E. Harasyn
W. O. Harms
P. N. Haubenreich
R. L. Heestand
(10) M. R. Hill
H. W. Hoffman
J. T. Hogan
J. A. Horak
W. R. Huntley
H. Inouye
G. G. Kelley
G. D. Kerbel
R. L. Klueh
C. C. Koch
E. Lamb
J. M. Leitnaker
C. T. Liu
(10) E. L. Long, Jr.
H. M. Long
M. S. Lubell
R. E. MacPherson
F. C. Maienschein
W. R. Martin
D. McAlees
H. E. McCoy
H. C. McCurdy
R. E. McDonald
C. J. McHargue
J. R. McNally, Jr.
A. J. Miller
A. J. Moorhead
O. B. Morgan
E. M. Oblow
P. Patriarca
F. G. Perey
R. E. Reed
M. Roberts
M. T. Robinson
J. A. Rome
M. W. Rosenthal
A. C. Schaffhauser
J. L. Scott
J. E. Selle
Myrtleen Sheldon
G. M. Slaughter
D. Steiner
J. O. Stiegler
R. A. Strehlow

D. B. Trauger
T. N. Washburn
J. S. Watson
J. R. Weir, Jr.
C. R. Weisbin
E. R. Wells
F. W. Wiffen
F. W. Young
A. Zucker

EXTERNAL DISTRIBUTION

AIR FORCE SYSTEMS COMMAND, Andrews AFB, MD 20331

G. R. Crane

AIR FORCE MATERIALS LABORATORY, Wright-Patterson AFB, OH 45433

L. N. Hjelm
L. Perlmutter

AIR FORCE KIRTLAND AIR FORCE BASE, Kirtland AFB, NM 87117

A. Noonan
Directorate of Nuclear Safety

AMES LABORATORY, Iowa State University, P.O. Box 1129,
Station A, Ames, IA 50010

O. N. Carlson

ARGONNE NATIONAL LABORATORY, 9700 S. Cass Avenue, Argonne, IL 60439

S. Greenberg
T. F. Kassner
J. M. McKee
A. A. Solomon

ATOMICS INTERNATIONAL, P.O. Box 309, Canoga Park, CA 91304

R. L. McKisson
H. Pearlman

BATTELLE MEMORIAL INSTITUTE, 505 King Avenue, Columbus, OH 43201

Defense Materials Information Center
W. Pardue

BROOKHAVEN NATIONAL LABORATORY, 29 Cornell Avenue, Upton, Long Island, NY 11973

D. H. Gurinsky
H. S. Isaacs
J. R. Weeks

BUREAU OF MINES, Albany Metallurgy Research Center, P.O. Box 70,
Albany, OR 97321

Haruo Kato

DONALD W. DOUGLAS LABORATORIES, 2955 George Washington Way, Richland, WA 99352

D. Watrous

E. I. DU PONT DE NEMOURS AND COMPANY, Savannah River Laboratory, Aiken, SC 29801

P. E. Smith
D. R. Turno

GENERAL ELECTRIC COMPANY, P.O. Box 8661, Philadelphia, PA 19101

R. J. Katucki
E. H. Sayell
H. Straub

GULF ENERGY AND ENVIRONMENTAL SYSTEMS, P.O. Box 608, San Diego, CA 92112

N. Elsner

ISOTOPES, INC., Nuclear Systems Division, 110 West Timonium Road, Timonium, MD 21093

G. Linkous

JET PROPULSION LABORATORY, 4800 Oak Grove Drive, Pasadena, CA 91103

R. G. Ivanoff
V. Truscello

JOHN HOPKINS UNIVERSITY, APPLIED PHYSICS LABORATORY, 8621 Georgia Road, Silver Springs, MD 20910

LOS ALAMOS DCIENTIFIC LABORATORIES, P.O. Box 1663, Los Alamox, NM 87544

R.N.R. Mulford

MINNESOTA MINING AND MANUFACTURING COMPANY, 3M Center, St. Paul, MN 55101

E. F. Hampl

MONSANTO RESEARCH CORPORATION, Mound Laboratory, P.O. Box 32, Miamisburg, OH 45342

W. T. Cave
D. L. Coffee
E. W. Johnson
D. P. Kelly

NATIONAL AERONAUTICS AND SPACE ADMINISTRATION, MANNED SPACECRAFT CENTER, Mail Code EZ, Houston, TX 77058

T. E. Redding

NAVAL FACILITIES ENGINEERING COMMAND, DEPARTMENT OF THE NAVY, Code 042, Washington, DC 20390

M. D. Starr

PACIFIC NORTHWEST LABORATORY, P.O. Box 550, Richland, WA 99352

Director

TRW SYSTEMS, One Space Park, Redondo Beach, CA 90278

I. Jones

USERDA, DAYTON AREA OFFICE, P.O. Box 66, Miamisburg, OH 45342

R. L. Wainwright

USERDA, DIVISION OF APPLIED TECHNOLOGY, Washington, DC 20545

R. W. Shivers

USERDA, DIVISION OF BIOMEDICAL AND ENVIRONMENTAL RESEARCH, Washington, DC 20545

USERDA, DIVISION OF REACTOR RESEARCH AND DEVELOPMENT, Washington, DC 20545

T. A. Nemzek
J. M. Simmons

USERDA, SAN FRANCISCO OPERATIONS OFFICE, 1333 Broadway, Oakland, CA 94612

R. DuVal

USERDA, DIVISION OF SPACE NUCLEAR SYSTEMS, Washington, DC 20545

R. T. Carpenter
G. P. Dix
D. S. Gabriel
N. Goldenberg
H. Jaffe
J. J. Lombardo
G. A. Newby
C. O. Tarr
E. J. Wahlquist

USERDA, OAK RIDGE OPERATIONS, P.O. Box E, Oak Ridge, TN 37830

Reactor Division
Research and Technical Support Division

USERDA, TECHNICAL INFORMATION CENTER, Office of Information Services, P.O. Box 62, Oak Ridge, TN 37830

(2) Manager

FUSION REACTOR TECHNOLOGY DISTRIBUTION 1